A Calibration Chamber for Thermo-hydro-mechanical Studies of Soil Behavior

via Resonant Column Testing

by

Daniel R. C. Green

Presented to the Faculty of the Graduate School of

The University of Texas at Arlington in Partial Fulfillment

of the Requirements

for the Degree of

Master of Science in Civil Engineering

The University of Texas at Arlington

August 2018

Acknowledgments

I would like to thank my mother and father for their unwavering support and constant presence throughout my life. Words cannot express my gratitude for the opportunities they have provided me and allowed me to pursue.

I would like to thank my advisor Dr. Laureano Hoyos for his guidance during my research and for pushing me to finish this thesis. I would also like to thank Dr. Xinbao Yu for lending me his thermal camera and being on my thesis committee. I want to also extend my gratitude to Dr. Sahadat Hossain for being a part of my thesis committee.

Finally, I want to thank Roya Davoodi-Bilesavar for her help with research and testing. She was a constant figure in the lab to discuss my thesis with and helped me regularly every step of the way from crushing soil to resonant column testing. I am truly grateful.

Abstract

A Calibration Chamber for Thermo-hydro-mechanical Studies of Soil Behavior

via Resonant Column Testing

Daniel R. C. Green

The University of Texas at Arlington, 2018

Supervising Professor: Dr. Laureano Hoyos

A considerable portion of the emerging geothermal infrastructure in the country is located in earthquake prone areas while being supported and/or surrounded by soil deposits located well above the groundwater table. Geotechnical earthquake research in the country, however, continues to be mostly focused on soil response under saturated conditions, especially soil liquefaction phenomena, while most of the work on dynamic response of compacted soils has not taken suction or thermal conditioning of pore-fluids into account as critical environmental factors. To date, there is hardly any comprehensive study at the laboratory scale that has focused on a thorough assessment of the dynamic properties of unsaturated soils, particularly material damping ratio, for a relatively large range of cyclic shear strain amplitudes (0.001% to 0.1% shear strain amplitudes) under controlled moisture and simultaneous thermal conditioning of pore-fluids.

An existing Resonant Column apparatus has been upgraded to investigate the dynamic response of compacted low plasticity clay, particularly in terms of shear-wave velocity, shear modulus and damping ratio, under controlled moisture, confinement, and thermal conditioning of the pore-fluids, from 20-60°C. A digital convection heater, featuring two heating elements, two internal fans, and a thermocouple, has been adapted to the main cell of the RC apparatus for measurement and control of thermal conditioning of the pore-fluids. However, because

thermocouple probes cannot be inserted into the sample during testing for risk of disturbing the compacted soil and puncturing the latex membrane, a thorough thermo calibration of the Resonant Column chamber is necessary prior to testing to ensure proper heating and heat distribution within the soil.

For calibration, a second heating chamber, similar to the one used for RC testing was developed to determine optimum temperatures and heating times for the soil to reach a desired temperature. The primary scope of this thesis is the thermo calibration of the Resonant Column chamber and preliminary thermo-controlled RC testing to investigate the potential impact of heat on stiffness parameters, particularly shear modulus and damping ratio of a low plasticity clay.

Table of Contents

List of Figures

List of Tables

Chapter 1

Justification and Introduction

1.1 - Introduction

Geothermal power is a continually developing trend in green energy that has been growing rapidly not only in the United States, but also in countries around the world since the late 1970s. Globally, geothermal capacity of existing geothermal power plants totaled 11,700 megawatts as of 2013, with an additional 11,700 megawatts in additional capacity either in early stages of development or currently under construction in 70 countries around the world. Existing plants produced approximately 68 billion kilowatt-hours of electricity, enough to meet the demands of nearly 6 million homes in the United States (Geothermal Energy Association, 2013). Currently, 3386 megawatts of the global geothermal power infrastructure reside in the United States, making it the global leader in geothermal capacity. Eighty percent of the United States geothermal capacity is located in California where 40 power plants provide close to 7 percent of the state's electricity (Geothermal Energy Association, 2013).

High underground temperatures are a necessity for geothermal power. The areas with the highest underground temperatures are located in regions with active or young volcanoes where tectonic plate boundaries and thin layers in the earth's crust let heat through. These favorable locations and identified hydrothermal sites can be seen in figure 1-1. These regions with the highest potential for geothermal power are seismically active. Earthquakes cause movement and stresses in the rock which allows naturally heated water to circulate more freely, sometimes leading to geysers and natural hot springs. Geothermal power plants tap into these geothermal reservoirs drawing hot water or steam from the earth and convert the heated fluid into electricity for commercial use.
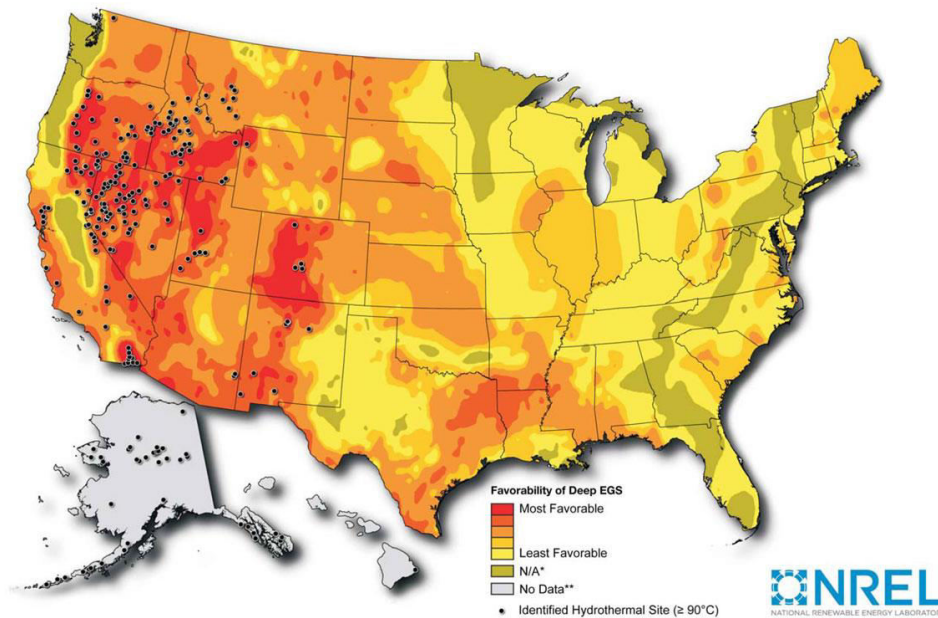
Figure 1-1: U.S. geothermal resources. (U.S. Energy Information Administration, Annual Energy Review 2011)

While geothermal energy has the potential for electrical power generation on a large scale, it also is being used in heating and cooling systems for homes and buildings through the use of ground source heat pumps. Geothermal power generation requires high underground temperatures; however, geothermal heating and cooling systems utilize the constant temperature zone located anywhere from five to a few hundred feet below the ground where the temperature remains about 55°F regardless of seasonal changes. In residential areas or small buildings these geothermal systems can be installed at relatively shallow depths of five feet in a horizontal configuration or at deeper depths of a few hundred feet for vertical configurations.

For larger structures, geothermal energy is harvested primarily through energy piles, heat exchanger piles, or geothermal piles. The idea of geothermal piles is the same as the ground source heating and cooling previously stated. However, instead of having a separate pipe system underground, the heat exchanger pipes are located in the foundation itself by adding one or more loops of plastic pipes down the length of the pile inside of the rebar reinforcement cage. A common geothermal pile schematic is shown in figure 1-2. The circulation loops located in the

structural support piles are connected to a ground source heat pump that provides heating and cooling to the building. The ground source heat pump functions the same way as the more common air source heat pump, however it has the advantage of the ground being warmer than the air in the winter (therefore able to provide more heat) and cooler than the air in the summer (therefore able to absorb more heat). These dual-purpose piles provide an efficient and renewable source of energy potential with great environmental and economic benefits.
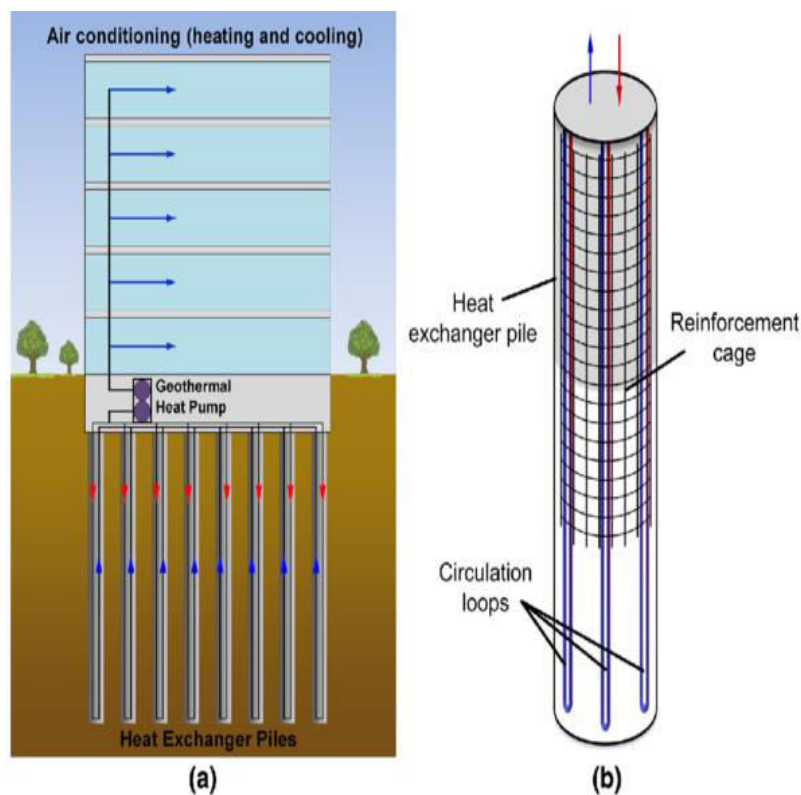
Figure 1-2: a) Schematic showing a building supported by heat exchanger piles, b) typical configuration of a heat exchanger pile with integrated circulation loops (Olgun et al., 2015)
.

Even though geothermal energy is more environmentally friendly and economical than traditional energy generation methods, it is not without its challenges. The addition of cyclic thermal loading applications to foundation systems and soil require further investigation to fully

understand the effects of heat on soil properties. Current design practices for geothermal piles relies primarily on experience and empirical rules, incorporating high values of factor of safety which excessively increase construction and installation costs, as well as undermine the potential economic and environmental benefits (Ghasemi-Fare and Basu, 2015).

While numerous thermo-controlled soil tests have been performed and the results are well documented, the majority of these tests are focused on how temperature influences the strength properties and preconsolidation pressure of soil using thermo-controlled triaxial and thermo-controlled oedometer experiments. Cekerevac and Laloui studied the effects of temperatures ranging from 22 to 90°C on the mechanical behavior of a saturated clay (Cekerevac and Laloui, 2003). To complete their work, they developed and calibrated a new thermo-controlled triaxial device specifically focused on the thermo-mechanical testing of saturated soil (Cekerevac and Laloui, 2005). Tang et al. developed an isotropic cell to study the thermo-mechanical behavior of unsaturated soils (Tang et al., 2007). Uchaipichat and Khalili modified a triaxial apparatus for testing of unsaturated soils at elevated temperatures from 20 to 60°C (Uchaipichat and Khalili, 2009). Alsherif and McCartney used drained triaxial compression tests to study the effects of temperature and suction on the hardening mechanisms of soil under different testing paths (Alsherif and McCartney, 2015).

Stiffness properties of soil, such as damping ratio and shear modulus have also been well documented through use of resonant column testing. Ashmawy et al. thoroughly reviews material damping ratio and resonant column testing (Ashmawy et al., 1995). Lanzo and Vucetic established trends between plasticity index and damping ratio of soils (Lanzo and Vucetic, 1999). Vucetic and Dobry studied the effects of soil plasticity on cyclic response and stiffness properties to potentially aid in seismic microzonation of earthquake prone areas (Vucetic and Dobry, 1991). Suction controlled resonant column testing has also been thorough. Vassallo et al. used a suction controlled resonant column apparatus to investigate the effect of suction history on small strain stiffness of a clayey silt (Vassallo et al., 2007). Despite the advances mentioned, there is a distinct lack of information on the stiffness properties of soil under thermo-controlled loading

conditions. However, as geothermal energy becomes more prevalent and geothermal piles become more common the demand for this information will continue to grow.

This thesis focuses primarily on calibration of a resonant column chamber for future thermo-controlled testing to better understand the effects of elevated temperatures on stiffness properties of soil. Preliminary thermo-controlled resonant column test data is also shown; however, more thorough testing is necessary.

1.2 – Research Objectives

As previously stated, the primary scope of this research work is the thermo-calibration of a resonant column chamber for future investigation into stiffness properties of soil under thermo-controlled loading from temperatures between 20 to 60°C. The secondary objective of this research is to present preliminary data on soil stiffness properties under elevated temperatures for use as a starting point for further research into thermo-controlled resonant column testing. Specific tasks within the scope of this thesis are described below.

- ➢ To identify the need for a better understanding of soil stiffness properties under elevated temperatures.
- ➢ To review literature on previous thermo-controlled testing devices and studies, including triaxial and oedometer apparatuses
- ➢ To review literature on previous resonant column testing both with and without suction control.
- ➢ To design a chamber similar to the resonant column testing device for thermo calibration.
- ➢ To precisely classify the soil used during testing through ASTM standard methods for liquid limit, plastic limit, plasticity index, specific gravity, sieve and hydrometer analysis.
- ➢ To identify the maximum dry density and optimum moisture content of the soil using the compaction curve obtained from the ASTM standard proctor method
- ➢ To perform heating and cooling cycles using source temperatures of 40, 50, 60, and 70°C on three soil samples with moisture contents ranging from slightly dry to slightly wet
- ➢ To identify possible moisture loss during heating cycles

- To identify optimum heating and cooling times for soil samples to reach peak temperatures and return to room temperature

- To use the data gathered to establish trends during heating and cooling for calibration of the resonant column chamber

- To perform resonant column tests under room and elevated temperatures to gather preliminary thermo-controlled testing data.

- To provide useful data for future, more thorough investigation of elevated temperatures on soil stiffness properties.

1.3 – Thesis Organization

A brief summary of the chapters included in this thesis are as follows:

Chapter 2 restates the importance of understanding thermo-dynamic properties of soil and examines progress that has been made in thermo-controlled testing in triaxial and oedometer cells. Resonant column tests with and without suction control are also discussed to give a reference point for thermo-controlled resonant column testing. This chapter will consist primarily of a literature review of the papers previously mentioned and briefly introduced in the introduction.

Chapter 3 details the design and assembly of the thermo-calibration chamber. This chapter describes the design process and materials used, including the specifications of the thermometer and temperature controller. A thorough step by step assembly guide, with photos, outlines the assembly process in a detailed manner.

Chapter 4 presents the soil properties and results obtained during classification and the thermo calibration of the resonant column chamber. Soil tests and results obtained are presented and analyzed to provide a justification for the classification of the soil. The reasoning behind temperatures selected and methods used for thermo calibration will be discussed. Data is presented, and trends are drawn from the thermo calibration test results.

Chapter 5 presents preliminary thermo-controlled resonant column testing results. Damping ratio and shear modulus under normal and elevated temperatures is compared in an effort to observe the effect of heat on stiffness properties of soil.

Chapter 6 includes a summary of the thesis and results obtained from both thermo calibration and preliminary thermo-controlled resonant column experiments. Conclusions pertaining to the data obtained are stated and recommendations for improvements to methods used are given to provide guidance for future research.

Chapter 2

Literature Review

2.1 - Introduction

This chapter will discuss the growing need for a better understanding of how elevated temperatures effect dynamic and stiffness properties of soil, in particular shear modulus, G, and damping ratio, D.

Advancements in thermo-mechanical testing of soils are reviewed not only to show that temperature has a significant effect on mechanical and strength properties of soil, but also to look at different heating methods used in thermo-controlled triaxial and oedometer tests. Differences between heating methods used, mediums for heat transfer, and challenges faced are examined to provide a basis for thermo calibration of the resonant column chamber.

The procedure of a typical resonant column test is provided, and typical results are presented to establish a basic understanding of how dynamic soil properties are obtained and what they signify.

2.2 - Growing trends in thermal energy.

The Geothermal Energy Association reported in 2013 that 11,765 Megawatts of geothermal power are operating globally with 11,766 Megawatts of additional capacity either in development or early stages of construction across 70 countries (Geothermal Energy Association, 2013). The 2016 Geothermal Energy Association report showed that the global market reached 13.3 Gigawatts of operating capacity as of January 2016 with 12.5 Gigawatts of additional planned capacity across 82 countries. Current models show the global geothermal market on pace to reach 18.4 Gigawatts by 2021, and if all countries follow through on their geothermal power development goals the global market could exceed 32 Gigawatts by the early 2030s. The United Nations and the International Renewable Energy Agency pledge a lofty five-fold growth increase in geothermal capacity and two-fold growth increase in geothermal heating by 2030 compared to current levels. The Geothermal Energy Association estimates that countries

around the world have only tapped into 6 to 7 percent of the total global potential for geothermal power based on current geologic knowledge and technology. The untapped resources are vast and could provide renewable energy to power grids across the globe (Geothermal Energy Association, 2016).
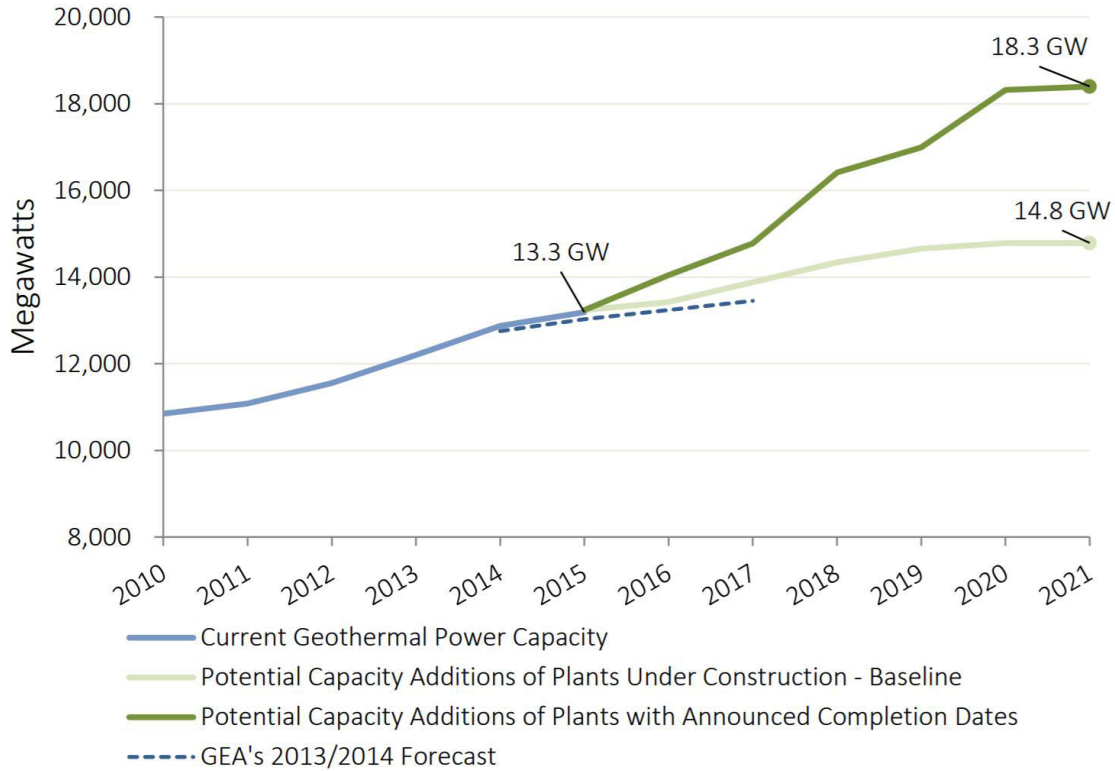
Figure 2-1: International geothermal power nameplate capacity (MW)
(Geothermal Energy Association, 2016)

The majority of current geothermal power capacity is located in the United States. As of 2013 the United States has approximately 3,386 Megawatts of installed geothermal capacity. Furthermore, 3,250 Megawatts of the United States current geothermal capacity are in two of the three most seismically active states. The second most seismically active state, California, contains over 80 percent of the current geothermal capacity, with an additional 15 percent located in Nevada, the third most seismically active state. California will continue to be a national leader

in geothermal power due to their 2005 Energy Action Plan, which proposes a goal of 33 percent of electricity generation from renewable sources by 2020. The plan was codified in 2011. Geothermal energy in Nevada is also expected to continue growing. Nevada currently has 517 Megawatts of geothermal capacity with 2,275 Megawatts in development over 75 projects (Geothermal Energy Association, 2013).
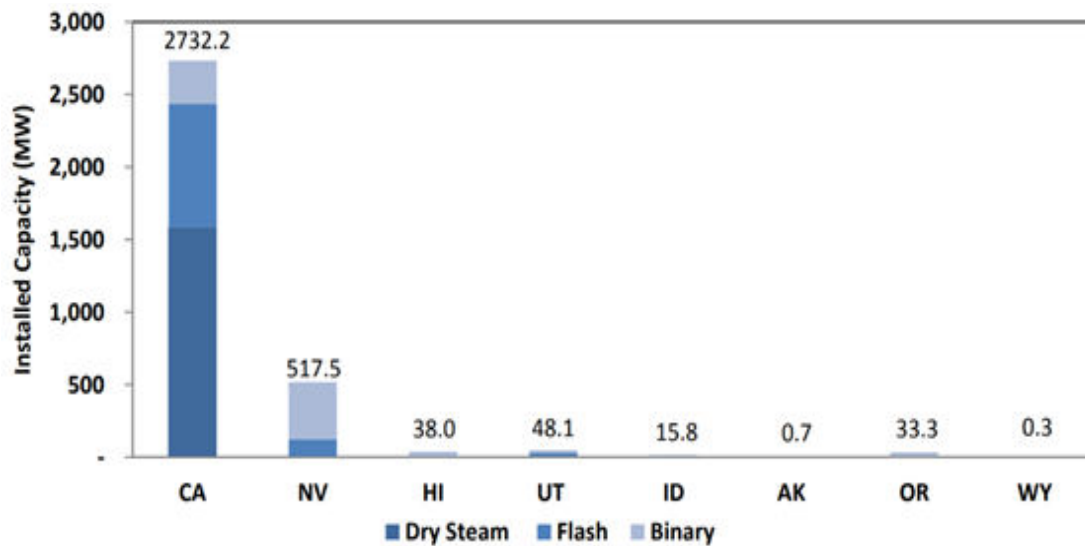
Figure 2-2: February 2013, US Geothermal Installed Capacity by State (MW)
(Geothermal Energy Association, 2013)

As geothermal energy continues to grow, a complete understanding of elevated temperatures on strength and stiffness properties of soil will be crucial to ensure safe and cost-effective designs of geothermal infrastructure. Potential environmental and economic benefits of geothermal energy have made the use of geothermal pile support systems more popular all over the world. However, despite the growing popularity of harvesting shallow geothermal energy through building foundation systems, the present design practices use empirical methods and high factors of safety, which undermine the economic and environmental benefits associated with renewable geothermal energy (Ghasemi-Fare and Basu, 2015).

2.3 - Review of thermo-mechanical soil testing and devices

Thermal effects on the mechanical behavior of a saturated soil are well documented. The first soil testing devices modified for thermo mechanical testing were oedometers. The apparatus was usually modified with a heating element located in the water bath surrounding the sample. The heating element would heat up the water which would heat up the sample. Oedometers operate under an assumption of zero lateral strain, however with thermo induced volume change that assumption is invalid. Difficulty with analysis of thermo-controlled oedometer results led to the development of temperature controlled triaxial cells (Cekerevac and Laloui, 2005).

Many temperature controlled triaxial devices have been used with different heating methods, however, most heating methods fall into two categories, heating by circulating fluid or heating with internal heaters. Despite their differences, both methods use water as the confining fluid and medium for heat transfer. Triaxial cells that heat via circulating fluid have an external heat pump that circulates hot water into the chamber. The hot water being circulated into the cell was used both as a heat source and confining fluid. Triaxial cells with internal heaters submerge heating elements directly into the water filled cell and use a motorized propeller to evenly distribute heat throughout the water. Heating elements have varied from metal rods to foil to a coil that surrounds the sample like a cage (Cekerevac and Laloui, 2005).

Cekerevac and Laloui conducted a thorough study on clay using a temperature controlled triaxial device. Triaxial shear, consolidation, and drained thermal heating experiments were conducted for temperatures between 20 and 90°C. However, similar to the purpose of this thesis, they first had to modify and calibrate their existing triaxial device for thermo-controlled testing. They developed a new thermo-mechanical triaxial system with the following requirements in mind:

➢ The heating system should work independently from the other parts of the cell

➢ The heating system should impose a uniform temperature field to the sample

➢ The time needed to bring the sample to a uniform temperature should be as short as possible

➢ The heater should be as close to the sample as possible to improve temperature control

The triaxial device they designed incorporated both heating by circulating fluid through a heat pump and heating by an internal submerged heat source. A closed loop system consisting of a metal tube spiraled around the sample is attached to a 2000-watt heater that uses a pump to circulate hot water through the coiled tubing. A diagram of the triaxial cell designed by Cekerevac and Laloui is shown in figure 2-3 below (Cekerevac and Laloui, 2005).
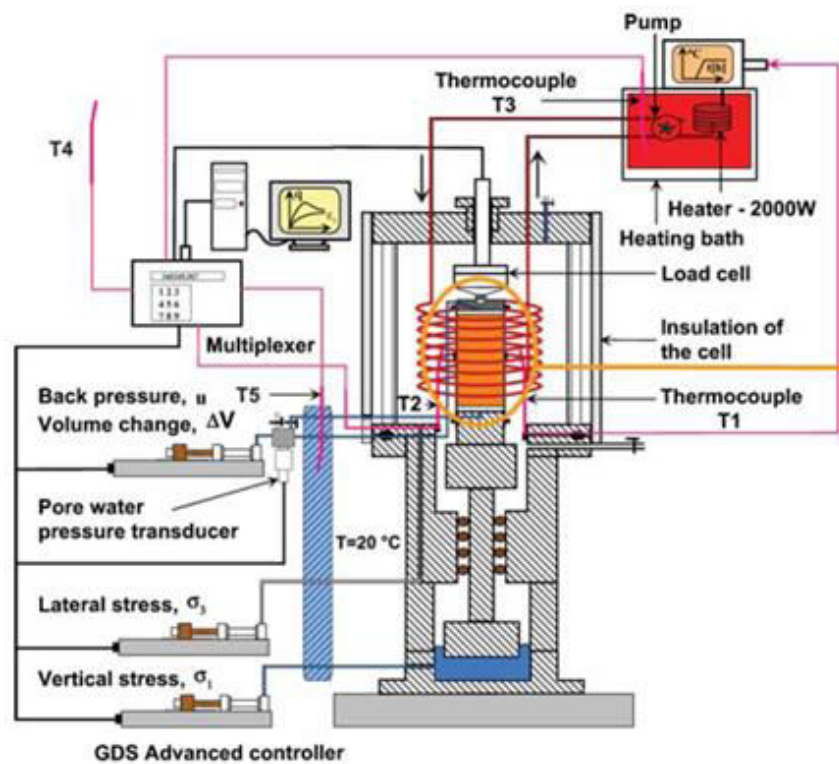
Figure 2-3: Triaxial apparatus with controlled temperatures. (Cekerevac and Laloui, 2005)

To calibrate their triaxial device they used three main thermocouples, one to control the temperature of the circulating fluid, one to measure water temperature near the sample, and one inserted into the middle of the sample to measure the soil temperature. The temperature of the circulating fluid was increased in increments of 10°C and held constant until the temperature of the sample and the heating water reached equilibrium. The calibration tests showed small

differences between the temperature of the heating fluid and the sample that ranged from 0.3°C

at an imposed temperature of 30°C to 1.0°C at 90°C. Furthermore, the calibration tests also

showed the time for equilibration between the heating water and sample to be 60 minutes for

temperature steps of 10°C. After 60 minutes, figure 2-4 shows a constant temperature with

relatively small fluctuations (Cekerevac and Laloui, 2005).
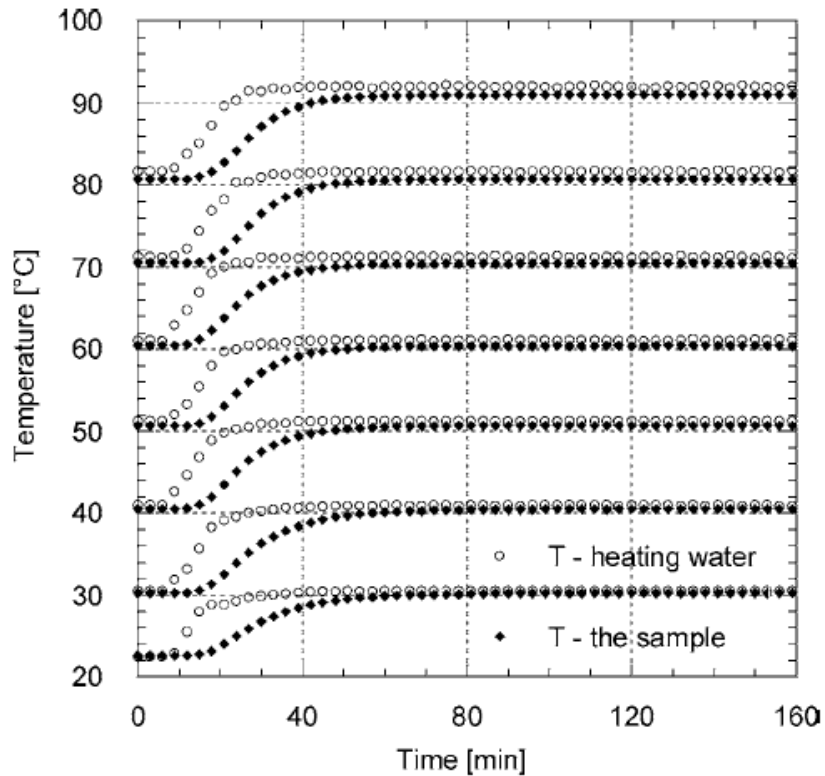
Figure 2-4: Temperature changes of heating water and the sample during the heating from 20-90°C; confining pressure 600kPa. (Cekerevac and Laloui, 2005)

Temperature increases in the heating water can have unforeseen consequences. High

temperature causes water to expand, which can manifest in a dilation of the drainage system or

contraction of the sample. High temperatures can also compromise the integrity of the latex

membrane surrounding the sample, allowing a significant inflow of water into the sample.

Cekerevac and Laloui found that the volume change associated with both of these issues was

significant and needed to be accounted for to ensure accurate experimental results (Cekerevac and Laloui, 2005).

Initial testing on normally and overconsolidated clay samples showed that isotropic drained heating produces volume changes that can be expansive or contractive depending on the overconsolidation ratio of the soil. Samples tested at higher temperatures demonstrated a more brittle behavior than samples tested at room temperature, however, the increase in deviator stress was much higher for normally consolidated samples than samples with high overconsolidation ratios. Densification was observed for heating of normally consolidated samples and dilation was observed for heating of overconsolidated samples. Despite the effects observed during heating, the critical state line was shown to be independent of temperature for ranges of 20 to 90°C (Cekerevac and Laloui, 2005).

In a subsequent paper, Cekerevac and Laloui more thoroughly investigated the thermal effects on the mechanical behavior of clay, expanding on the preliminary results presented in their triaxial cell calibration paper to include: triaxial shear tests, consolidation tests, and further volumetric tests. The tests in this study were performed on a low plasticity clay with a liquid limit of 45 and plasticity index of 21 (Cekerevac and Laloui, 2003).

Similar to the preliminary test results obtained during calibration, more thorough volumetric tests reproduced the initial findings of overconsolidation ratio on volumetric strain. Heating of normally consolidated samples produced thermal contraction. Heating of slightly overconsolidated samples produced less contraction when compared to normally consolidated samples, however, heating of highly overconsolidated samples produced thermal expansion. Thermal induced volumetric strain is shown visually in figure 2-5. The overconsolidation ratio which causes a transition between contraction and dilation behavior depends highly on the soil type (Cekerevac and Laloui, 2003).

14
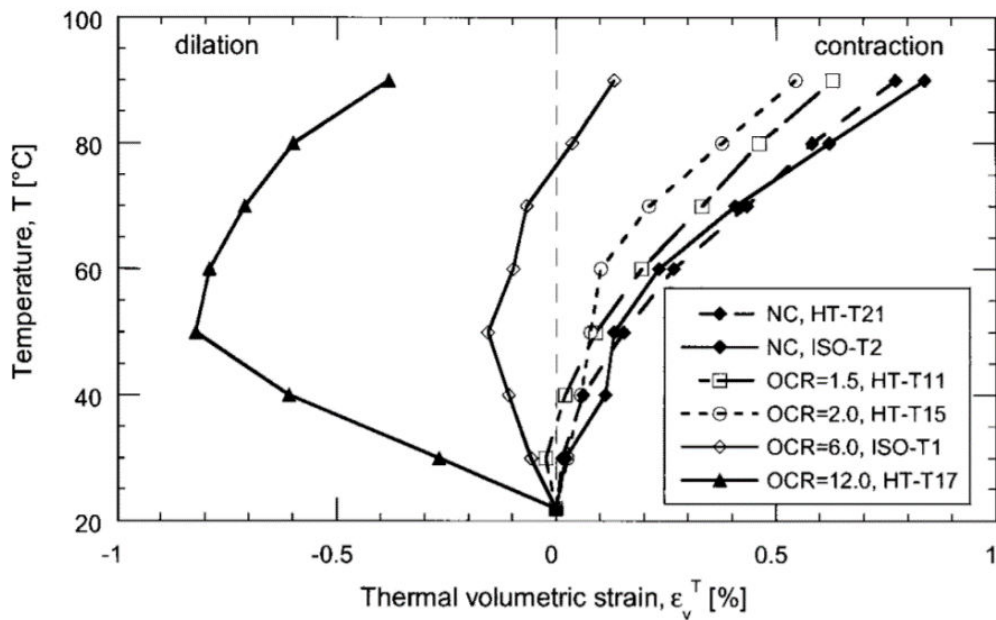
Figure 2-5: Volumetric strain of Kaolin during heating from 22 to 90°C.
(Cekerevac and Laloui, 2005)

Thermal effects on preconsolidation pressure were also investigated. Preconsolidation pressure refers to the maximum effective vertical overburden stress that a particular soil sample has sustained in its history. It is evaluated as the value at the intersection of the two linear parts of the compression curve. To analyze thermal effects on preconsolidation pressure four consolidation tests were performed at temperatures of 22, 60, and 90°C. The steps followed during testing are depicted visually in figure 2-6 (Cekerevac and Laloui, 2003).
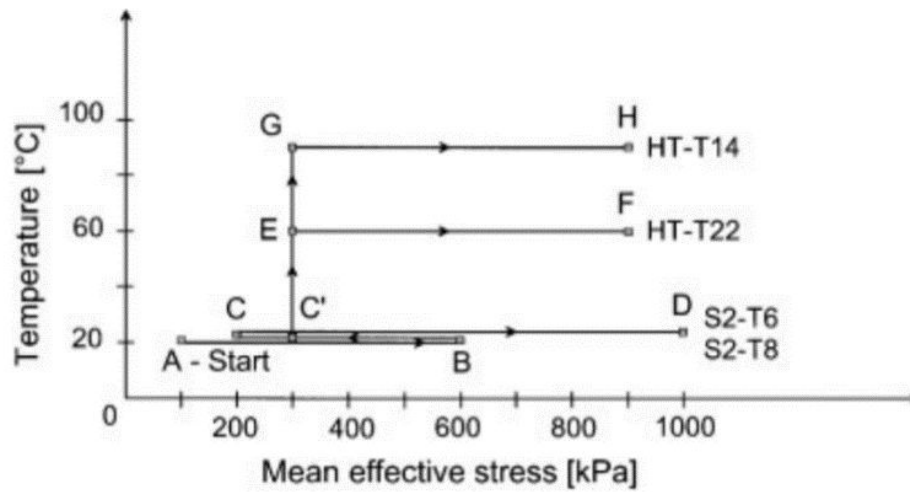
Figure 2-6: Isotropic thermo-mechanical paths. (Cekerevac and Laloui, 2003)

As shown in figure 2-6, all samples were subjected to mechanical isotropic consolidation to 600 kPa then unloaded to 300 kPa for high temperature tests HT-T22 and HT-T14 or 200 kPa for room temperature control tests S2-T6 and S2-T8. Samples S2-T6/T8 were subsequently re-consolidated to 1000 kPa while high temperature samples HT-T22/T14 were first heated and then re-consolidated to 900 kPa. The results shown in figure 2-7 clearly show an inverse relationship between temperature and preconsolidation pressure. As temperature increases, preconsolidation pressure decreases (Cekerevac and Laloui, 2003).

16
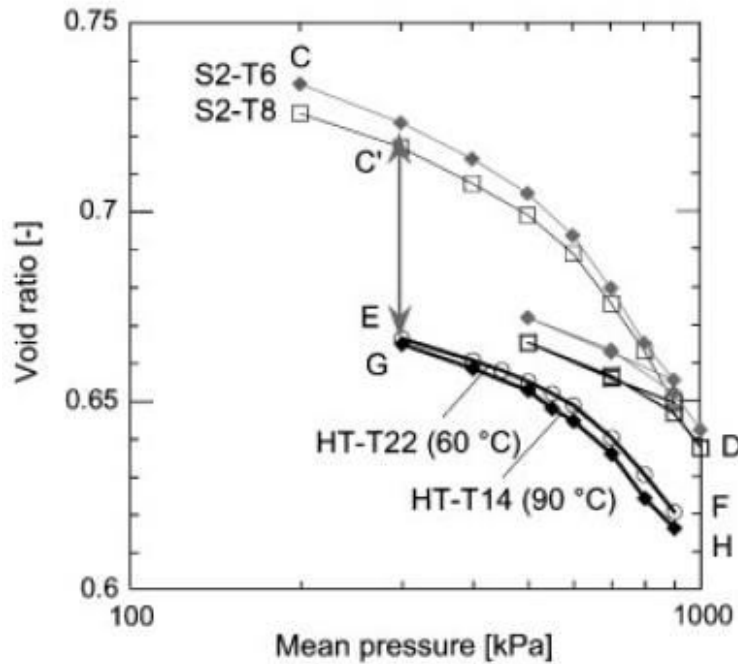
Figure 2-7: Influence of temperature on preconsolidation pressure of Kaolin clay.
(Cekerevac and Laloui, 2003)

Through extensive experimental testing, Cekerevac and Laloui proposed and validated the following expression to represent the thermal influence on preconsolidation pressure:

$$\sigma'_c(T) = \sigma'_c(T_0)\{1 - \gamma \log[T/T_0]\}$$

where preconsolidation pressure at a given temperature, T is a function of the preconsolidation pressure at reference temperature, T_0 and material parameter γ (Cekerevac and Laloui, 2003).

Thermal effects on shear strength were also investigated. Drained triaxial compression tests were conducted on samples at 22 and 90°C for varying overconsolidation ratio values. The results shown in figure 2-8 indicate a clear increase in shear strength for the samples tested at higher temperatures, however, this increase is less pronounced for samples with higher overconsolidation ratios. Elastic modulus, E also increases with an increase in temperature for both normally consolidated and overconsolidated samples (Cekerevac and Laloui, 2003).
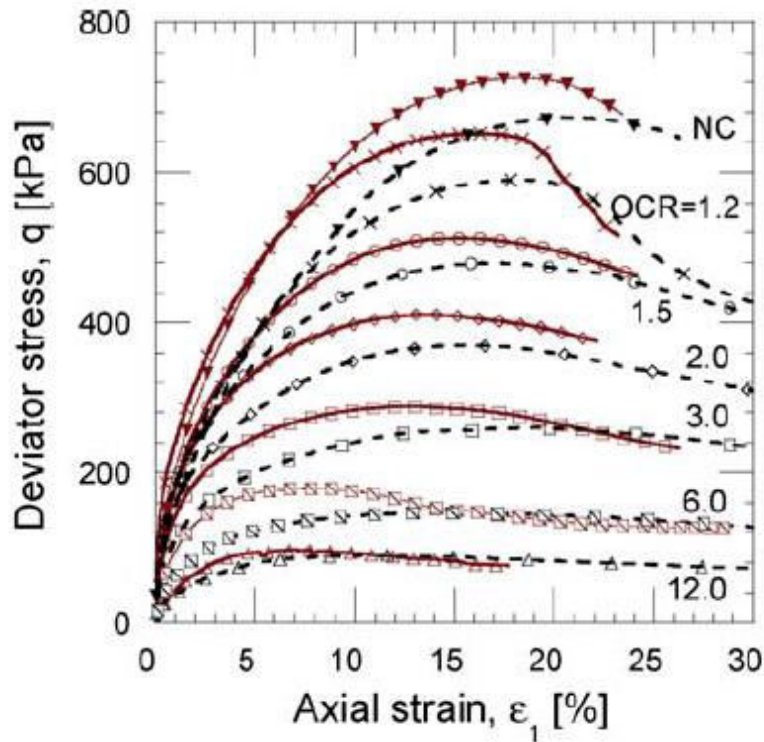
Figure 2-8: Drained triaxial tests at ambient (22°C) and high (90°C) temperatures; Consolidation pressure 600 kPa, 22°C – dashed lines, 90°C – solid lines; Deviator stress vs axial strain. (Cekerevac and Laloui, 2003)

Temperature did not seem to influence the slope of the normal consolidation line or the critical state line. The compression index or slope of the normal consolidation line for both 22 and 90°C is shown in figure 2-9. The lines are virtually parallel, with thermal compaction causing the lower values at 90°C. The slope of the critical state line was also constant for temperatures of 22 and 90°C, shown in figure 2-10. Comparing figures 2-9 and 2-10 the slopes are slightly different with compression index values of 0.24 and 0.18 despite the usual observed trend of the NCL and CSL being parallel with each other (Cekerevac and Laloui, 2003).
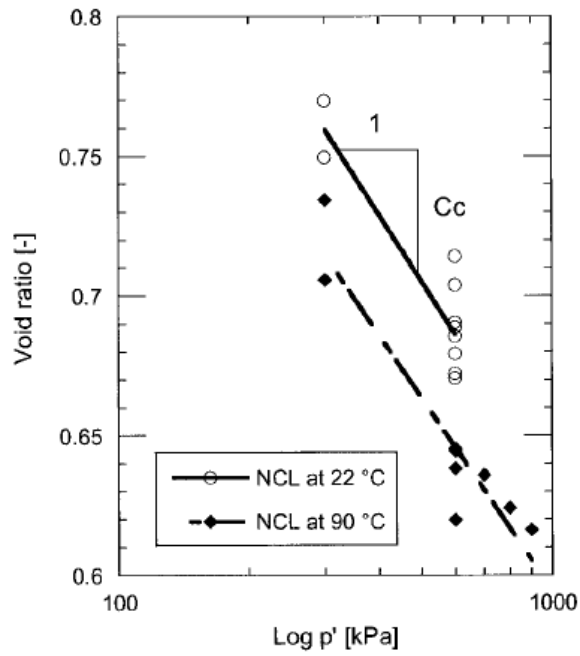
Figure 2-9: Normal consolidation lines (NCL) for samples consolidated at 22 and 90°C.
(Cekerevac and Laloui, 2003)
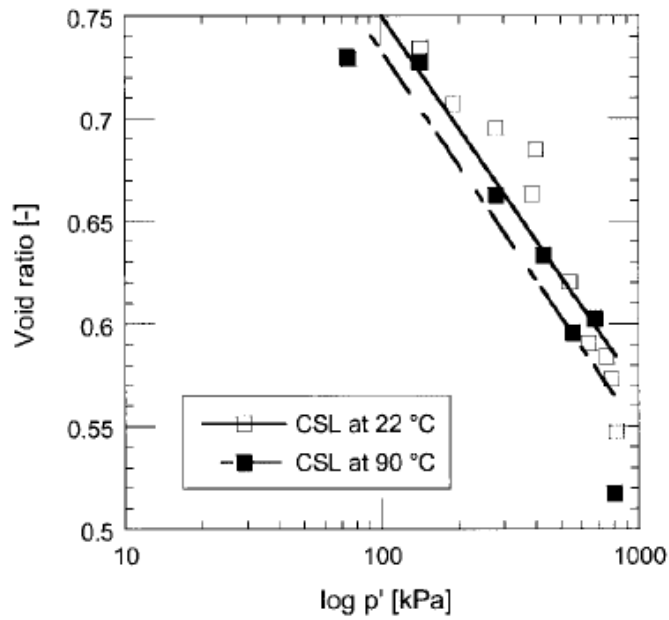
Figure 2-10: Influence of temperature on critical state line (CSL) in the volumetric plane.
(Cekeravac and Laloui, 2003)

Tang et al. describe similar findings in their paper detailing the development of an isotropic cell capable of high suction (500 MPa), high temperature (20 – 80°C), and high pressure (64 MPa). The suction is applied via the vapor equilibrium technique, which uses a salt solution placed inside the chamber to draw water from the sample and induce suction. Heating is achieved by placing the entire isotropic cell into a temperature controlled bath with thermocouples monitoring the water temperature inside and outside the chamber. Confining pressure is applied by a pressure controller using the water inside of the cell. A schematic of the isotropic cell is shown in figure 2-11 (Tang et al., 2007).
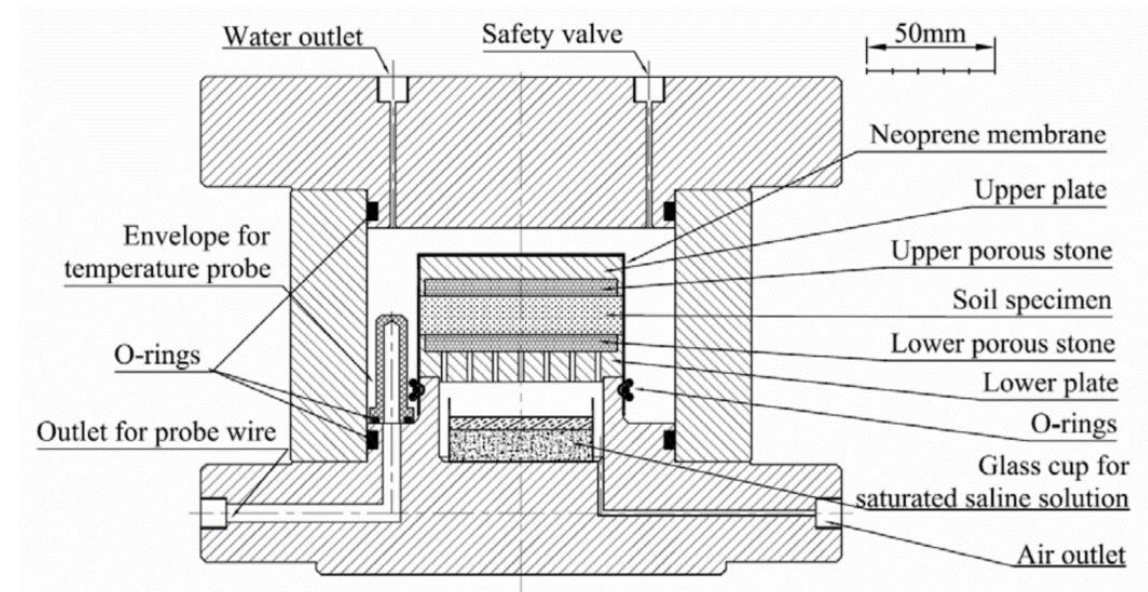
Figure 2-11: Basic scheme of the suction-temperature controlled isotropic cell. (Tang et al., 2007)

The results echoed those of Cekerevac and Laloui, even under 39 MPa suction. A thermal dilation effect was observed during heating, however, the overconsolidation ratio was not mentioned. Neither the compression index nor the swelling index showed significant change during heat application, further reaffirming prior data suggesting the CSL and NCL are independent from temperature. Preconsolidation pressure showed a significant dependence on

temperature, decreasing from 1.9 MPa to 0.8 MPa under thermal loading when temperature was increased from 20 to 60°C (Tang et al., 2007).

Uchaipichat and Khalili investigated the thermo mechanical behavior of an unsaturated silt. For their experiments, a standard suction controlled triaxial device was modified to allow temperature control by means of a heating element and motorized agitator. The motorized agitator acts like a propeller and circulates the confining water to achieve a uniform heat distribution. Suction was controlled using the axis translation technique. A schematic of the modified triaxial cell is shown in figure 2-12 (Uchaipichat and Khalili, 2009).
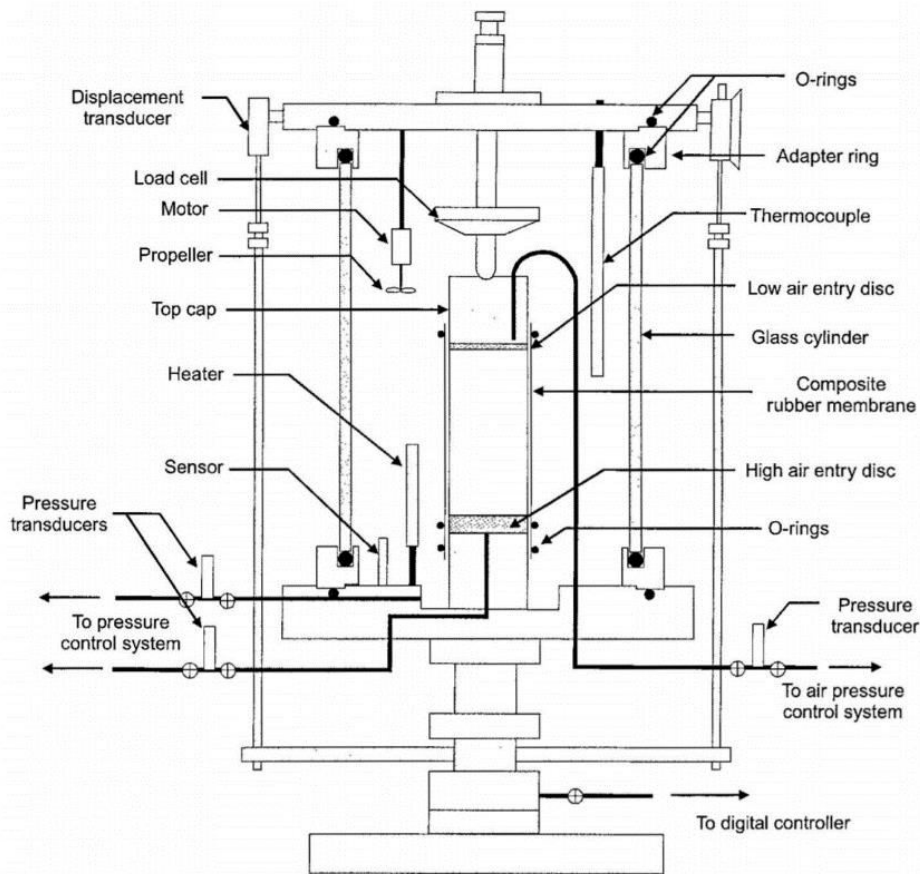
Figure 2-12: Modified Bishop-Wesley cell (Uchaipichat and Khalili, 2009)

Uchaipichat and Khalili report similar findings to both Tang and Cekerevac. Increasing matric suction beyond the air entry value results in a hardening effect of the soil, with preconsolidation values increasing significantly. However, increasing temperature results in the same thermal softening effect, with preconsolidation pressure decreasing (Uchaipichat and Khalili, 2009).

They also observed the same dilation and contraction effects during heating as Cekerevac and Laloui. For high overconsolidation ratios dilation occurred, and for normally consolidated and low overconsolidation ratios contraction occurred. Their results also showed contraction during heating becomes more pronounced with increasing matric suction. This is due to matric suction causing an increase in effective stress, which lowers the overconsolidation ratio and thus making the sample more susceptible to thermal contraction (Uchaipichat and Khalili, 2009).

The findings of Uchaipichat and Khalili pertaining to shear strength disagree with those of Cekerevac and Laloui. For various confinement pressures and matric suction values, Uchaipichat and Khalili report thermal softening trends, which can be seen in figure 2-12. As compared with figure 2-8, which shows a clear increase in shear strength for samples tested at higher temperatures. It is important to note that Cekerevac and Laloui tested a low plasticity clay and Uchaipichat and Khalili tested a silt (Uchaipichat and Khalili, 2009).
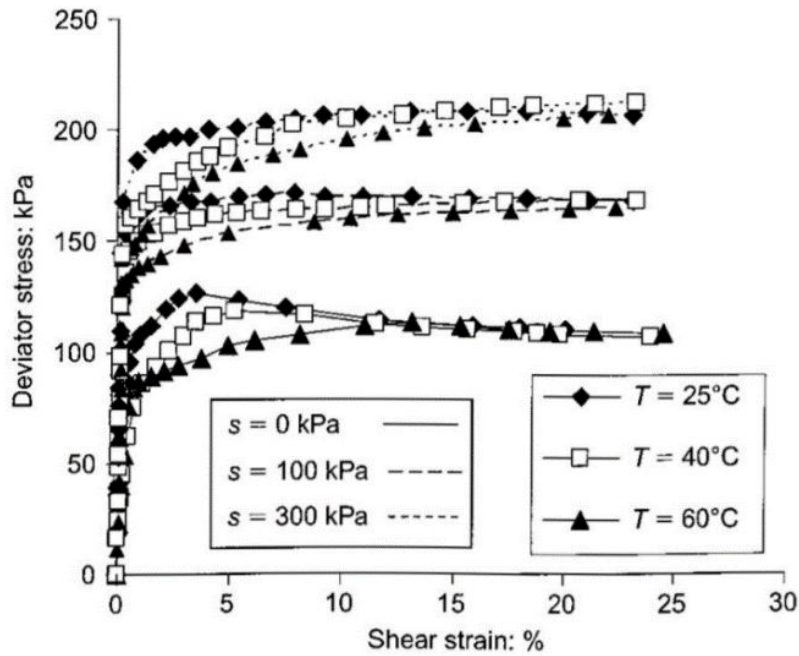
Figure 2-13: Suction and temperature controlled conventional compression shear tests at initial mean effective stress of 50 kPa (Uchaipichat and Khalili, 2009)

Uchaipichat and Khalili also found that the critical state line appeared to be independent of temperature. This finding is in accordance with the findings of both Tang et al. and Cekerevac and Laloui (Uchaipichat and Khalili, 2009).

Alsherif and McCartney further investigated the effects of high temperatures and high suction on soil. They proposed that the order of application of heat and suction may play a crucial role in hardening or softening trends of the soil. They used a thermo-hydro-mechanical triaxial cell to conduct their experiments. The vapor equilibrium technique was used to apply high values of suction, and the samples were heated using heating elements submerged in the confining fluid with a pump to circulate the water to achieve uniform heat distribution (Alsherif and McCartney, 2015).

To evaluate their assumptions, they used three testing paths. The first set of tests followed the application of a high suction magnitude to soil specimens at 23°C (room temperature). The second set, called the temperature-suction path, was performed by first

23

heating the samples to 65°C and then applying a high suction value to the soil. The third set, called the suction-temperature path, was performed by first applying a high suction value to the soil and then heating the soil specimens to 65°C (Alsherif and McCartney, 2015).

Samples evaluated under the second testing path, high temperature application followed by high suction, showed a thermal softening effect when compared to samples tested under high suction at room temperatures. However, sampled tested following the third path, high suction application followed by high temperatures, showed a hardening trend. The results from Alsherif and McCartney are depicted in figure 2-13 (Alsherif and McCartney, 2015).
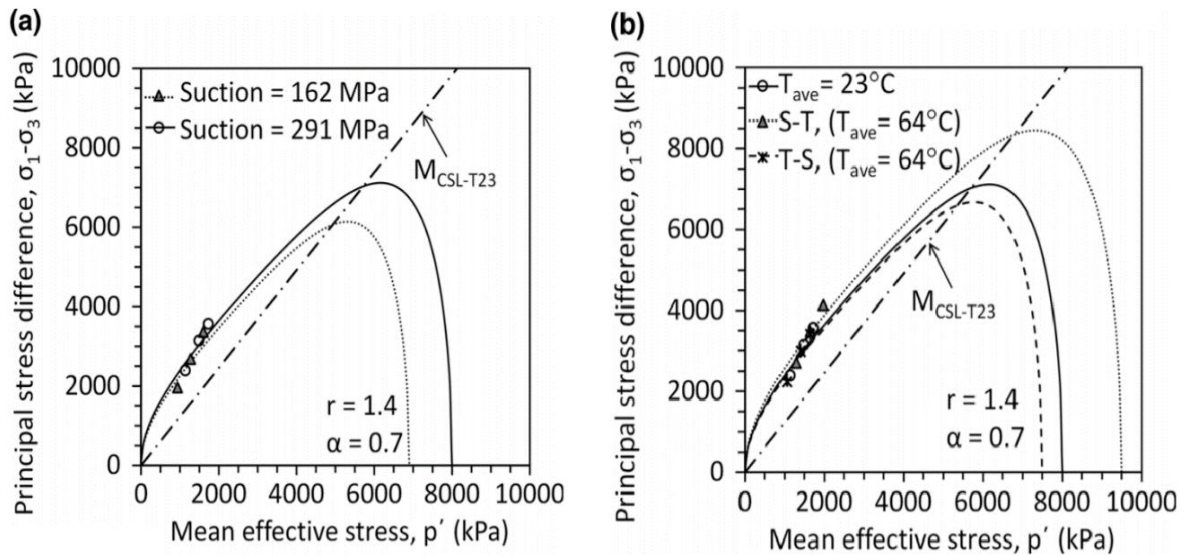
Figure 2-14: Evaluation of changes in preconsolidation stress; a) impact of suction and net confining stresses at ambient temperature; b) impact of temperature and testing path (Alsherif and McCartney, 2015)

The thermal softening trend shown in figure 2-13b agrees with the previous observations made by Tang, Uchaipichat and Khalili that elevated temperatures cause a reduction in preconsolidation pressure and shear strength. However, the hardening effect, that occurred when temperature was applied after suction, emphasizes the need to consider the observed path dependent nature on the mechanical behavior of unsaturated soil. Also shown in figure 2-13 is

the independent nature of the critical state line under varying temperature and suction values, which is in accordance with the findings previously reported by Cekerevac and Laloui, Tang, and Uchaipichat and Khalili (Alsherif and McCartney, 2015).

2.4 - Review of stiffness properties and resonant column testing

Shear modulus, G, and damping ratio, D, are two of the main properties needed to evaluate the dynamic response of soil. The determination of shear modulus can be made from experimental results similar to figure 2-14, which shows both Gmax, the maximum or small strain shear modulus, and G or Gsec the large strain or secant shear modulus.
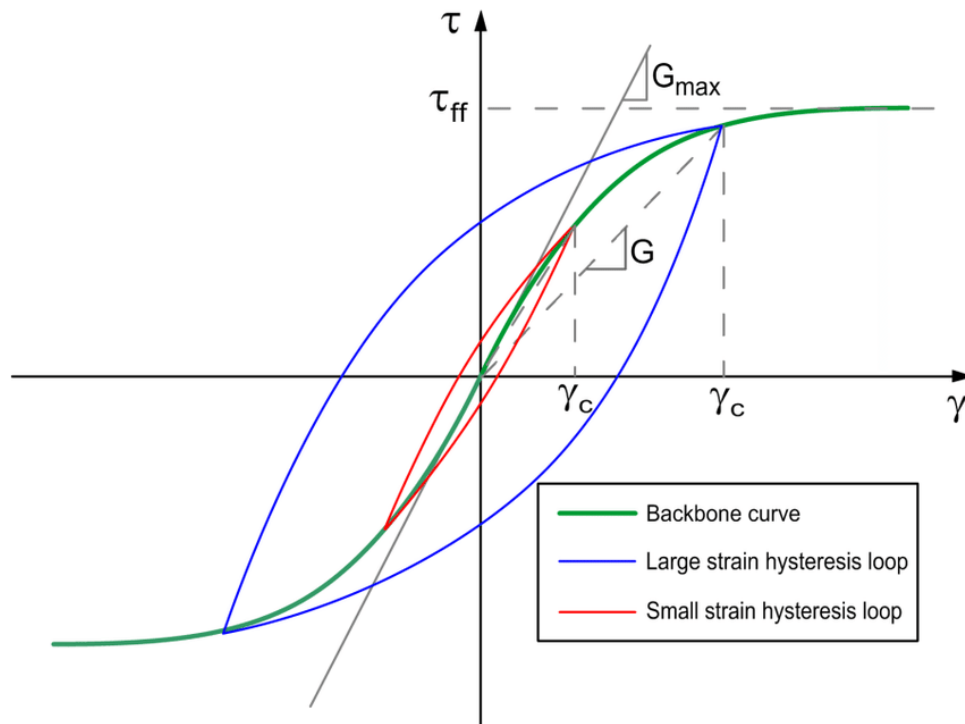
Figure 2-15: Schematic illustration of backbone curve and small strain and large strain hysteresis loops. Gmax is the maximum (small strain) shear modulus, G is the secant shear modulus for a given strain level. (Stewart et al., 2014)

Proper evaluation of shear modulus is necessary for geotechnical engineers to safely design deep foundation systems and any other structure subject to dynamic soil structure

interaction, especially when the area is prone to stability problems or is located in earthquake prone or seismically active areas where dynamic interaction is more common.

Once soil is subjected to dynamic or cyclic loading from an earthquake, damping ratio, D, is the soil property responsible for the dissipation of energy propagating through the material. Damping is defined as the loss of energy within a vibrating or cyclically loaded system, usually dissipated in the form of heat. There are two types of damping, internal and external. Internal damping refers to the energy dissipation within the material itself. For soils internal damping can be attributed to inter-particle sliding and friction, structural rearrangement, and pore fluid viscosity. Internal damping is an inherent soil material property and is usually the term being referred to by the less specific "damping ratio". External damping also called system damping is not an inherent material property and refers to a transmission of energy away from the source via radiation (Ashmawy et al., 1995).

Laboratory determination of the material damping ratio is usually done through three methods: resonant column, torsional shear, and cyclic triaxial. In the resonant column test, two methods of damping measurement are typically used: logarithmic decrement and the magnification factor. Logarithmic decrement refers to imposing an initial vibratory condition on the soil sample then allowing the sample to vibrate freely while recording the decay in peak amplitude. Magnification factor or half-power method refers to using the steady state peak amplitude at resonance to determine the damping ratio. Logarithmic decrement and magnification factor methods are depicted in figure 2-15 (Ashmawy et al., 1995).

$$\delta = \frac{1}{n} ln \left| \frac{x_1}{x_{n+1}} \right|$$

$$\text{Damping} = \zeta = \frac{\delta}{\sqrt{4\pi^2 + \delta^2}}$$

$$\text{Damping} = \zeta = \frac{\omega_2 - \omega_1}{2\omega_n}$$
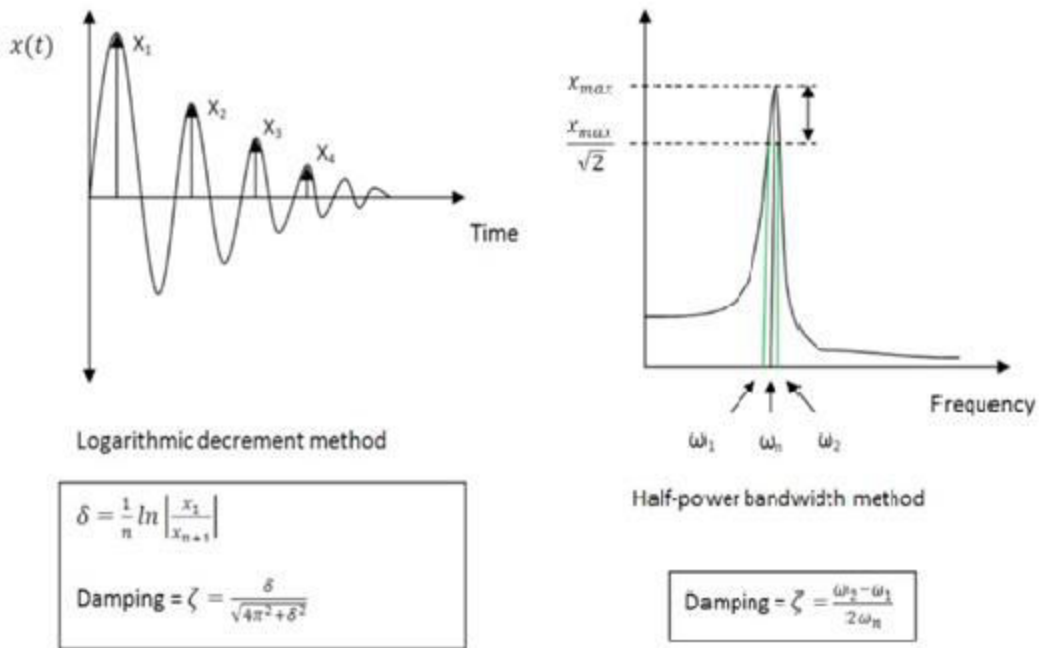
Figure 2-16: Damping determination via logarithmic and magnification factor methods
(Perpetual Industries, 2011)

Lanzo and Vucetic investigated the variation of damping ratio at small cyclic shear strain amplitudes < 0.01% and large cyclic shear strain amplitudes > 0.01% with a focus on the effect that plasticity index, PI, has on the damping ratio at small cyclic shear strains. At small cyclic shear strain amplitudes, a soil deposit could be in the range of excitation frequencies without the pronounced effect of an earthquake. The low-level frequencies generate low value cyclic strains which elicit a small damping response allowing resonance to occur and large amplifications to take place (Lanzo and Vucetic, 1999).

Their data suggests at small cyclic shear strains < 0.001% the viscous damping ratio of clays is generally larger than the damping ratio of sands. At these small values of cyclic strain, the damping ratio follows a trend of increasing as the plasticity index increases. However, as cyclic shear strains increase past 0.01% this trend reverses, showing a decrease of damping ratio with increasing plasticity index. This trend is visible in figure 2-16 (Lanzo and Vucetic, 1999).
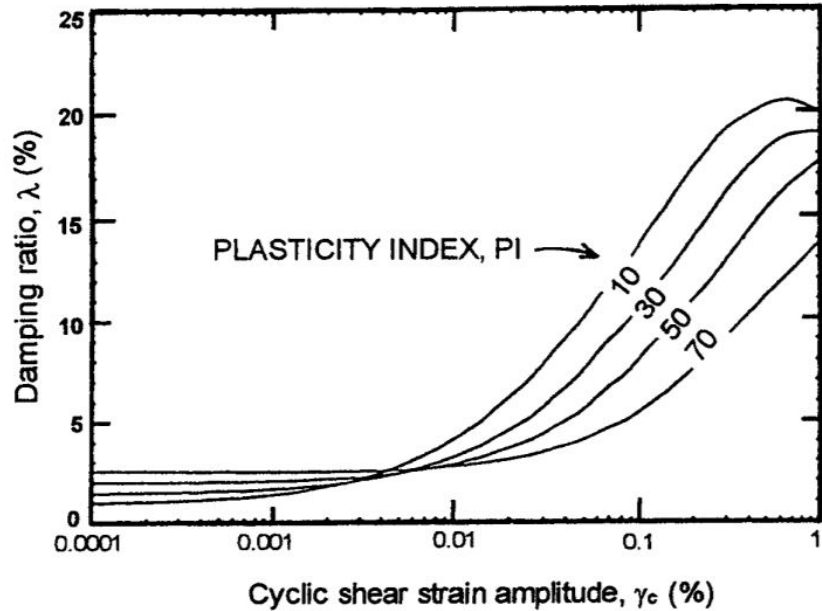
Figure 2-17: Effect of PI on damping ratio curves derived analytically for clays by
Pyke (EPRI, 1993) (Lanzo and Vucetic 1999)

Vucetic and Dobry conclude that plasticity index is one of the most significant index
properties for site-response evaluations and seismic microzonation. Not only can shear modulus
and damping be accurately predicted using plasticity index, but the determination of plasticity is a
basic, inexpensive test that is used on almost every geotechnical project. As the plasticity index
of the soil increases the level of cyclic shear strain needed to induce a significant nonlinear
stress-strain response and stiffness degradation also increases (Vucetic and Dobry, 1991).

Suction controlled resonant column tests have also been performed. Vassallo et al. used
a suction controlled triaxial cell and a resonant column torsional shear cell to investigate the
possible effects unsaturated conditions may have on shear stiffness and damping. Using the axis
translation technique, suction values of 50, 100, 200, and 400 kPa were imposed on the samples.
Vassallo's experimental results showed a significant increase in the soil stiffness with increasing
values of matric suction. He attributed the hardening phenomenon during suction to the variation
of the volumetric state of the soil sample (Vassallo et al., 2007).

Chapter 3

Calibration Chamber Design, Components, and Assembly

3.1 - Introduction

The calibration chamber was designed to be similar to the thermo-controlled resonant column chamber, but with space to allow monitoring and recording of soil temperature. The resonant column chamber was designed to hold air pressure and did not have an opening for the thermocouple probes needed to measure soil temperature. The resonant column chamber also has many internal components inside the chamber making it congested for the three thermocouple probes.

The full design consisted of the plexiglass calibration chamber, GCTS HTC-250 heat controller, and Extech SDL200 4-Channel Thermometer/Datalogger. The calibration chamber consists of a 10" diameter x 18" long x 0.5" thick plexiglass cylinder, two 12" x12" x 0.5" aluminum plates, and four 3/8" diameter threaded aluminum rods. The GCTS HTC-250 heat controller consists of an Omega CN132 Temperature controller, power cable, Omega Type E thermocouple, two 120V heating elements, and two Orion 12V DC fans. The Extech SDL200 4-Channel Thermometer/Datalogger consists of the 4-channel temperature meter, three Type K thermocouple probes, Type K thermocouple wire, and 120V AC Adapter.

This chapter shows detailed assembly of the three main components of the thermo calibration chamber, as well as the position of the probes inserted into the soil sample. The following pictures are annotated to clear identify each part previously described.

3.2 - Thermometer and sample configuration

The Extech SDL200 4-Channel Thermometer/Datalogger consists of the 4-channel digital thermometer, three Type K thermocouple probes, Type K thermocouple wire probe, two gigabyte SD card, and 120V AC adapter. The Extech thermometer automatically logs temperature data into an excel file. For temperature calibration the logging interval was set to 300 seconds. The Type K thermocouple probes are useable in the range of -40 to 200°C. The Type K thermocouple probes have an accuracy of $\pm(0.4\% + 1°C)$. The Extech digital thermometer is calibrated by FLIR Systems, Inc. Figures 3-1 through 3-5 show the components of the thermometer and positions of the probes in the soil sample.
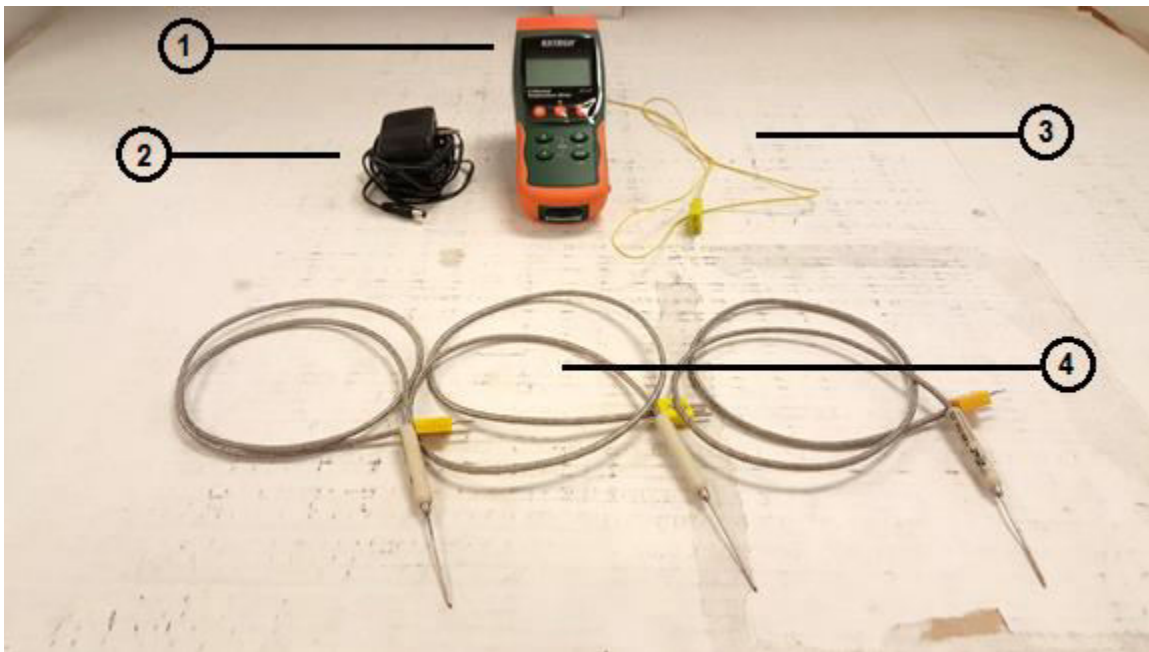
Figure 3-1: Extech SDL200 4-Channel thermometer/datalogger and components: 1) SDL200 4-Channel thermometer/datalogger, 2) 120V AC adapter, 3) Type K thermocouple wire, 4) 3 Type K thermocouple probe
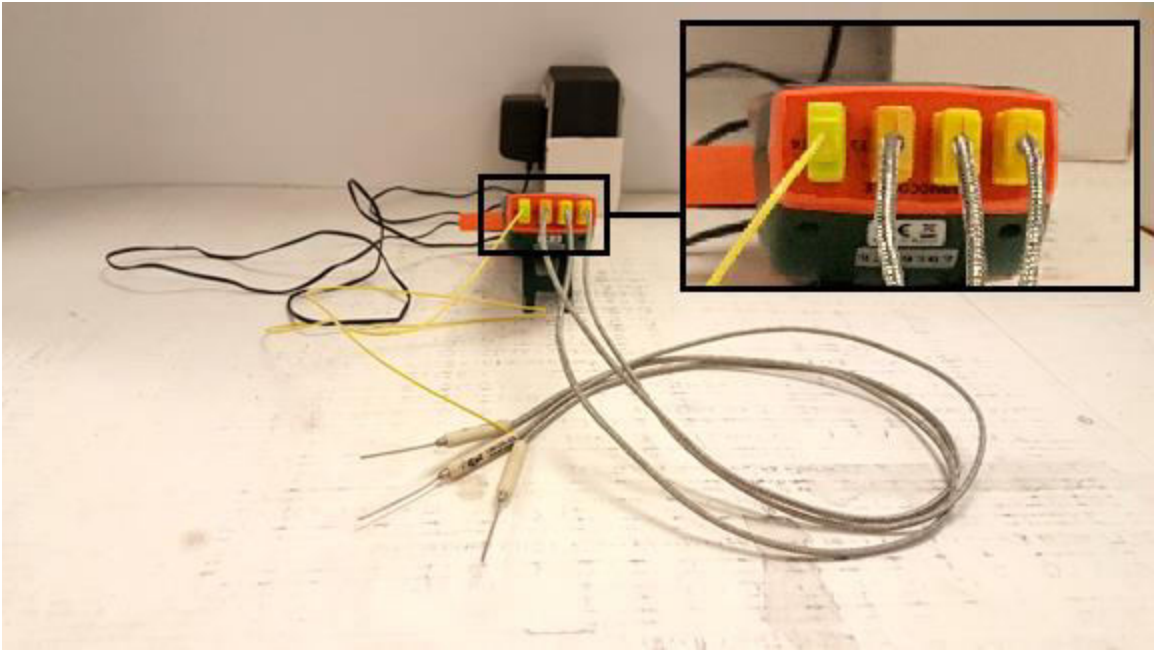
Figre 3-2: Thermocouple probe and wire plugins

Figure 3-3: SDL200 4-Channel thermometer with 1) SD card
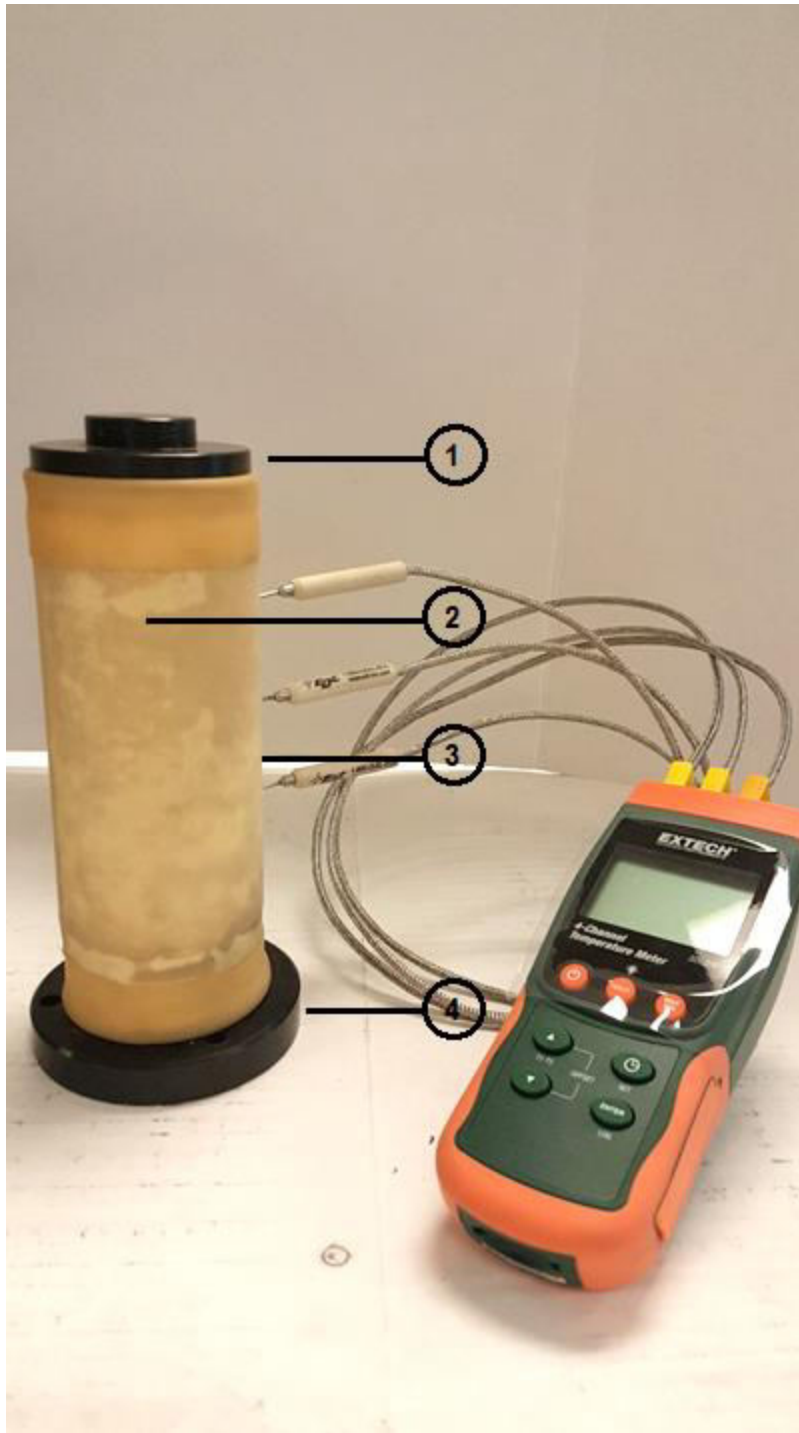
Figure 3-4: Sample enclosure with 1) top cap, 2) soil sample, 3) latex membrane, and 4) base
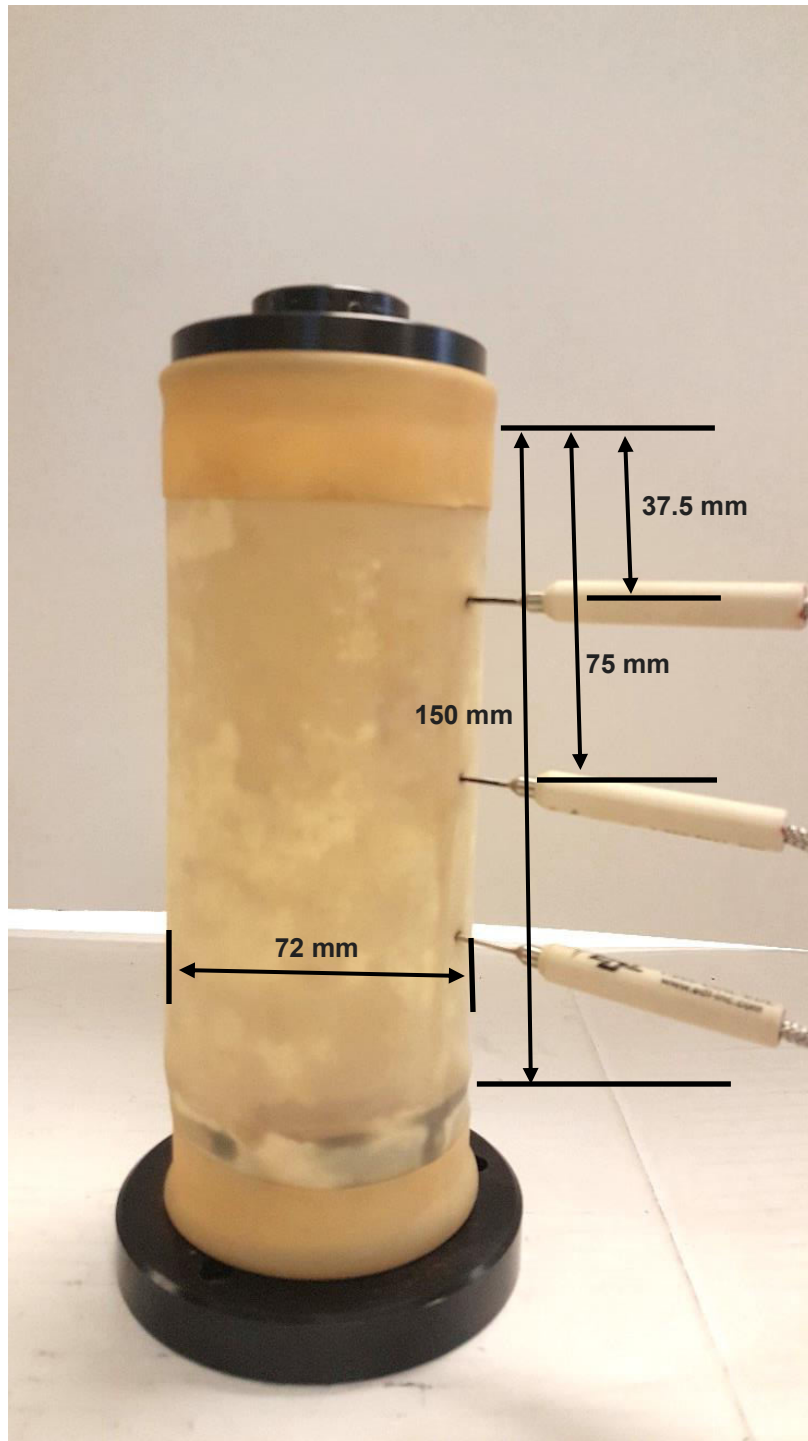
Figure 3-5: 3 Type K thermocouple probes inserted into cylindrical soil sample, 72 mm diameter x 150 mm length, probes spaced equally at 37.5 mm

3.3 - Heat controller assembly

The GCTS HTC-250 heat controller consists of an Omega CN132 Temperature controller, power cable, Omega Type E thermocouple, two 120V heating elements, and two Orion 12V DC fans. GCTS Testing Systems assembles the components into their HTC-250 heat controller. The heating elements, thermocouple, and fans are mounted to the top cap of the calibration chamber. The Omega Type E thermocouple is mounted near the heating elements and measures the air temperature at the top of the chamber. The thermocouple controls the temperature of the heating elements and regulates the temperature setting of the controller. Figures 3-6 through 3-10 show the components and assembly of the GCTS HTC-250 heat controller.

Figure 3-6: GCTS HTC 250 Heat controller and components. 1) GCTS HTC-250 heat controller, 2) Omega CN132 temperature controller, 3) power cable, 4) Omega Type E thermocouple, 5) 2 Orion 12V DC fans, and 6) 2 120V heating elements.
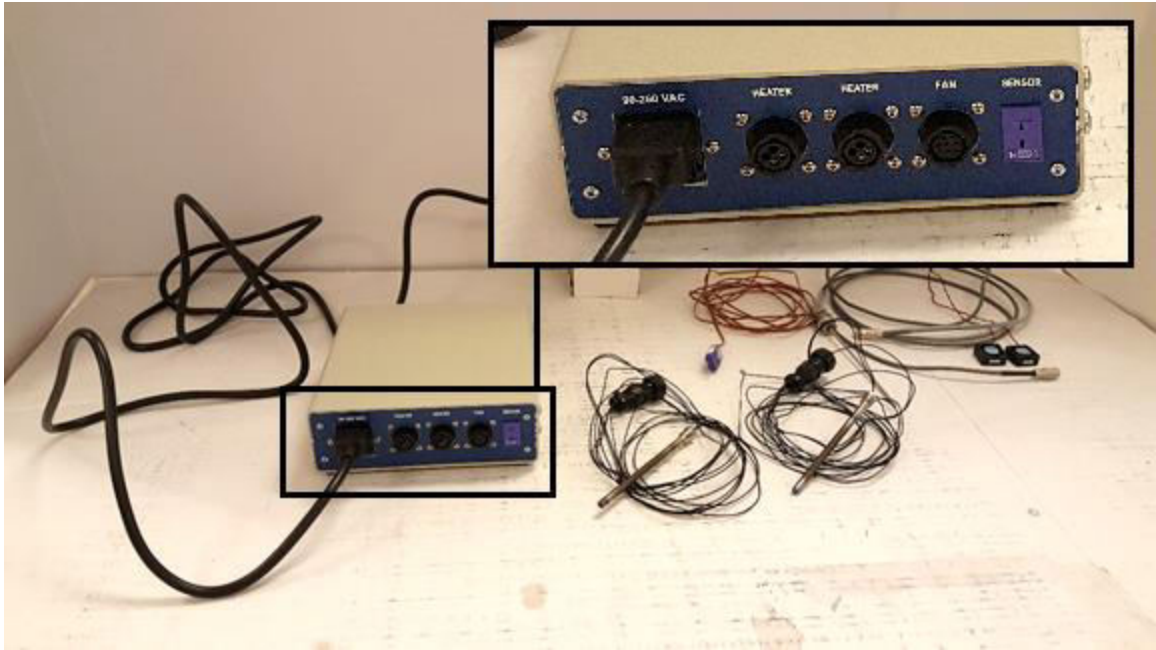
Figure 3-7: Heat controller assembly step 1: power cable
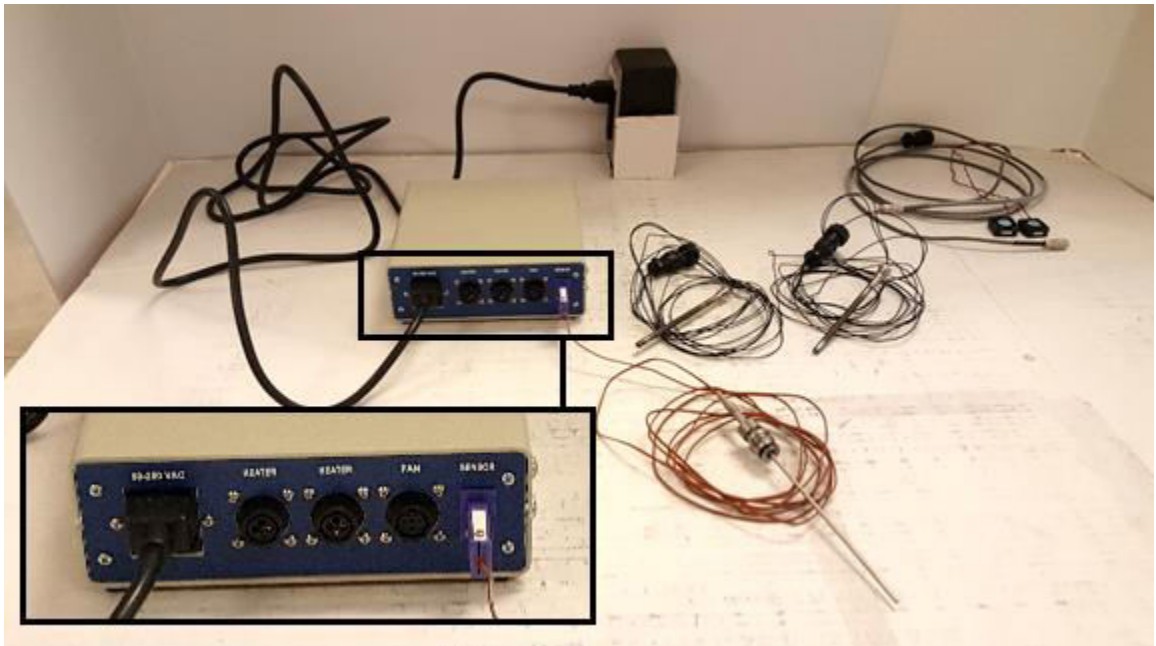
Figure 3-8: Heat controller assembly step 2: Omega Type E thermocouple sensor
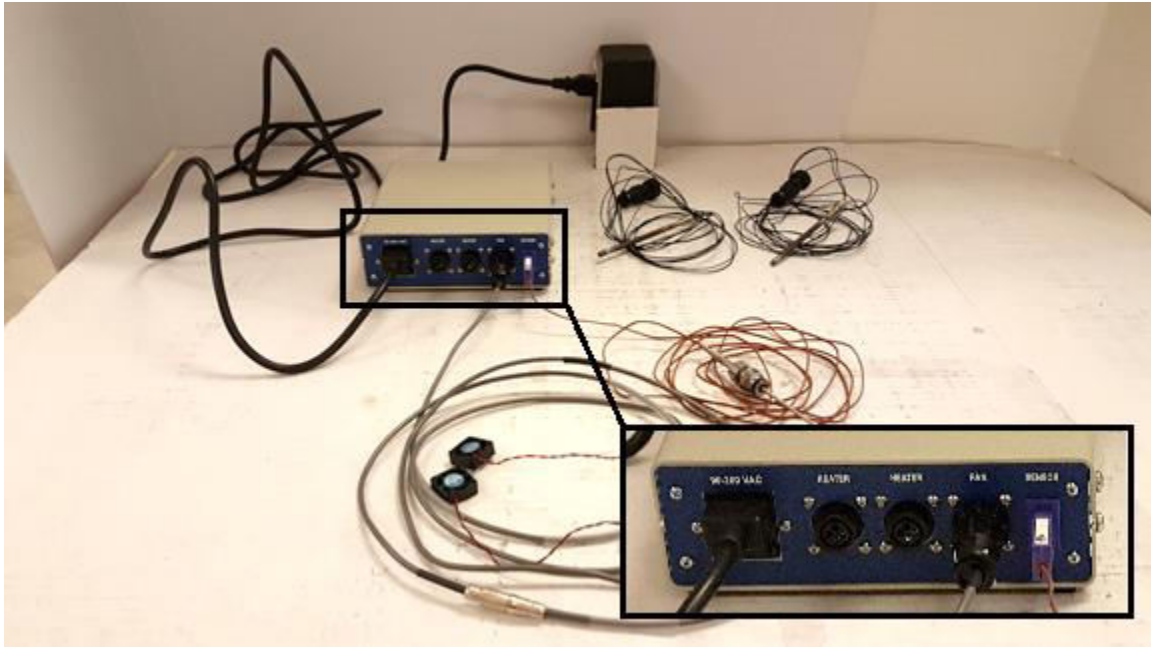
Figure 3-9: Heat controller assembly step 3: Orion 12V DC fans
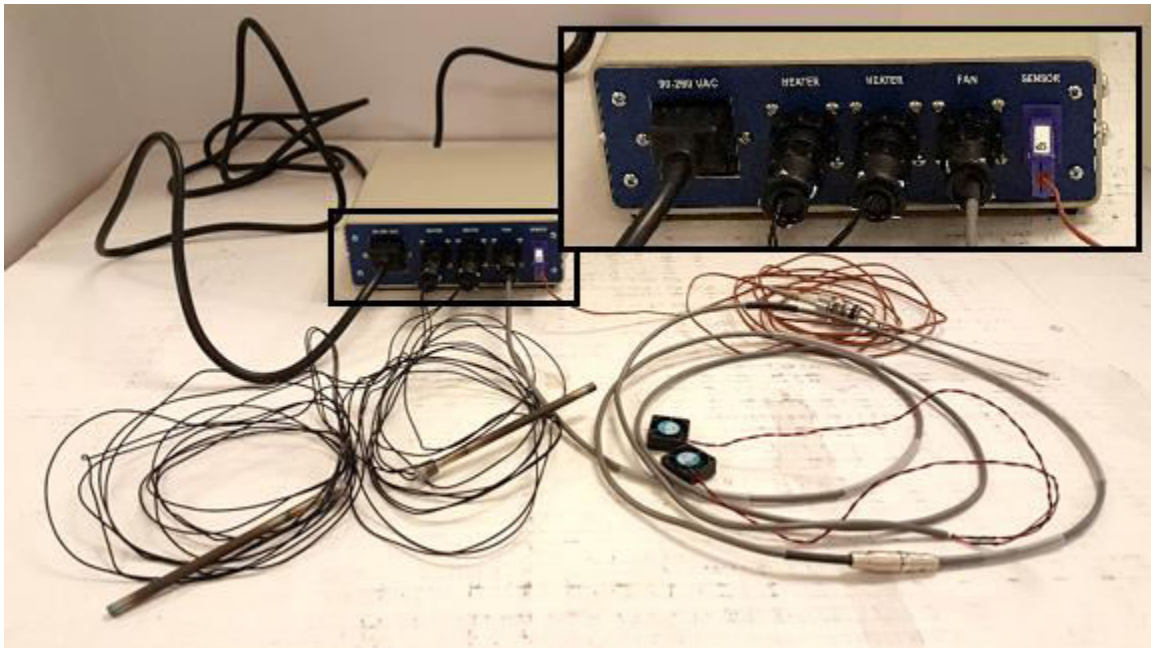
Figure 3-10: Heat controller assembly step 4: two 120V heating elements

3.4 - Calibration chamber assembly

The calibration chamber consists of a 10" diameter x 18" long x 0.5" thick plexiglass cylinder, two 12" x12" x 0.5" aluminum plates, and four 3/8" diameter threaded aluminum rods. Two rubber O-rings line the grooves cut in the aluminum top and base plates for the plexiglass cylinder. The top plate has threaded holes cut for the thermocouple sensor, heating elements, and L-bracket fan mount. It also has a square hole cut for the thermocouple probes to feed into the chamber from the digital thermometer. The black markings on the bottom plate help align the sample in the middle of the chamber. Eight washers and eight 3/8" threaded hex nuts fix the four threaded rods to the top and base plate and hold the chamber together. The fans are fixed to the L-bracket with eight small nuts, washers, and bolts. Figures 3-11 through 3-21 show the complete assembly of the calibration chamber.
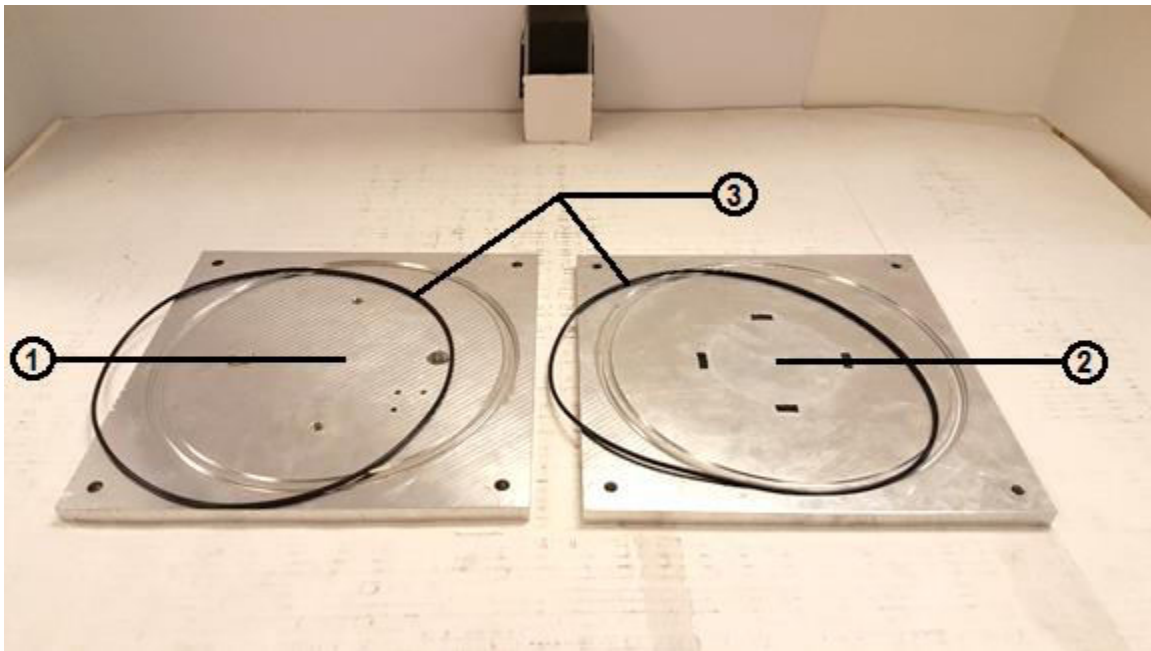
Figure 3-11: 1) Aluminum top plate, 2) aluminum base plate, 3) 2 rubber O-rings
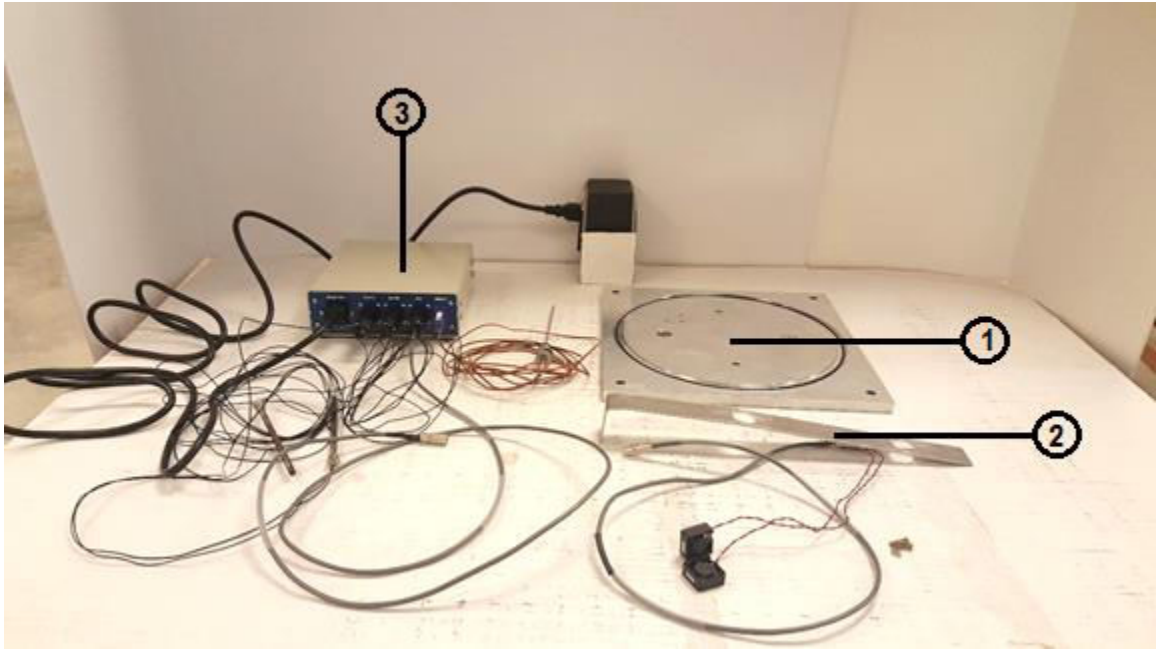
Figure 3-12: Top plate components: 1) aluminum top plate, 2) L-bracket fan mount,
3) assembled HTC-250 heat controller
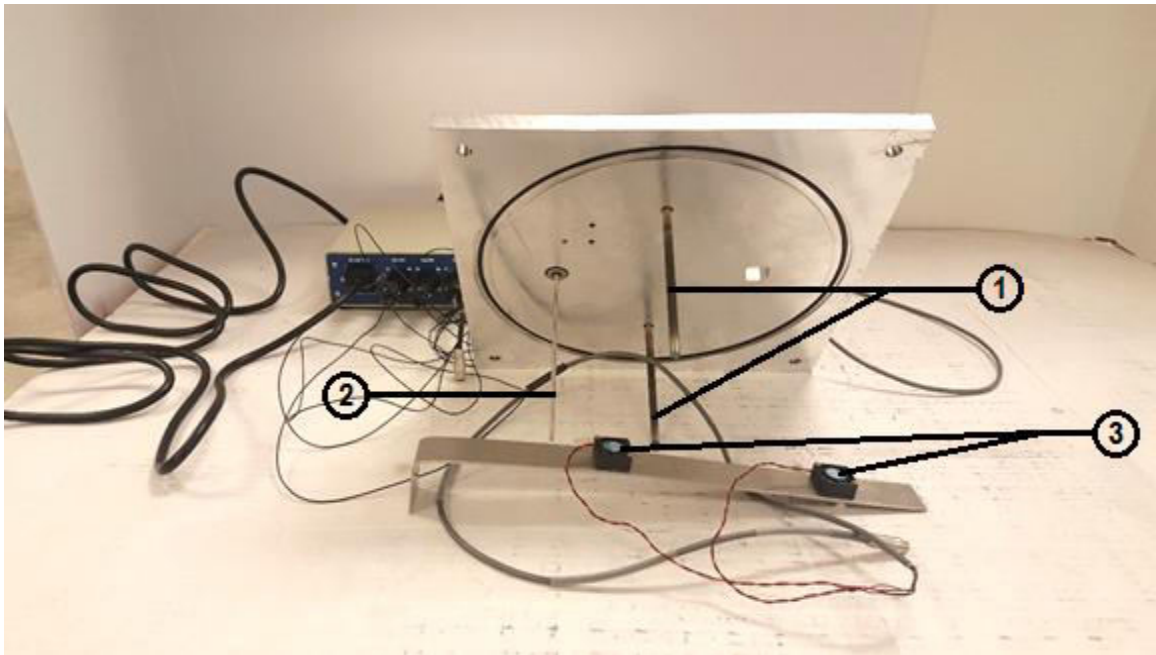
Figure 3-13: Top plate assembly step 1: attach 1) heating elements and 2) thermocouple sensor
to top plate, and 3) mount fans to L-bracket
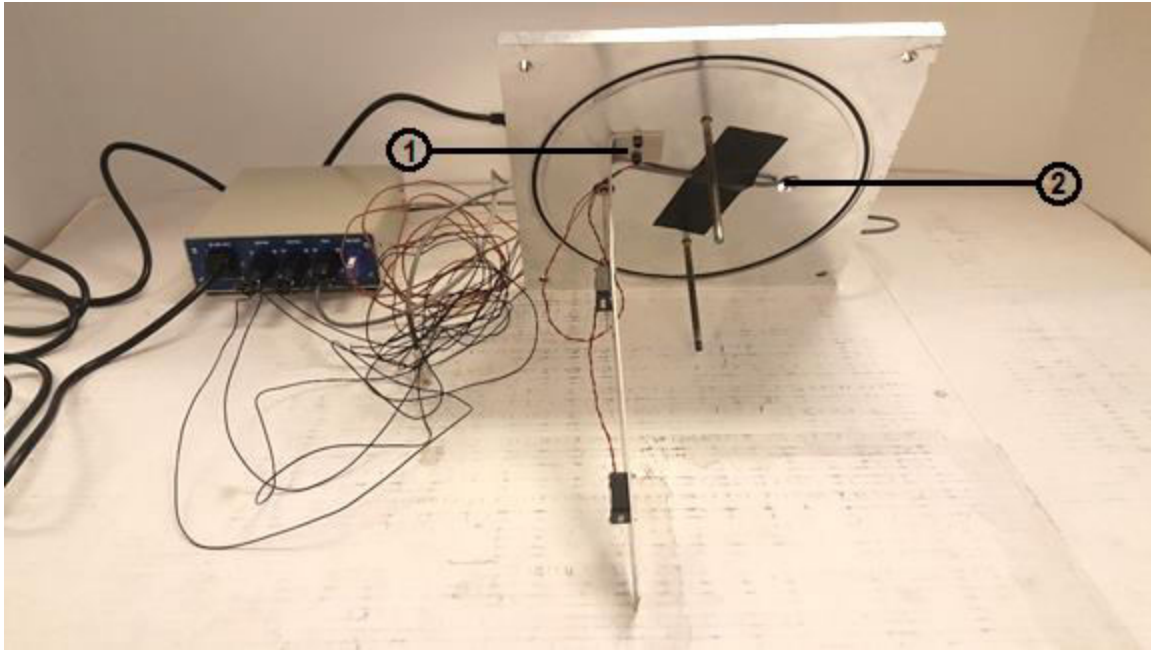
Figure 3-14: Top plate assembly step 2: 1) mount L-bracket to top plate and 2) pull fan cable through square opening
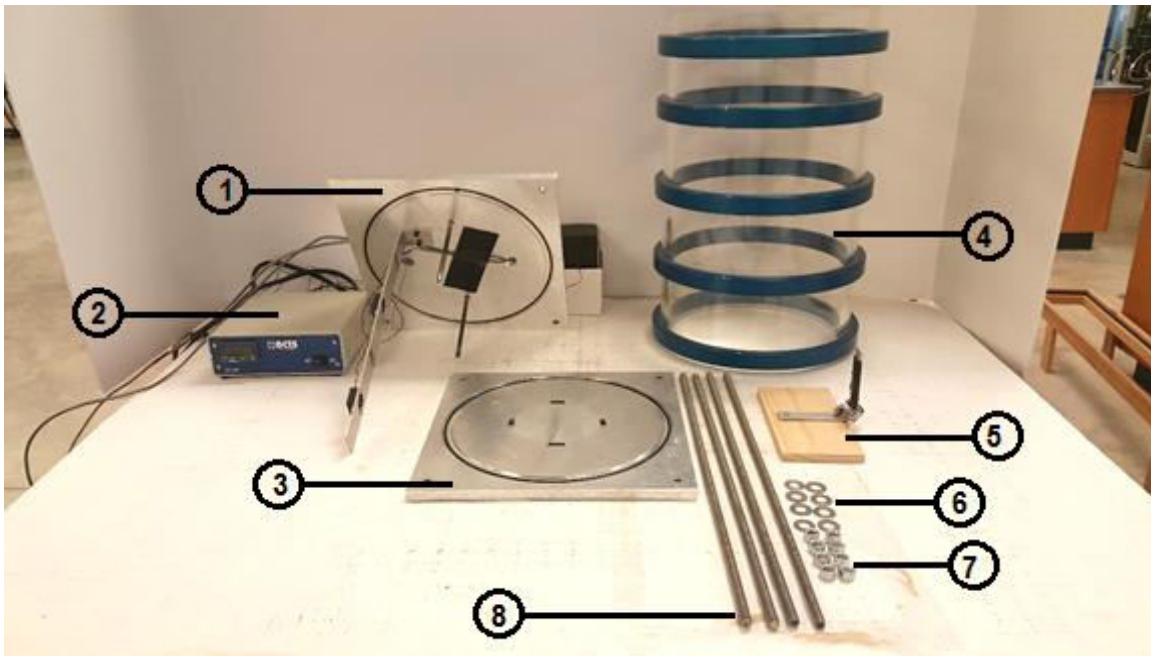
Figure 3-15: Calibration chamber components: 1) assembled top plate, 2) HTC-250 heat controller, 3) base plate, 4) plexiglass cylinder, 5) thermometer stand, 6) 8 washers, 7) 8 3/8" hex nuts, 8) 4 3/8" rods
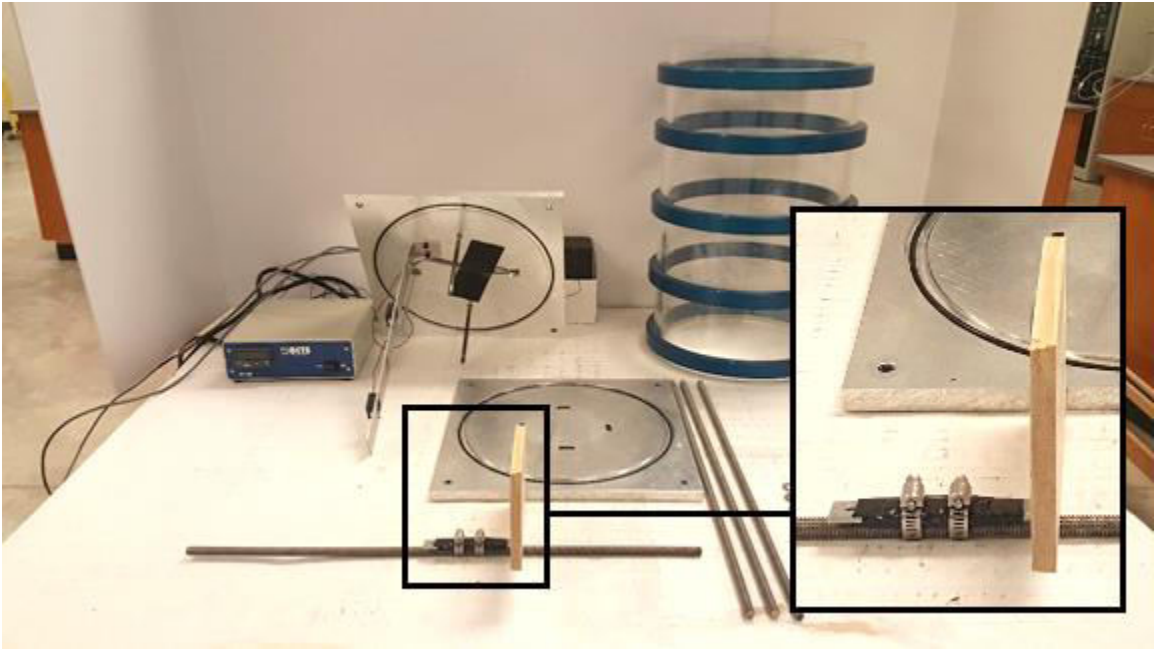
Figure 3-16: Chamber assembly step 1: attach thermometer stand to 3/8" rod
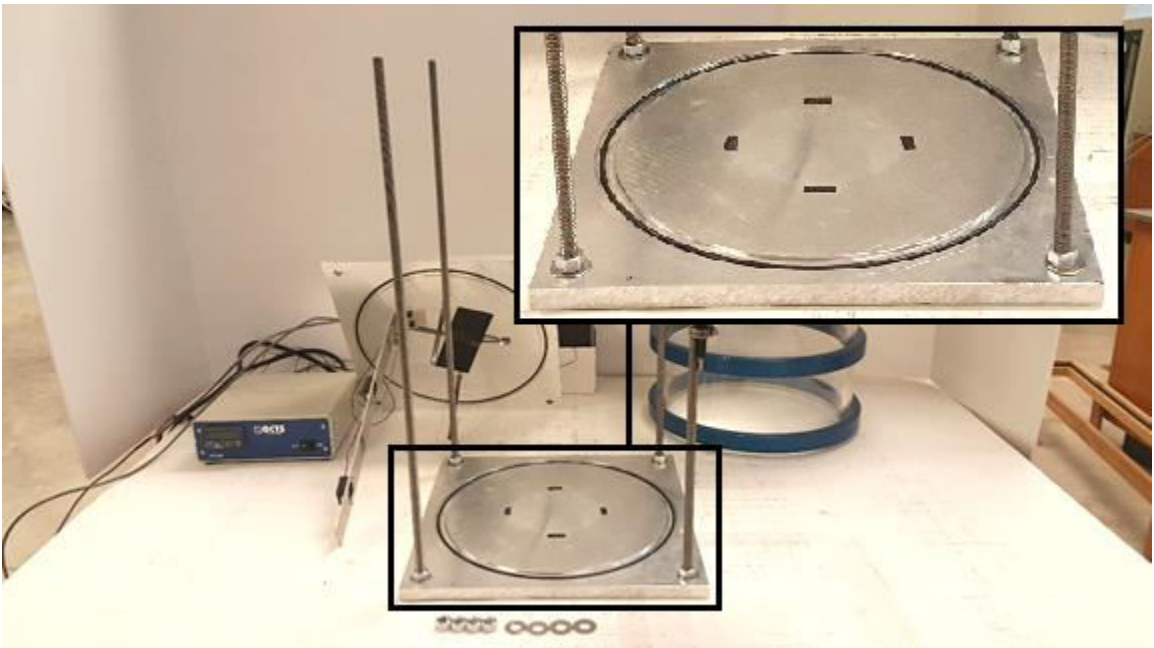
Figure 3-17: Chamber assembly step 2: attach 4 3/8" rods to base plate using
4 washers and 4 hex nuts
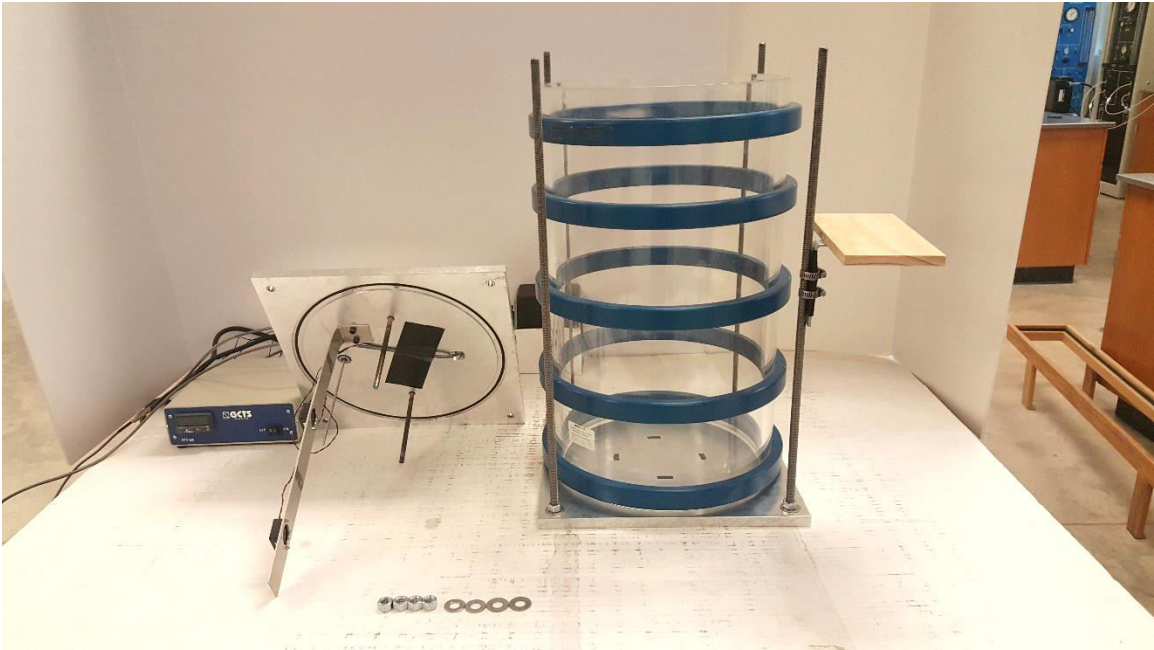
Figure 3-18: Chamber assembly step 3: fit plexiglass cylinder into groove in base plate
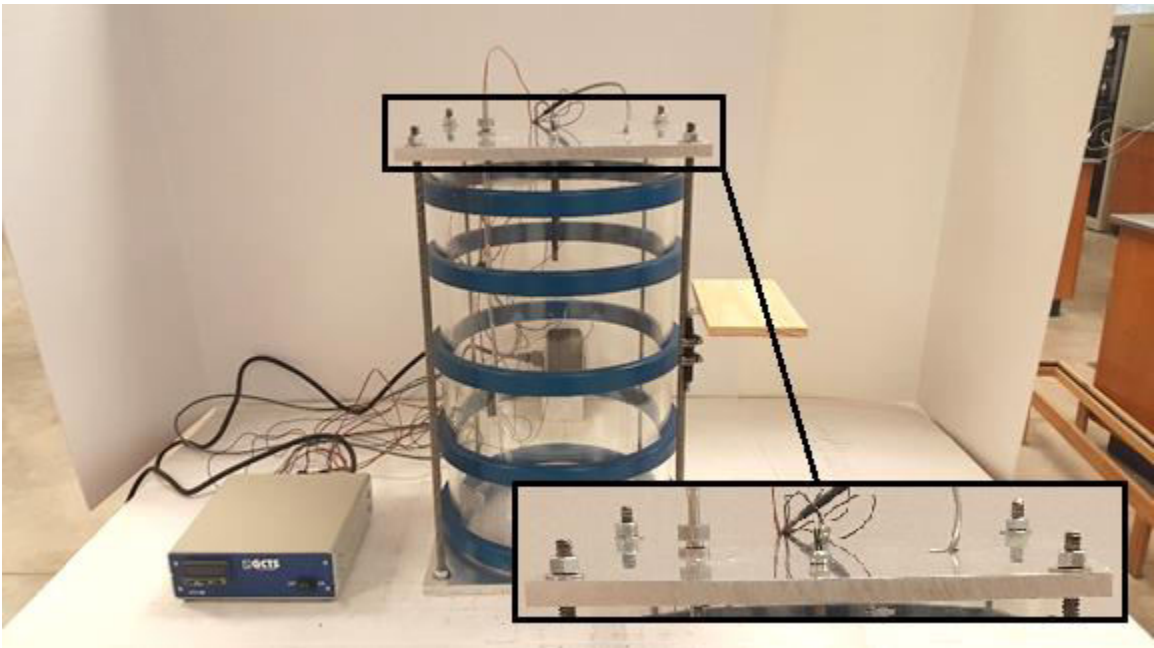
Figure 3-19: Chamber assembly step 4: secure top plate to plexiglass cylinder using the remaining 4 washers and 4 hex nuts
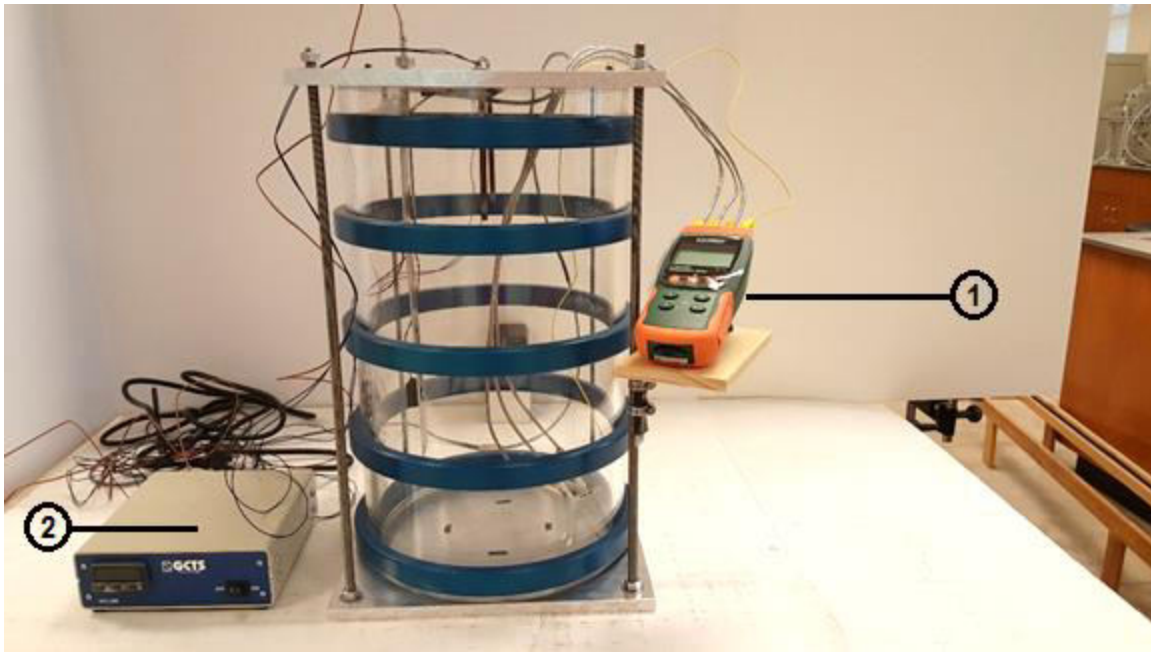
Figure 3-20: Calibration chamber with 1) digital thermometer and 2) HTC-250 heat controller
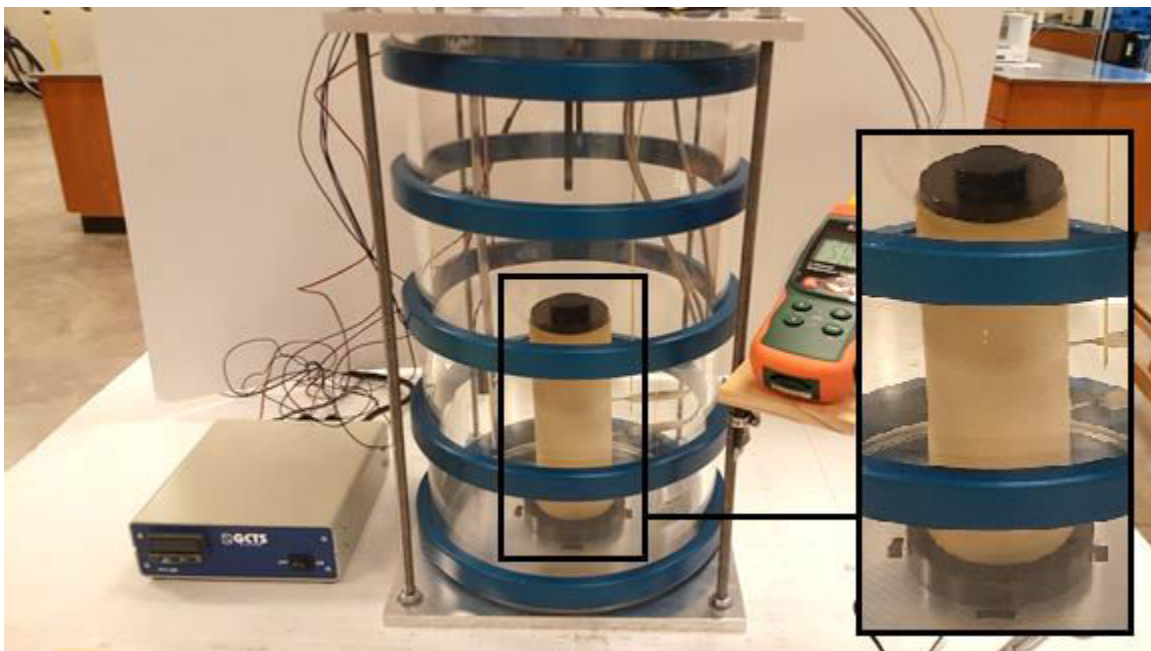
Figure 3-21: Calibration chamber with soil sample

Chapter 4

Calibration Testing and Variables

4.1 - Introduction

Soil classification tests were performed prior to testing. Visual inspection of the soil indicates a primarily silty soil with moderately sized chunks of clay. Prior to classification testing the soil sample was dried in an oven, crushed, and pulverized. Tests used during soil classification were specific gravity, sieve analysis, hydrometer analysis, and the Atterberg limits. ASTM test methods followed for soil classification were: ASTM D854 Specific gravity of soil solids by water pycnometer, ASTM C136 Sieve analysis of fine and coarse aggregates, ASTM D7928 Particle-size distribution of fine-grained soils using the sedimentation analysis, and ASTM D4318 Liquid limit, plastic limit, and plasticity index of soils.

After soil classification, a standard proctor was performed to determine maximum dry density and optimum moisture content. ASTM D698 Method A was followed. The compaction curve was used to determine dry density and moisture content of samples used during testing. Samples compacted under optimum moisture content, four percent above optimum moisture content, and four percent below optimum moisture content were selected for thermo calibration of the heating chamber.

Thermo calibration of the chamber consisted of performing heating and cooling cycles on samples compacted at optimum, dry, and wet moisture contents. For each moisture content a series of heating and cooling cycles was performed at temperatures of 40, 50, 60, and 70°C. For each temperature cycle the sample would be heated for 24 hours and then allowed to cool for 24 hours. Temperatures were recorded at three equally spaced points throughout the sample to not only observe heat transfer, but also determine heat distribution inside the sample. Pictures were taken with a fluke thermal imaging camera to give a visual representation of heat distribution in the chamber during heating, cooling, and throughout the sample.

4.2 - Specific Gravity Analysis

ASTM D854 Method B was used to determine the specific gravity of the soil. Excess air was removed from the pycnometer via suction. Two tests were performed with a difference of 0.34 percent, due to the precision of the first two tests a third test was determined to be unnecessary. Data from the specific gravity tests are presented in Table 4-1. The results from the specific gravity analysis suggest the soil is a low plasticity clay (CL) per ASTM D854. The test method states that a specific gravity of 2.67 with a standard deviation of 0.006 is expected for low plasticity clays.

Table 4-1: Specific gravity Analysis

Specific Gravity		
Sample	1	2
W1 (g)	661	660.9
T1 (°C)	22.4	23
W2 (g)	726.9	728.6
T2 (°C)	23	23
Bowl w (g)	178.1	168.1
Bowl+Soil (g)	283.4	276.5
Ws (g)	105.3	108.4
Ww (g)	39.4	40.7
Temp Corr.	0.9993	0.9993
Gs	2.67259	2.66339
Gs cor	2.6707	2.6615
% Diff	0.344478976	
Gs avg	2.67	

4.3 - Sieve and Hydrometer Analysis

ASTM C136 was the test method followed to determine the particle size distribution of the soil greater than 0.074 mm (#200 sieve). The results of the sieve analysis in Table 4-2 indicate

the soil is a silt-clay material with 41.32% passing the #200 sieve according to the AASHTO classification system.

Table 4-2: Sieve Analysis

Sieve #	Sieve Opening (mm)	Sieve Weight Empty (g)	Sieve + Soil (g)	Mass retained (g)	Percent Retained %	Cumulative Percent Retained %	Percent Finer %
16	1.19	451.8	451.9	0.1	0.02	0.02	99.98
20	0.841	423.1	424.4	1.3	0.26	0.28	99.72
30	0.595	631.9	642.6	10.7	2.14	2.42	97.58
40	0.42	339.2	359.9	20.7	4.14	6.56	93.44
50	0.297	328.8	386.9	58.1	11.62	18.18	81.82
60	0.25	308.8	346	37.2	7.44	25.62	74.38
80	0.177	306.6	345.7	39.1	7.82	33.44	66.56
100	0.149	299.6	349.6	50	10	43.44	56.56
200	0.074	288.3	503.9	76.2	15.24	58.68	41.32
Pan	0	496.3	564.5	197.8	39.56	98.24	0

In conjunction with the sieve analysis, a hydrometer analysis was performed on the portion of soil passing the #200 sieve. The hydrometer analysis gives a better understanding of the particle size distribution of the soil passing the #200 sieve, allowing a differentiation between silt and clay particles. ASTM D7928, particle size distribution of fine-grained soils using the sedimentation analysis, was used for determination. Hydrometer readings, correction factors, and results are shown in Tables 4-3, 4-4, and 4-5, and a full grain size distribution curve for the soil is shown in figure 4-1.

Table 4-3: Hydrometer readings

Hydrometer Readings			
#	Time (min)	Reading R	Temp C
1	0.25	51	22.8
2	0.5	47	22.8
3	1	42	22.8
4	2	37	22.8
5	4	33.5	22.8
6	8	28	22.8
7	15	25.5	22.8
8	30	23.5	22.6
9	60	22	22.4
10	120	20.5	21.8
11	240	20.5	21.5
12	480	20.5	20.7
13	1440	20	20.4
14	2880	17	21.4

Table 4-4: Hydrometer correction factors

Correction Factors			
Fz	Fm	Ft	Control Temp (°C)
8	0.5	0.575	21.7

Table 4-5: Hydrometer analysis

| Hydrometer Calculations and Results						
Rcp	Percent finer (%)	Rcl	L (cm)	A	D (mm)	Percent finer total (%)
43.58	0.86	51.5	7.85	0.0132	0.0740	35.69
39.58	0.78	47.5	8.5	0.0132	0.0544	32.41
34.58	0.69	42.5	9.3	0.0132	0.0403	28.32
29.58	0.59	37.5	10.15	0.0132	0.0297	24.22
26.08	0.52	34	10.7	0.0132	0.0216	21.36
20.58	0.41	28.5	11.6	0.0132	0.0159	16.85
18.08	0.36	26	12	0.0132	0.0118	14.80
16.08	0.32	24	12.4	0.0132	0.0085	13.17
14.58	0.29	22.5	12.6	0.0133	0.0061	11.94
13.08	0.26	21	12.9	0.0133	0.0044	10.71
13.08	0.26	21	12.9	0.0133	0.0031	10.71
13.08	0.26	21	12.9	0.0135	0.0022	10.71
12.58	0.25	20.5	12.95	0.0137	0.0013	10.30
9.58	0.19	17.5	13.4	0.0135	0.0009	7.84
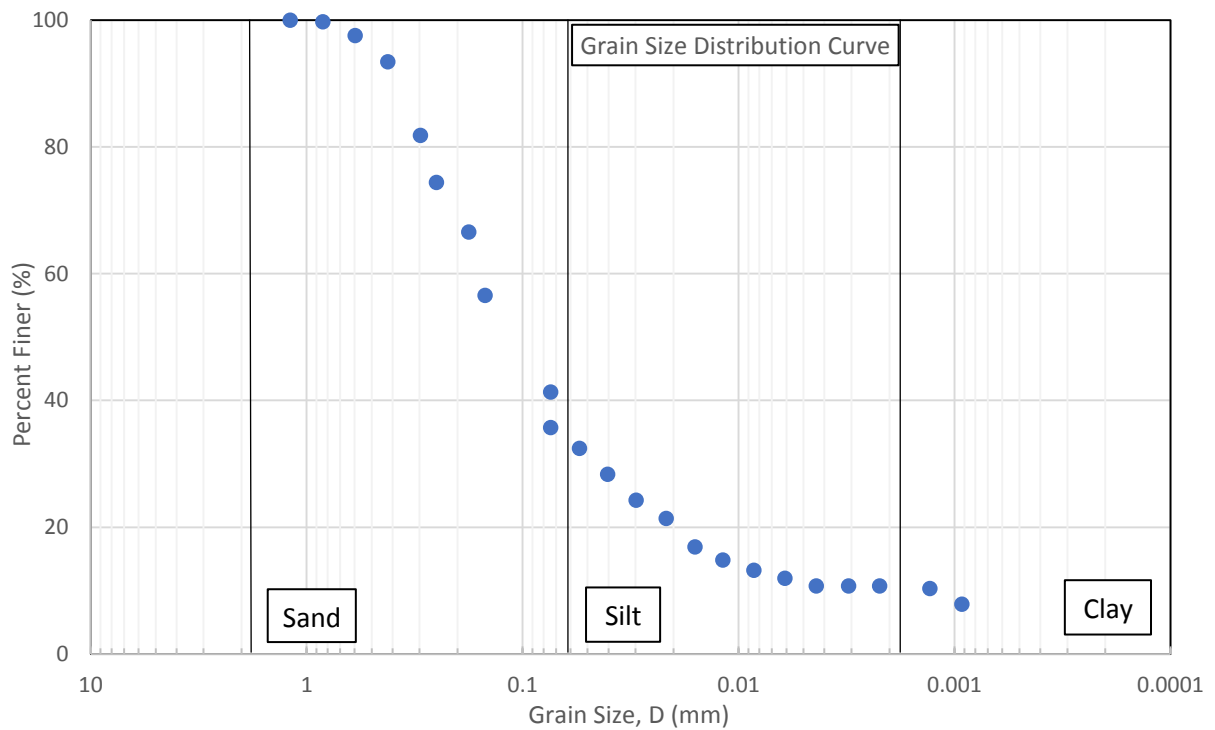
Figure 4-1: Full grain size distribution curve for sample soil

The sieve and hydrometer analysis suggest that the soil is composed of approximately 60 percent sand, 30 percent silt, and 10 percent clay. The coefficient of gradation (Cu) and coefficient of curvature (Cc) in Table 4-6, along with the general shape of the grain size distribution curve show that the soil is gap graded.

Table 4-6: Gradation classification parameters

D10	D30	D60	Cu	Cc
0.002	0.045	0.15	75	6.75

4.4 - Atterberg Limits

Both the liquid limit and plastic limit were also determined. The liquid limit refers to the moisture content at which a cohesive soil changes from a liquid state to a plastic state, and the plastic limit refers to the moisture content where the soil further changes from a plastic state to a semi-solid state. These two parameters are referred to as the Atterberg limits and can be used to calculate the plasticity index of the soil. ASTM D4318 was the test method used for determining the liquid limit, plastic limit, and plasticity index of the soil. Method A, multipoint test, was followed for liquid limit determination. Tables 4-7, 4-8, and 4-9 along with figure 4-2 show calculations for liquid limit, plastic limit, and plasticity index. The plasticity chart in figure 4-3 depicts the information in the tables, showing the soil sample in the low plasticity clay (CL) range. The results of the specific gravity, sieve, hydrometer, and plasticity index tests all indicate that the soil is a low plasticity clay (CL).

49

Table 4-7: Liquid limit analysis

Liquid Limit			
Sample	1	2	3
N	35	17	24
Tare (g)	21.2	21.8	21.5
T+S (g)	67.9	57.9	60
T+S dry (g)	57.5	49.2	51
w%	28.65014	31.75182	30.50847
LL	29.84065	30.30416	30.35815
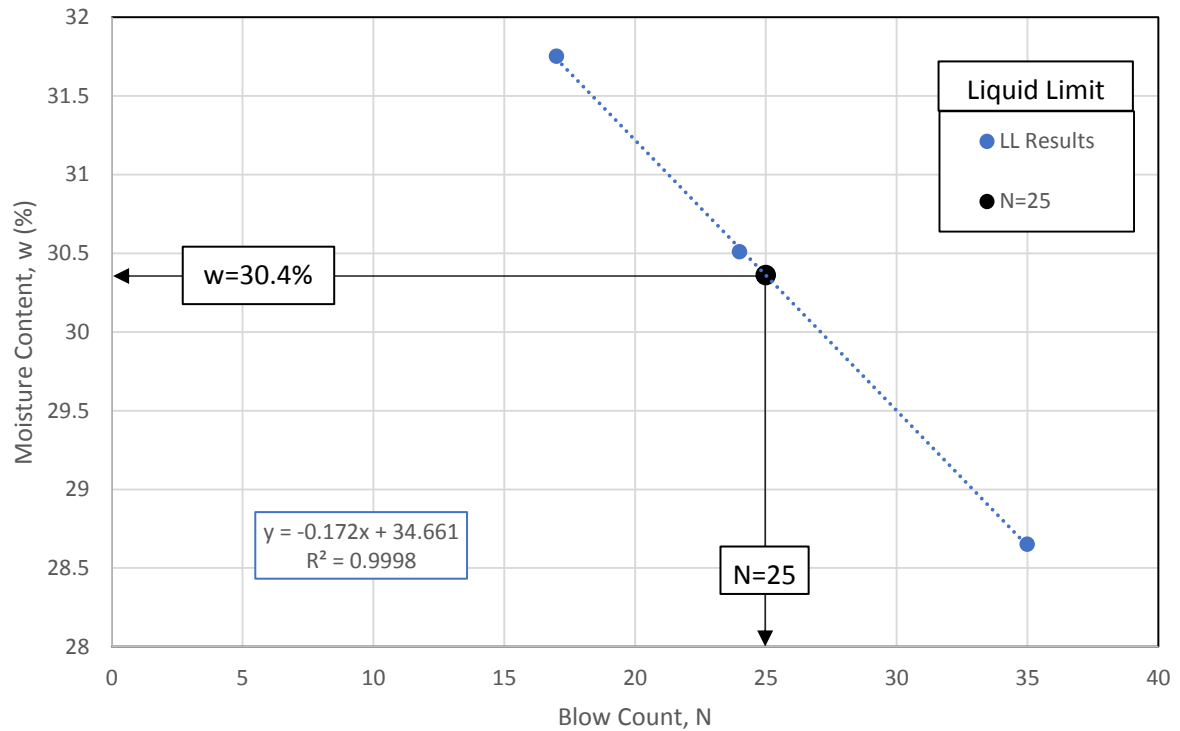
Figure 4-2: Liquid limit determination

Table 4-8: Plastic limit analysis

Plastic Limit			
Sample	1	2	3
Tare (g)	21.2	21.2	21.5
T+S (g)	28.1	27.8	27.5
T+S dry (g)	27.1	26.8	26.6
PL	16.94915	17.85714	17.64706
PL Avg	17.48445141		

Table 4-9: Plasticity index calculation

Plasticity Index		
LL	PL	PI
30.361	17.4844514	12.87655

Figure 4-3: Plasticity chart for sample soil

4.5 - Standard Proctor

ASTM D698 Method A was used to perform a standard proctor and determine the maximum dry density and optimum moisture content. Method A refers to using a 4-inch diameter mold and compacting the soil in three layers with 25 blows per layer. Table 4-10 and figure 4-4 show the results of the standard proctor. The maximum dry density and optimum water content determined dur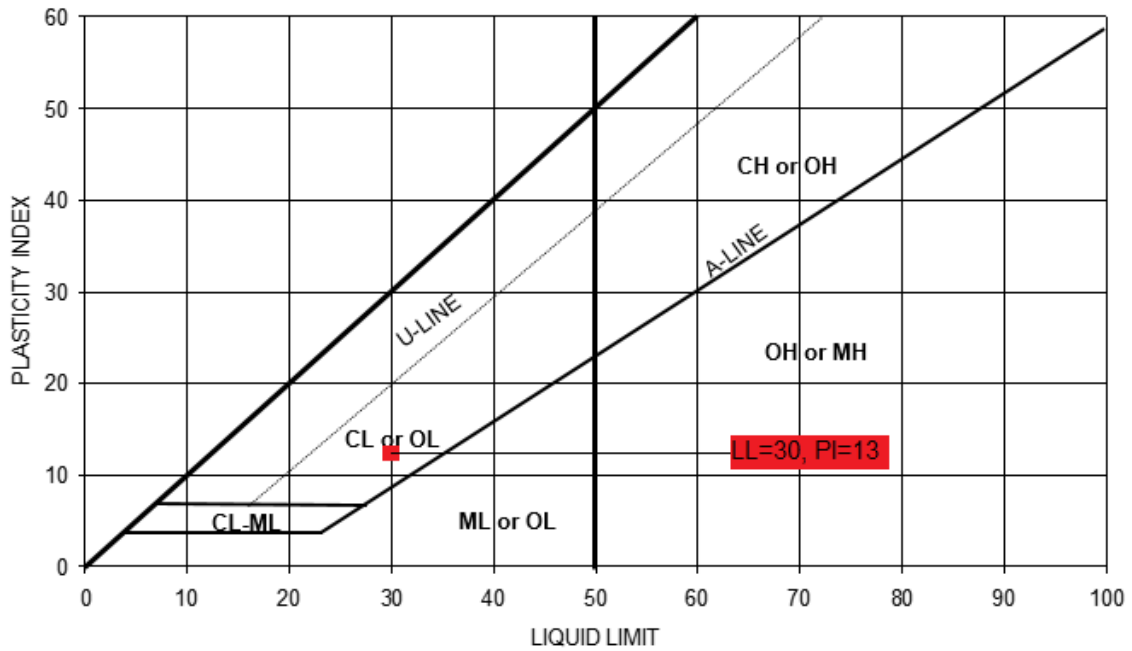ing testing agree with the other methods of soil analysis performed and further classify the soil as a low plasticity clay (CL). Optimum, dry, and wet moisture contents used during heat chamber calibration were obtained from the results of the test. The points used during thermo calibration are highlighted in Table 4-10: 13.6/110.9 (optimum), 9.9/109.3 (dry), and 17.6/108.2 (wet).

Table 4-10: Standard proctor analysis

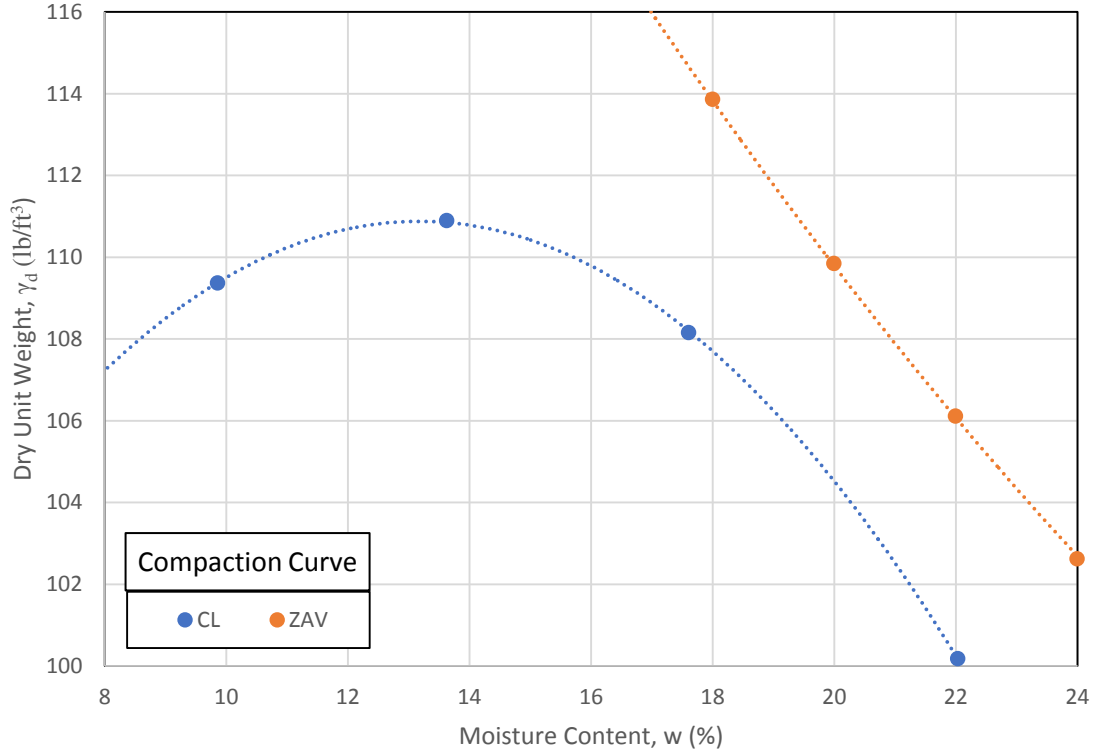| Standard Proctor				
	Air Dry +5%	Air Dry +8%	Air Dry +11%	Air Dry +14%
Mold (lb)	9.065	9.065	9.065	9.07
Soil+Mold (lb)	13.07	13.265	13.305	13.145
Moist Unit Weight (lb/ft^3)	120.15	126	127.2	122.25
Tare (g)	21.5	21.5	21.6	21
T+S moist (g)	60.5	68.2	57	64.2
T+S dry (g)	57	62.6	51.7	56.4
Moisture Content (%)	9.86	13.63	17.61	22.03
Dry Unit Weight (lb/ft^3)	109.37	110.89	108.16	100.18

Figure 4-4: Compaction curve

4.6 - Thermo calibration results and analysis

As stated in chapter 3, the current resonant column device was upgraded with two heating elements and a thermocouple to control temperature. However, there was no way to monitor temperature of the soil sample. A similar chamber was designed with the same heating elements and thermocouple configuration as well as space to accommodate additional thermocouples to measure soil and air temperature. In chapter 2 previous thermo-controlled triaxial and isotropic cells were discussed. Unfortunately, these cells use water as the confining fluid, and heating configurations ranged from heat pumps to submerged heating elements and water agitators. The resonant column device to be used in this thesis uses air as the confining fluid, and the fans used to circulate the hot air are too small to achieve a uniform heat distribution inside the chamber. Due to this challenge it was necessary to perform multiple heating and

cooling cycles at different temperatures and water contents to establish a reliable and verifiable calibration curve that provides a reasonably accurate method for identifying soil temperature in the resonant column device.

Target soil testing temperatures for the resonant column device were between 20 and 60°C. Heating calibration of resonant column device consisted of performing heating and cooling cycles in the thermo-controlled chamber at temperatures of 40, 50, 60, and 70°C. Each cycle consisted of a 24-hour heating period and a 24-hour cooling period. Data was collected using a 4-channel digital thermometer with three thermocouples inserted into the soil sample and one thermocouple measuring air temperature inside the chamber near the sample. Figures 4-5, 4-6, 4-7, and 4-8 show full heating and cooling cycles for soil samples compacted at maximum dry density and optimum water content.

Figure 4-5: Soil heating and cooling cycle for 40°C at 13.6% (optimum) water content

Figure 4-6: Soil heating and cooling cycle for 50°C at 13.6% (optimum) water content
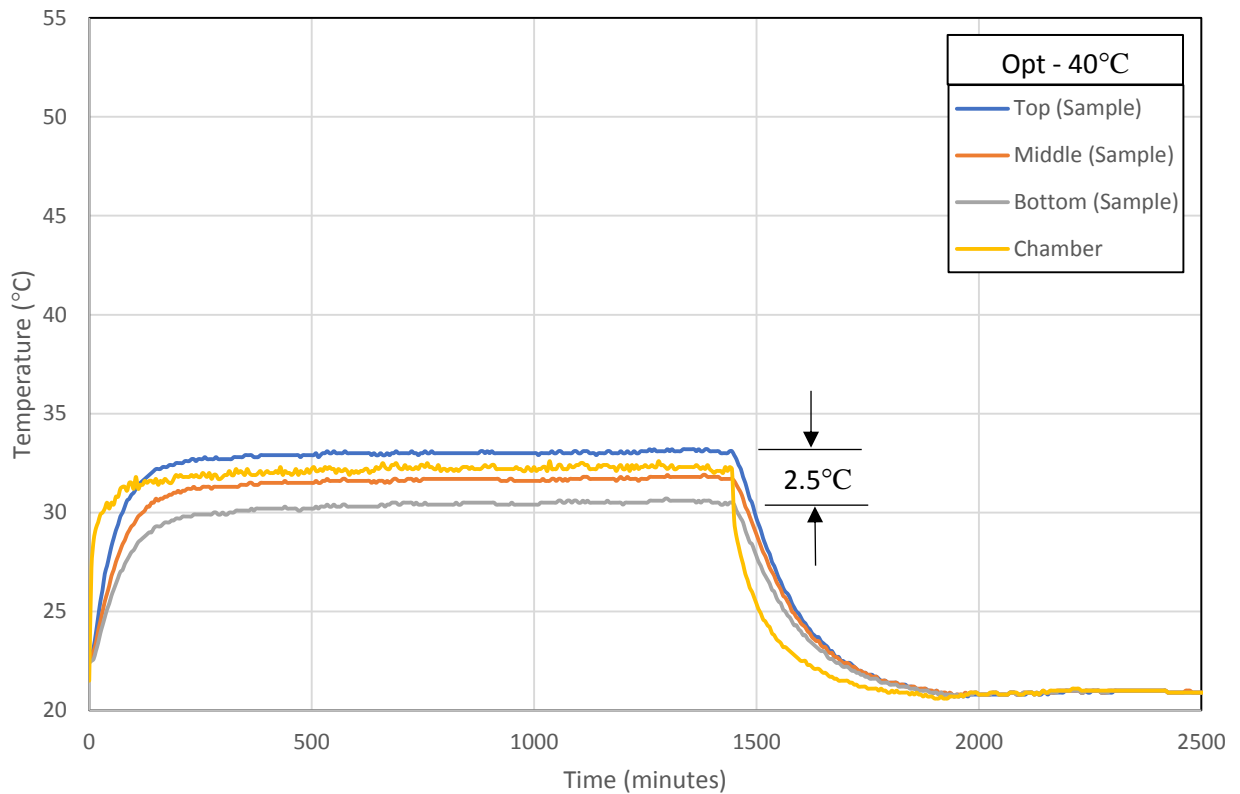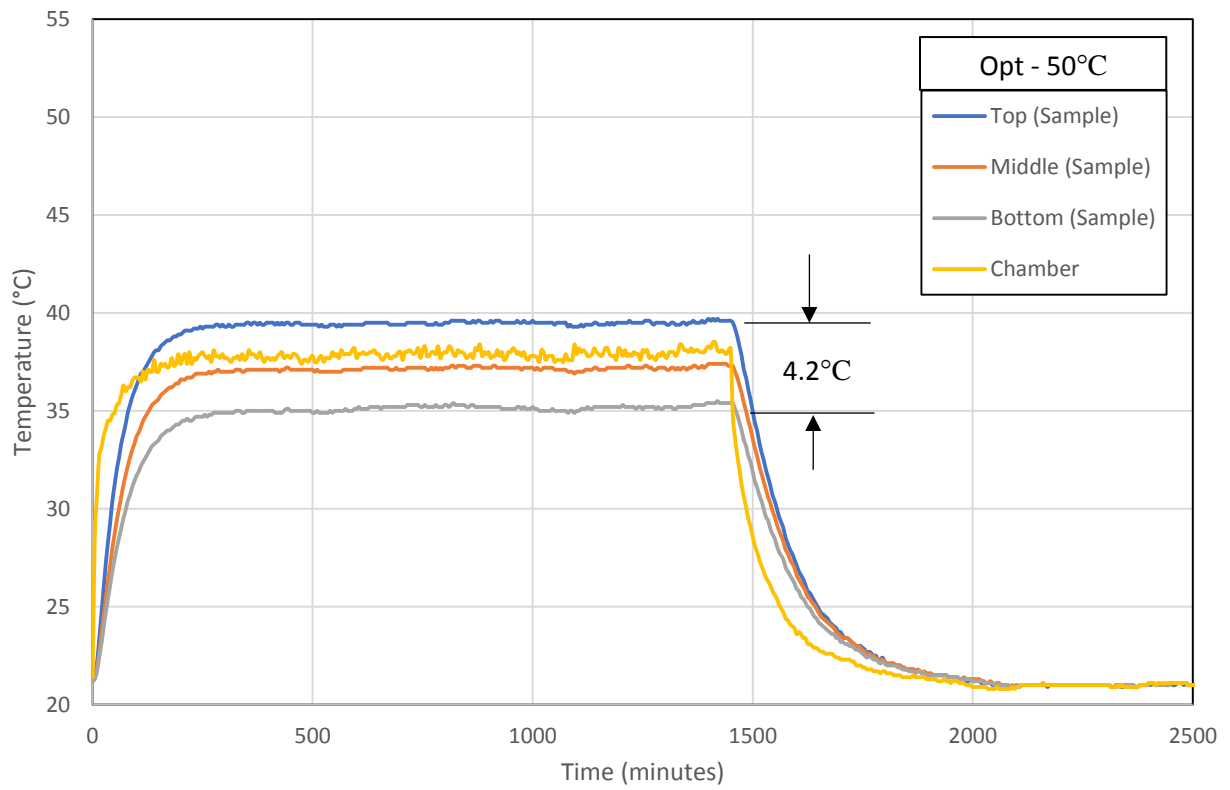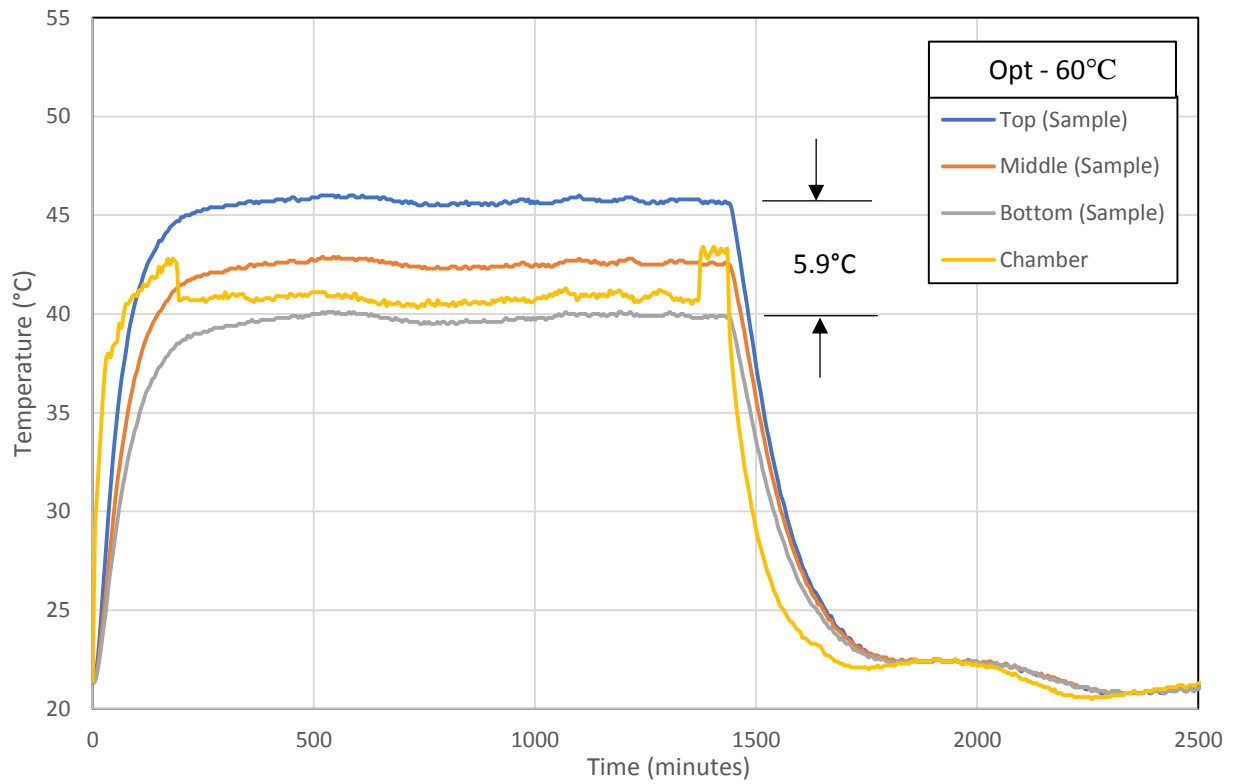
Figure 4-7: Soil heating and cooling cycle for 60°C at 13.6% (optimum) water content
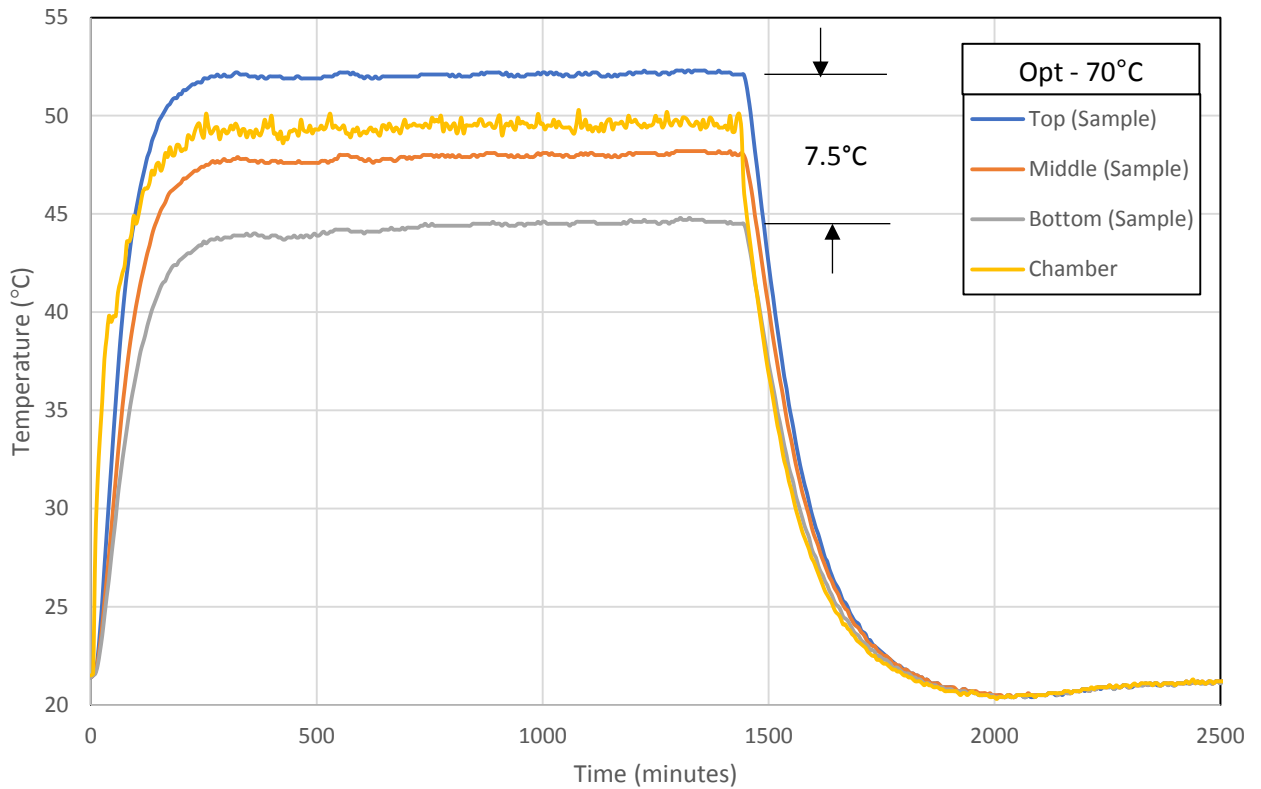
Figure 4-8: Soil heating and cooling cycle for 70°C at 13.6% (optimum) water content

All graphs show time in minutes on the x-axis versus soil temperature in degrees Celsius on the y-axis. The bounds for each axis are kept constant to clearly show the temperature differences from cycle to cycle. "Opt-40°C" refers to the soil samples being compacted at optimum moisture content and the temperature of the heating element being set to 40°C. As indicated in the legend of each graph, the blue line corresponds to the thermocouple probe inserted near the top of the sample, the orange line corresponds to the probe inserted into the middle of the sample, the gray line corresponds to the probe inserted near the bottom of the sample, and the yellow line corresponds to the thermocouple wire hanging inside the chamber near the middle of the sample measuring the temperature of the heated air. The noise seen in the yellow line is due to the thermocouple not being fixed properly and shifting inside the chamber. It can also be partly attributed to small variations in temperature while the heating mechanism

57

attempts to keep the chamber at a constant temperature. This can be seen more clearly in figure 4-7 where a drastic dip in the chamber temperature can be seen. This dip occurred due to the wire probe shifting, not because of an actual change of temperature as all three thermocouples in the soil report a steady reading during this time. All probes were inserted halfway into the soil since that point is furthest away from the surface and thus furthest away from the heated air inside the chamber.

Referring to figures 4-5 through 4-8 a few important observations can be made. It can be clearly seen that the soil never reaches the temperature of the heating element. Taking 21°C as room temperature, the graphs show that the middle of the soil sample only increases around 5°C for every increase of 10°C in the heating element. In figure 4-5 for example, the soil temperature starts at 21.4°C, and a constant temperature of 40°C is applied for 24 hours. However, the middle of the soil sample only reaches 32°C. A similar trend can be seen in graphs 4-6 through 4-8. It can also be seen that as temperature of the heating element increases, the temperature variation within the soil sample also increase from a 2.5°C difference at 40°C to a 7.5°C difference at 70°C. The data shows the rate of increase in soil temperature drops significantly after 300 minutes, with peak temperatures showing only minor fluctuations after 500 minutes. During cooling, soil samples return to room temperature 350 minutes after the heat source is shut off. The chamber air temperature, indicated by the yellow line on the graphs and measured near the middle of the sample, shows that the temperature variation between the heated air and the soil at the same depth in the chamber is relatively small (within 1-2°C).

Figures 4-9, 4-10, 4-11, 4-12 show the same heating and cooling cycles for soil samples compacted under dry conditions (9.9% moisture content). Heating times to peak temperatures and cooling times to room temperature are very similar to samples compacted under optimum conditions, however, the samples compacted under dry conditions peak at temperatures 1-2°C cooler than samples with optimum water content. The dry samples also show a slightly larger temperature variation when compared to optimum moisture samples from 0.2°C at 40°C to 0.8°C at 70°C.
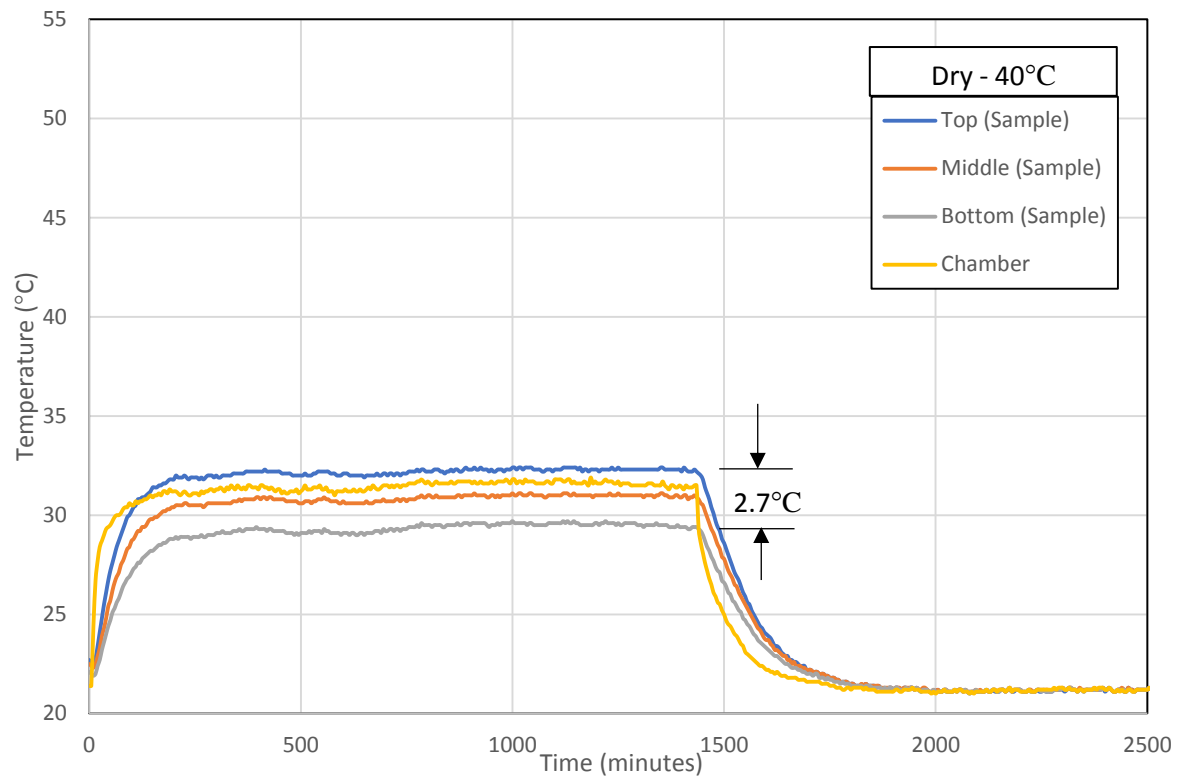
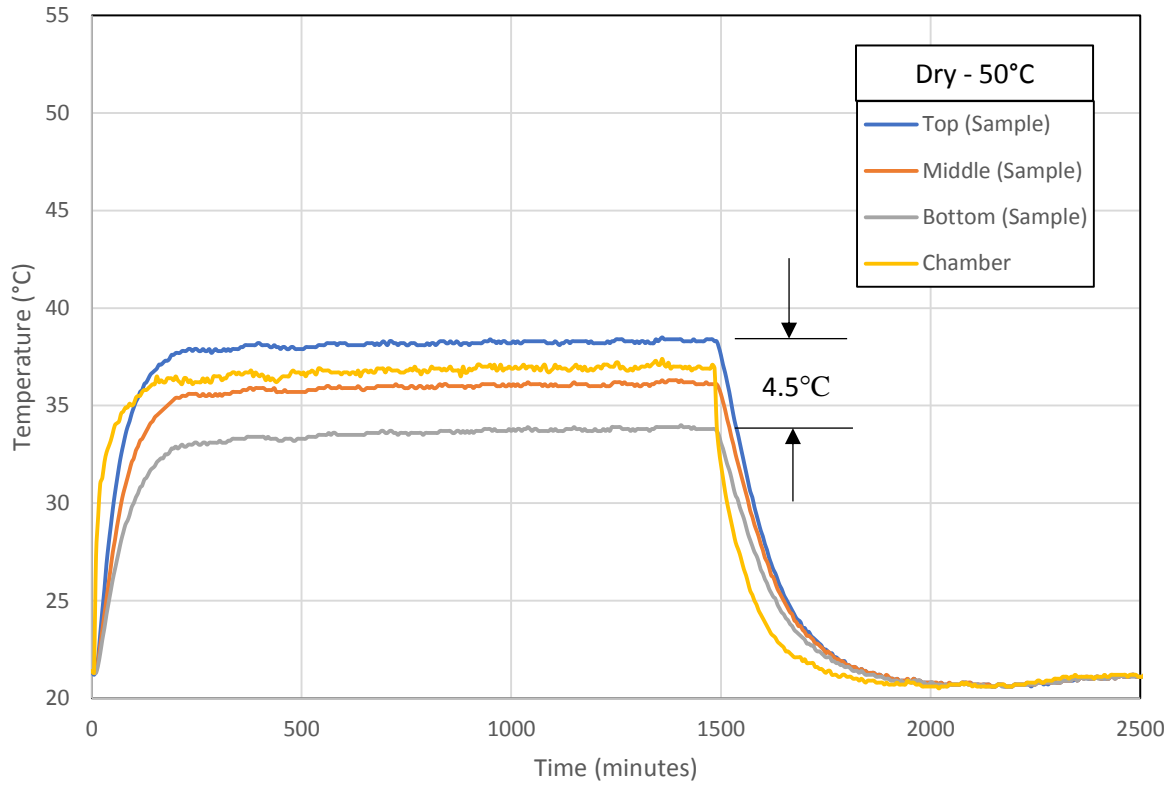Figure 4-9: Soil heating and cooling cycle for 40°C at 9.9% (dry) water content

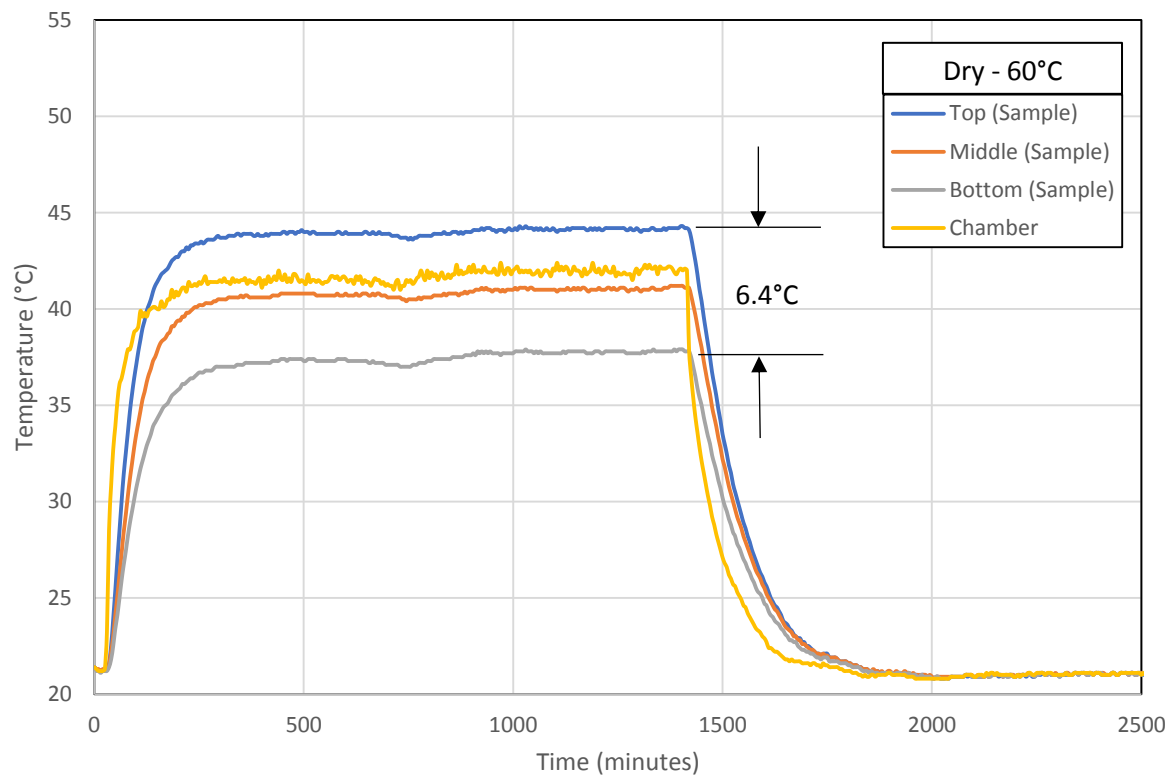Figure 4-10: Soil heating and cooling cycle for 50°C at 9.9% (dry) water content

Figure 4-11: Soil heating and cooling cycle for 60°C at 9.9% (dry) water content
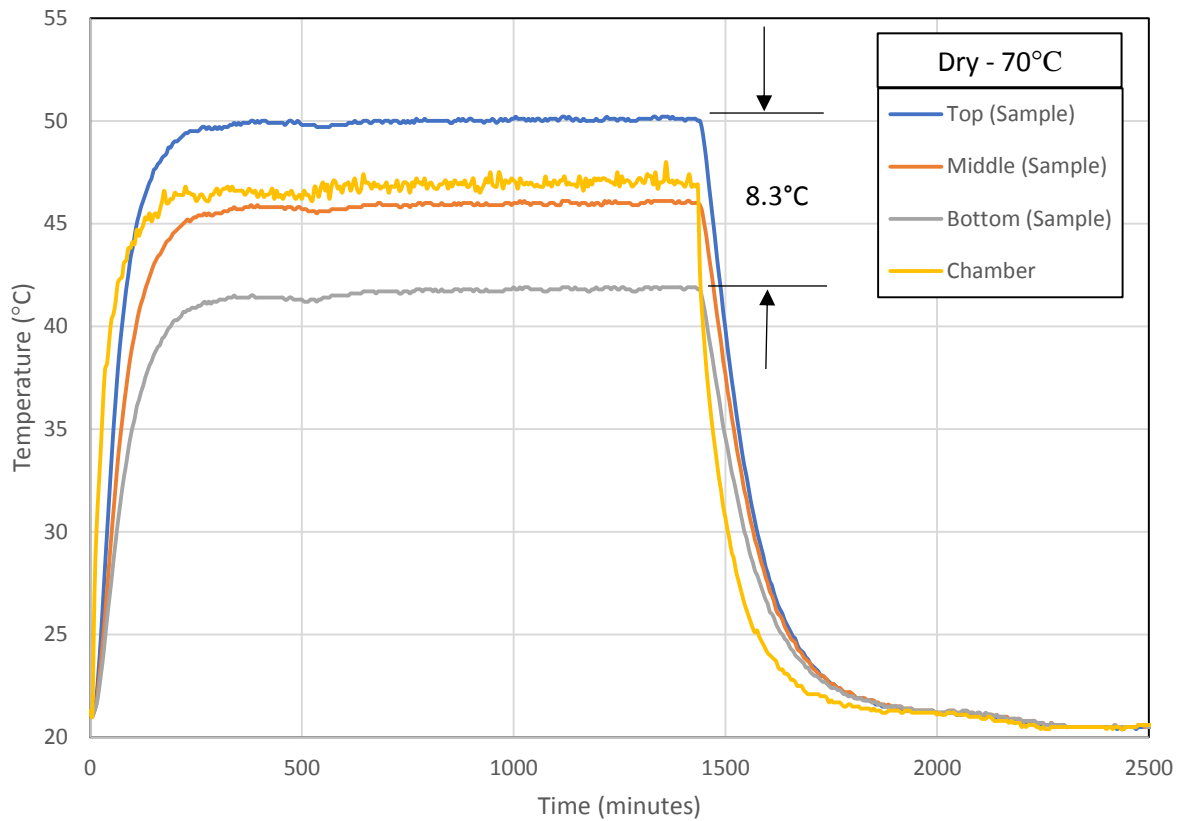
Figure 4-12: Soil heating and cooling cycle for 70°C at 9.9% (dry) water content

The same trends can be seen in the samples compacted under wet conditions (17.6% moisture content). While figures 4-13, 4-14, 4-15, and 4-16 show slightly higher peak temperatures than samples compacted under dry (9.9% moisture content) conditions, the temperatures of the wet samples still fall 1-2°C short of optimum moisture content samples. Temperature variation within the wet samples is also larger than both the optimum samples and dry samples. Heating time to peak temperatures and cooling time to room temperature is similar for all moisture contents.
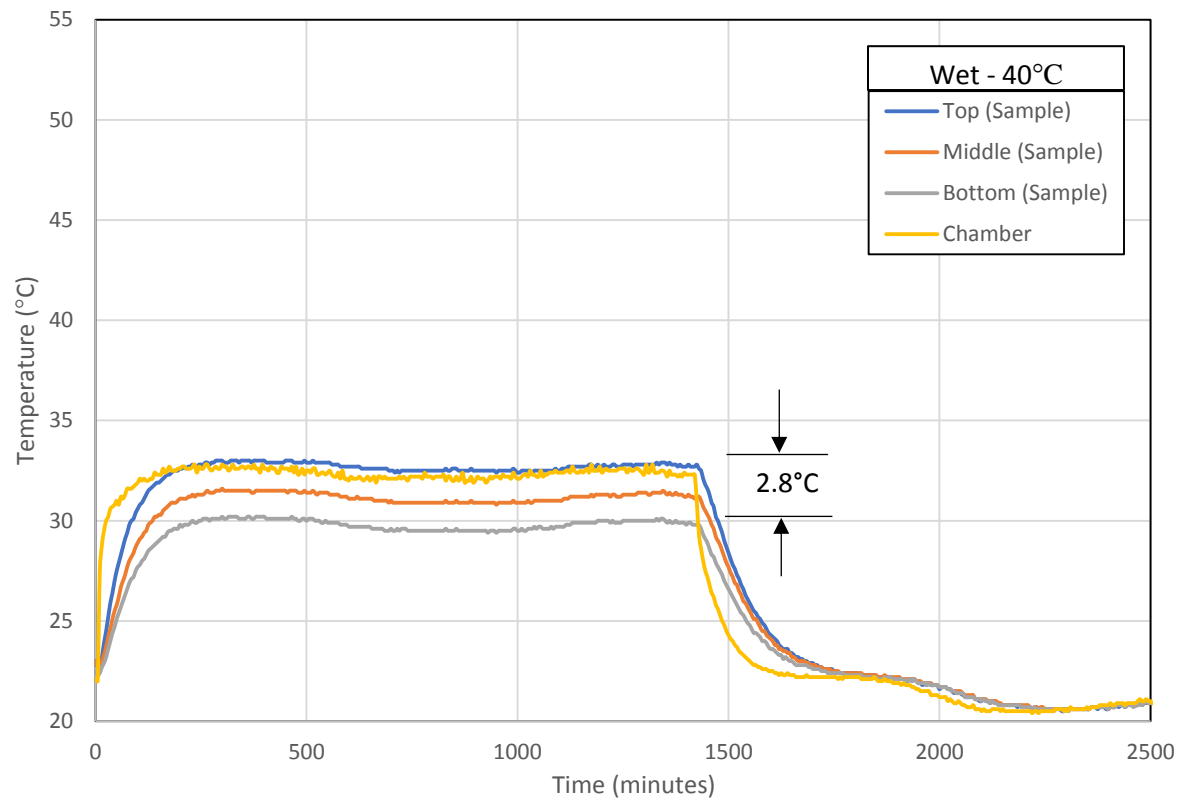
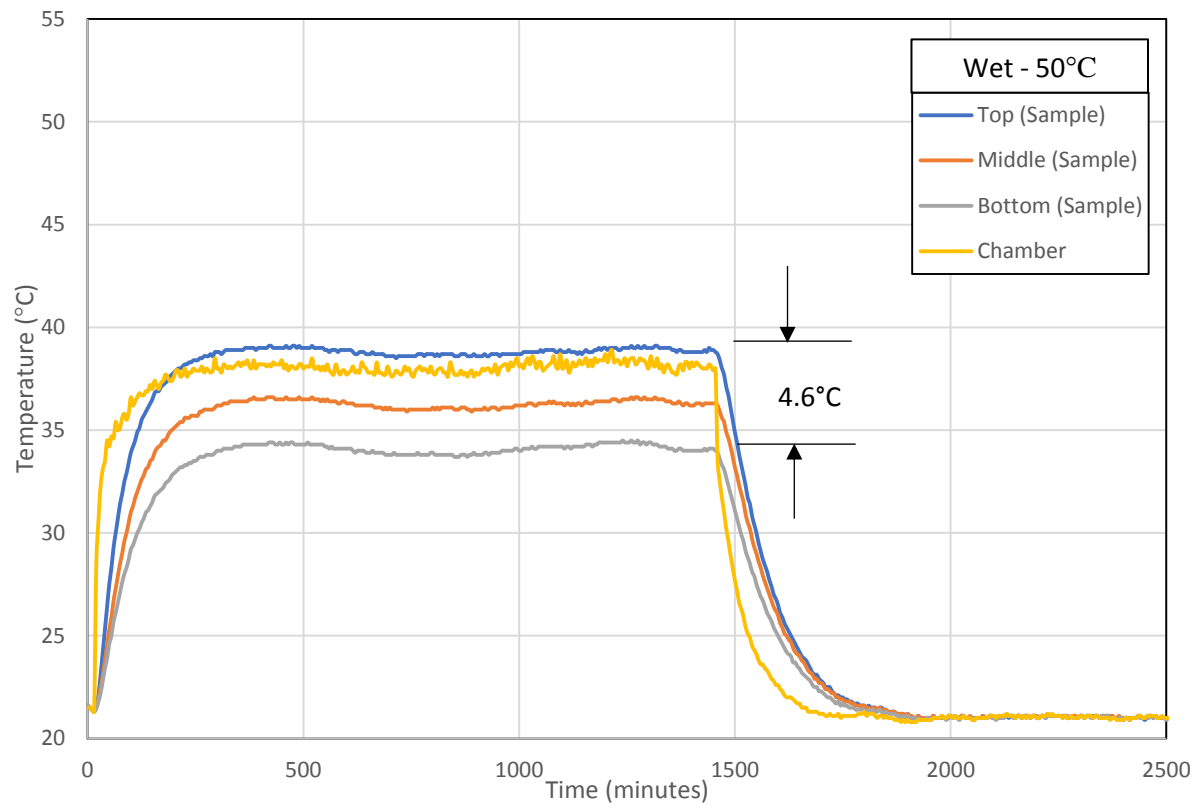Figure 4-13: Soil heating and cooling cycle for 40°C at 17.6% (wet) water content

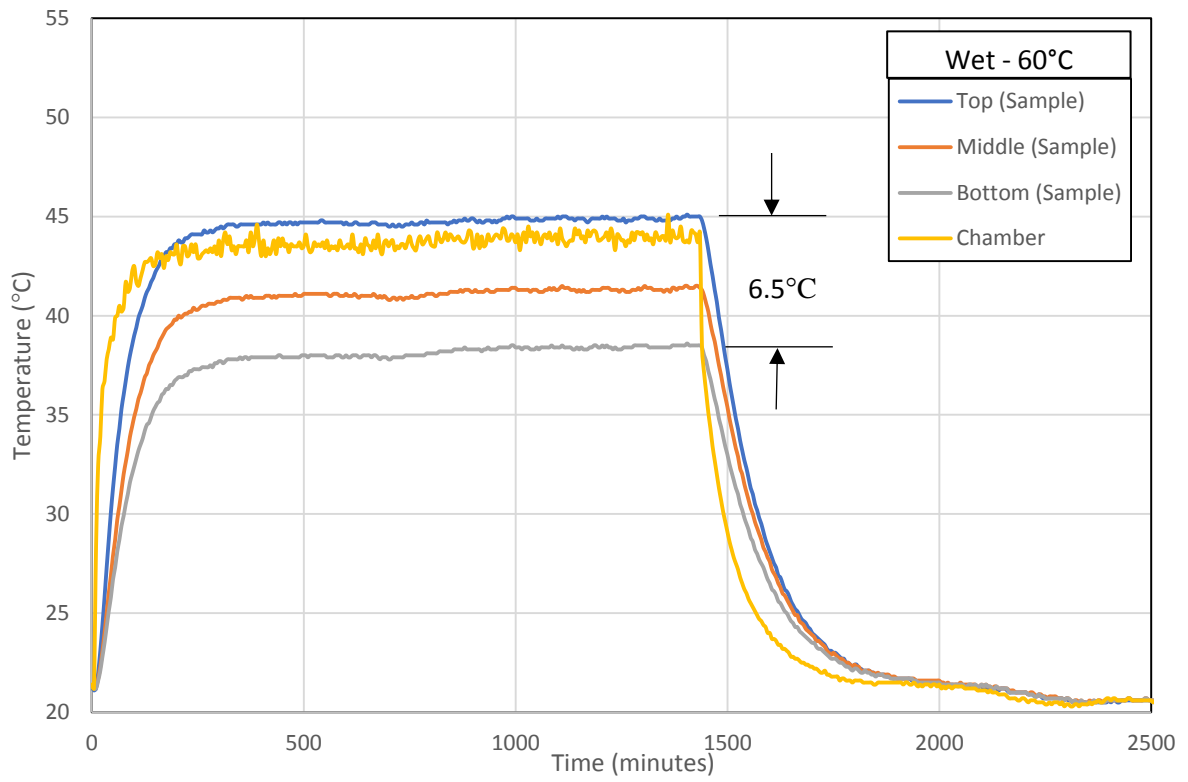Figure 4-14: Soil heating and cooling cycle for 50°C at 17.6% (wet) water content

Figure 4-15: Soil heating and cooling cycle for 60°C at 17.6% (wet) water content
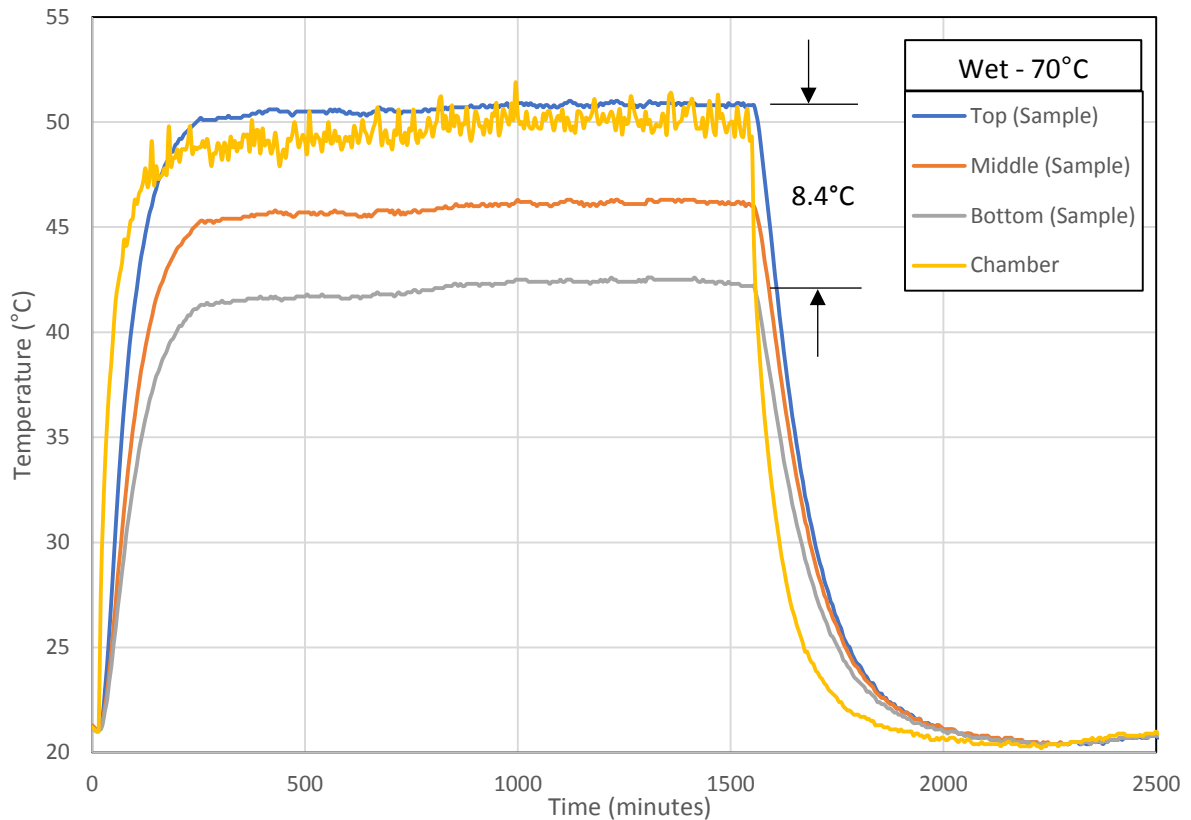
Figure 4-16: Soil heating and cooling cycle for 70°C at 17.6% (wet) water content

Figures 4-17, 4-18, 4-19, and 4-20 show comparisons between optimum, dry, and wet soil samples. The middle thermocouple probe data is shown for different water contents for 40, 50, 60, and 70°C temperature cycles. As previously stated, it can be clearly seen that the soil compacted under optimum water content reached higher peak temperatures than both dry and wet samples. The comparison graphs also show that as peak temperature increases, variation with water content also increases.

In their 2008 conference paper, "Thermal properties as a function of water content in a silty porous media under laboratory conditions," Rubio et al. examine soil properties that effect the thermal conductivity of a soil. They characterize the three major factors effecting heat transfer in a soil as particle size distribution, water content, and dry density. Thermal conductivity

increases with increasing particle size, being highest in sands and lowest in clays. Thermal conductivity increases with water content due to water having a thermal conductivity of 0.57 W/m K, about 30 times higher than that of air (0.018 W/m K). As water fills the voids around the soil particles heat transfer between particles increases thus increasing the thermal conductivity of the soil system. Dry density also plays an important role in thermal conductivity. As dry density increase thermal conductivity also increases due to less available pore space and thus less air. However, dry density appears to effect thermal conductivity at a lesser extent than moisture content (Rubio et al., 2008).

While particle size distribution of the samples tested in this thesis was fairly uniform, water content and dry density was altered for both dry and wet soil specimens. The values used during sample compaction are highlighted in Table 4-10. Comparing the values in Table 4-10 with figures 4-17 through 4-20 it is expected that the dry soil sample would reach lower peak temperature values than the optimum sample. The dry sample has a lower moisture content and lower dry density than the optimum sample and thus a lower thermal conductivity. The wet sample also reaches lower peak temperatures than optimum sample despite having a higher water content. As described by Rubio et al., this likely occurred due to the wet sample having a lower dry density than the optimum sample. This reasoning fits Rubio's comments that dry density effects thermal conductivity but at a lesser extent than moisture content and can be seen in the data shown in figures 4-17 through 4-20, where the wet sample (lower dry density, higher moisture content) reached slightly higher peak temperatures than the dry sample (higher dry density, lower moisture content).
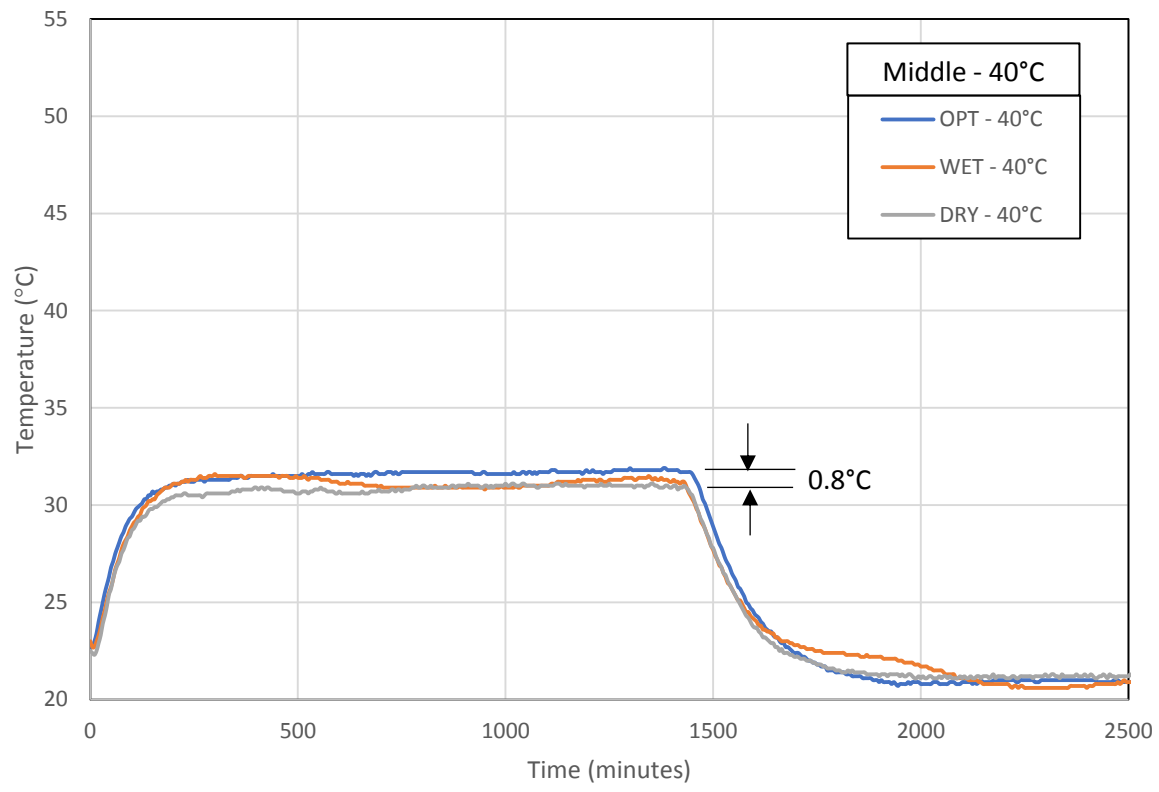
Figure 4-17: Middle thermocouple temperature variation for 40°C
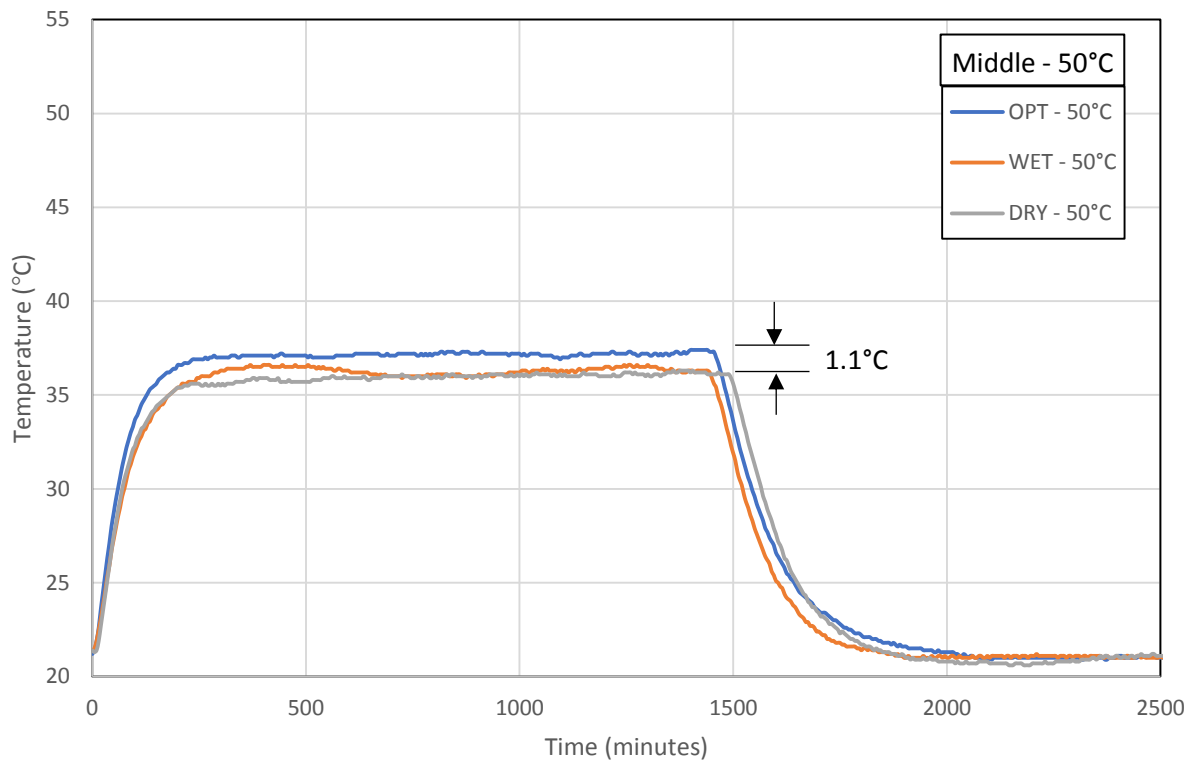
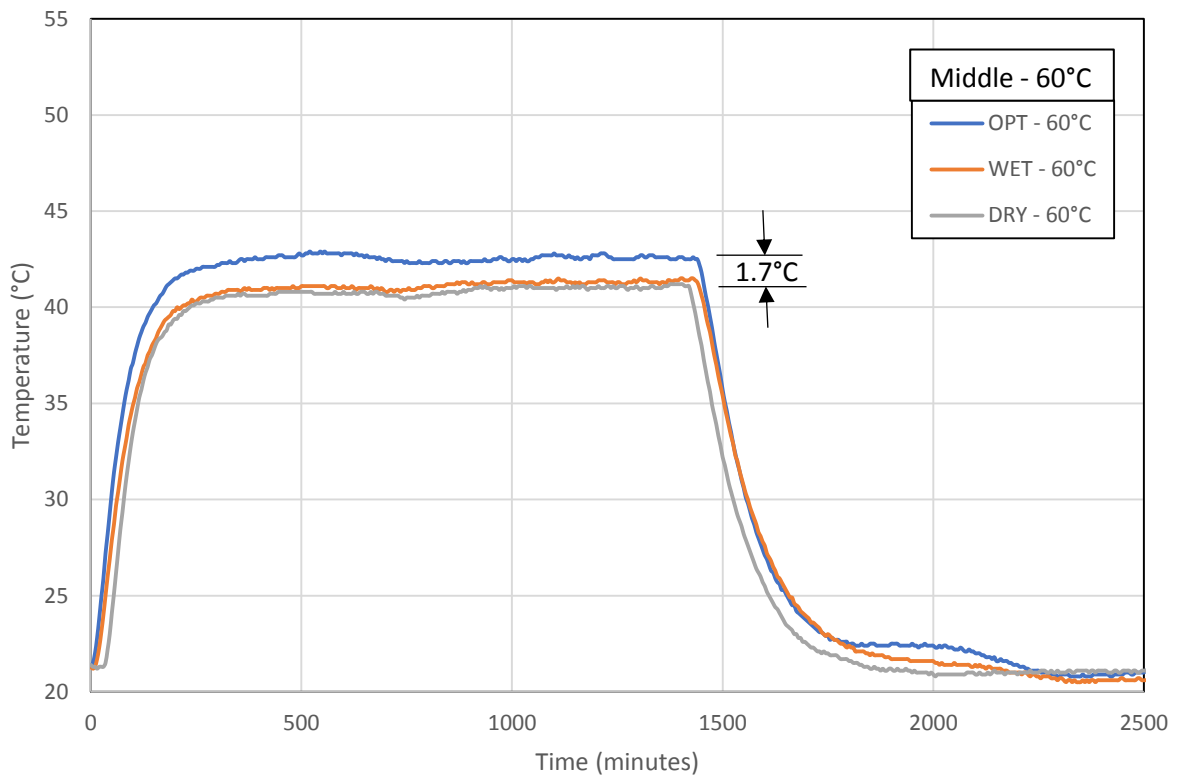Figure 4-18: Middle thermocouple temperature variation for 50°C

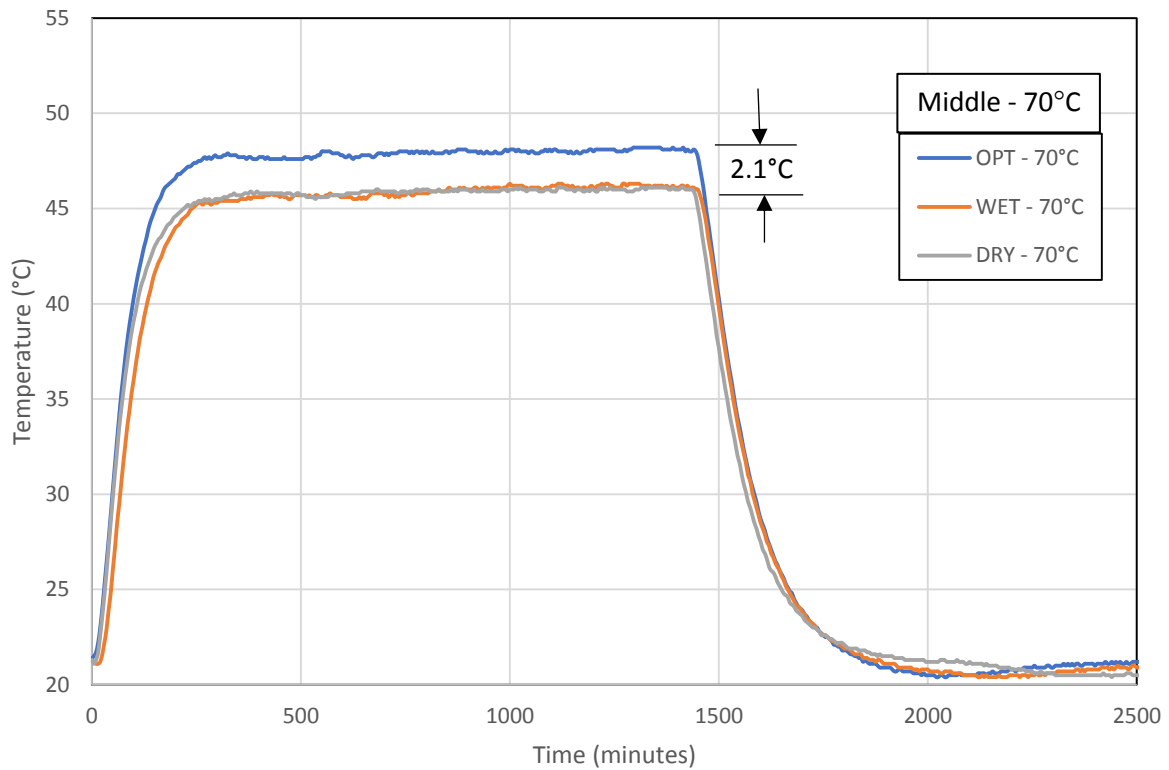Figure 4-19: Middle thermocouple temperature variation for 60°C

Figure 4-20: Middle thermocouple temperature variation for 70°C

Moisture contents were taken for each sample before soil compaction and after the 70°C heating cycle to determine moisture loss during heating. Results are shown in table 4-11, 4-12, and 4-13. Aside from the dry sample, the soil experienced a minor loss in moisture content during heating. The increase in moisture content shown in the dry sample is probably due to an unrepresentative portion of soil used to obtain a pre-compaction moisture content. An interesting trend can be seen in the dry sample and wet sample moisture contents after testing. The moisture content at the top of the samples where the air temperature in the chamber is hotter is lower than the moisture content at the bottom of the samples where the air temperature in the chamber is cooler. However, this trend is not seen in the optimum moisture content sample. It can be reasonably assumed that moisture content loss would be even less during an actual thermo-controlled resonant column test. The latex membrane has three holes caused by the

thermocouple probes during calibration heating and cooling. These holes facilitate moisture loss and would not be present during resonant column testing.

Table 4-11: Moisture content – optimum

Moisture Content				
Sample 1 - Optimum, target = 13.6%				
	Before Compaction	After Testing		
		Top	Middle	Bottom
Tare (g)	21.5	21.3	21	21.5
T+S (g)	55.4	35.8	34.2	35.1
T+S dry (g)	51.4	34.1	32.7	33.5
w%	13.38	13.28	12.82	13.33
avg		13.15		
%diff	1.74			

Table 4-12: Moisture content – dry

Moisture Content				
Sample 2 - Dry, target = 9.9%				
	Before Compaction	After Testing		
		Top	Middle	Bottom
Tare (g)	21.8	21.5	21.2	21.5
T+S (g)	55.8	40.7	38.6	35.9
T+S dry (g)	52.6	39	37	34.3
w%	10.39	9.71	10.13	12.50
avg		10.78		
%diff	3.76			

Table 4-13: Moisture content – wet

Moisture Content				
Sample 3 - Wet, target = 17.6				
	Before Compaction	After Testing		
		Top	Middle	Bottom
Tare (g)	21	21.5	21.5	21.2
T+S (g)	41.8	46.4	46	45.3
T+S dry (g)	38.7	42.8	42.4	41.7
w%	17.51	16.90	17.22	17.56
avg		17.23		
%diff	1.63			

Further analysis shows an interesting trend between the peak temperatures of each heating cycle for optimum, dry, and wet samples. Figures 4-21, 4-22, and 4-23 show a linear relationship between the temperature of the heating elements and the peak temperatures in the soil. The top, middle, and bottom thermocouple probe all report linear relationships between heating element temperature and peak soil temperature. These figures are the calibration curves that will be used in further resonant column testing to determine the necessary heating element temperature setting to impart a desired temperature on the soil sample. The equation of the trendline can be used to predict soil temperatures without the need for puncturing the latex membrane with thermocouples probes to verify the temperature of the sample. The trendlines in the calibration graphs are not parallel, reaffirming the observation that temperature variation within the sample increases with increasing temperature (figures 4-5 through 4-16). It can also be seen that the slope of the trendlines are steeper in the optimum moisture calibration graph than in either the dry or wet calibration graphs. The steeper slopes correlate to higher peak temperatures in the optimum moisture content samples (figures 4-17 through 4-20).
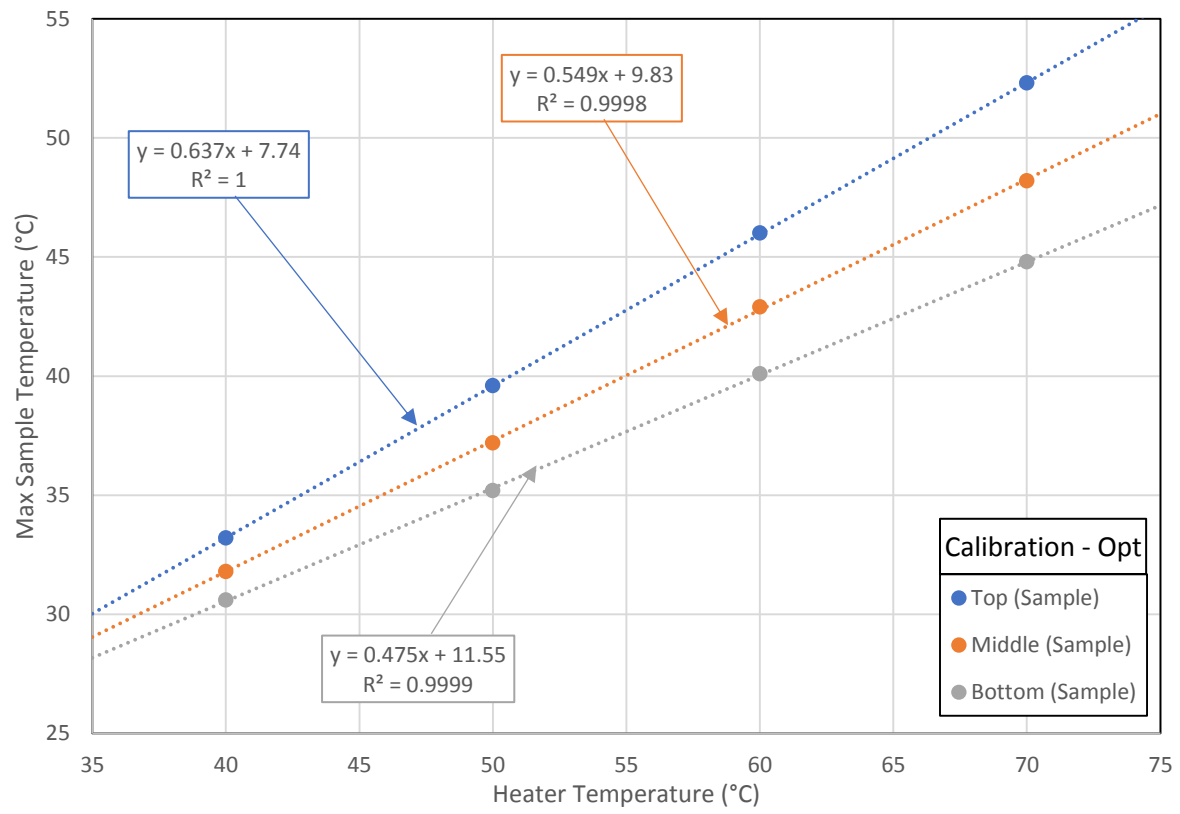
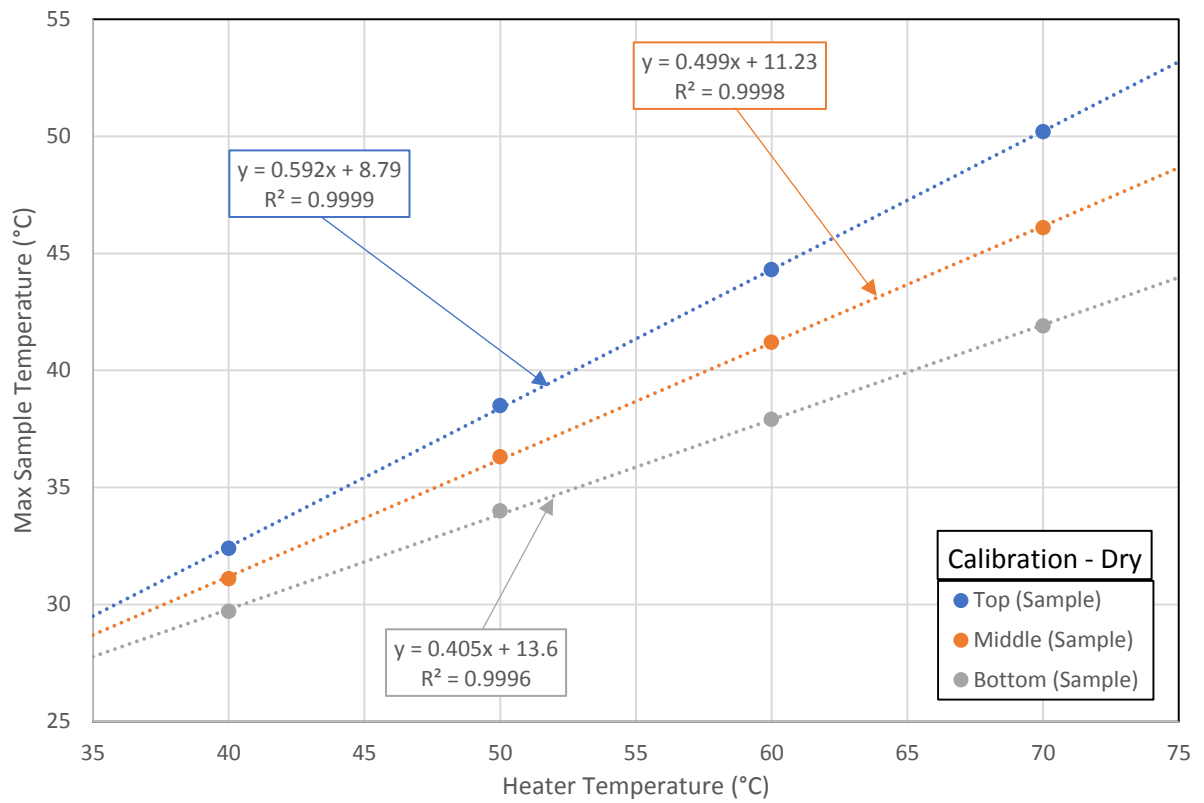Figure 4-21: Heating chamber calibration for 13.6% (optimum) moisture content

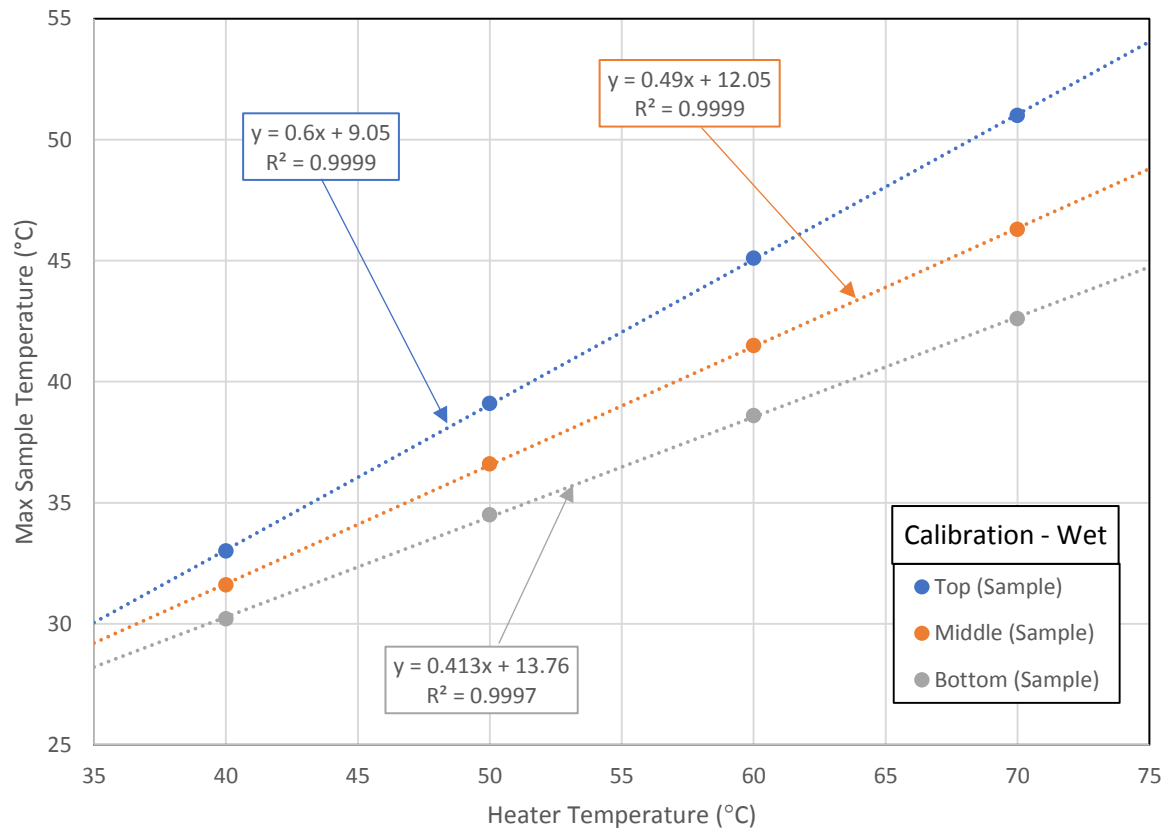Figure 4-22: Heating chamber calibration for 9.9% (dry) moisture content

Figure 4-23: Heating chamber calibration for 17.6% (wet) moisture content

Due to the increase in temperature variation of the soil samples during heating and more uniform temperature distribution during cooling, the cooling cycles were examined more closely. Since temperatures at the top, middle, and bottom of the sample converge to room temperature over time once the heating element is turned off, cooling trends were examined to determine feasibility of resonant column testing during cooling cycles. Figures 4-24, 4-25, 4-26, and 4-27 show a more focused view on the cooling portion of the optimum moisture content graphs in figures 4-5 through 4-8. The cooling cycle graphs were used to determine the temperature of the soil at which the temperature variation between the top and bottom thermocouple probe was less than 2°C and the time required for the cooling to occur. Figures 4-24 through 4-27 show that despite the starting temperature of the soil samples, all samples compacted under optimum

moisture conditions reached a temperature variation of less than 2°C at virtually the same temperature. Cooling times increased with higher starting temperatures, however, every sample reached a temperature variation of 2°C at a mean soil temperature of 30°C. The same trend can be seen in both the dry and wet samples, but at a slightly cooler temperature (graphs in appendix).
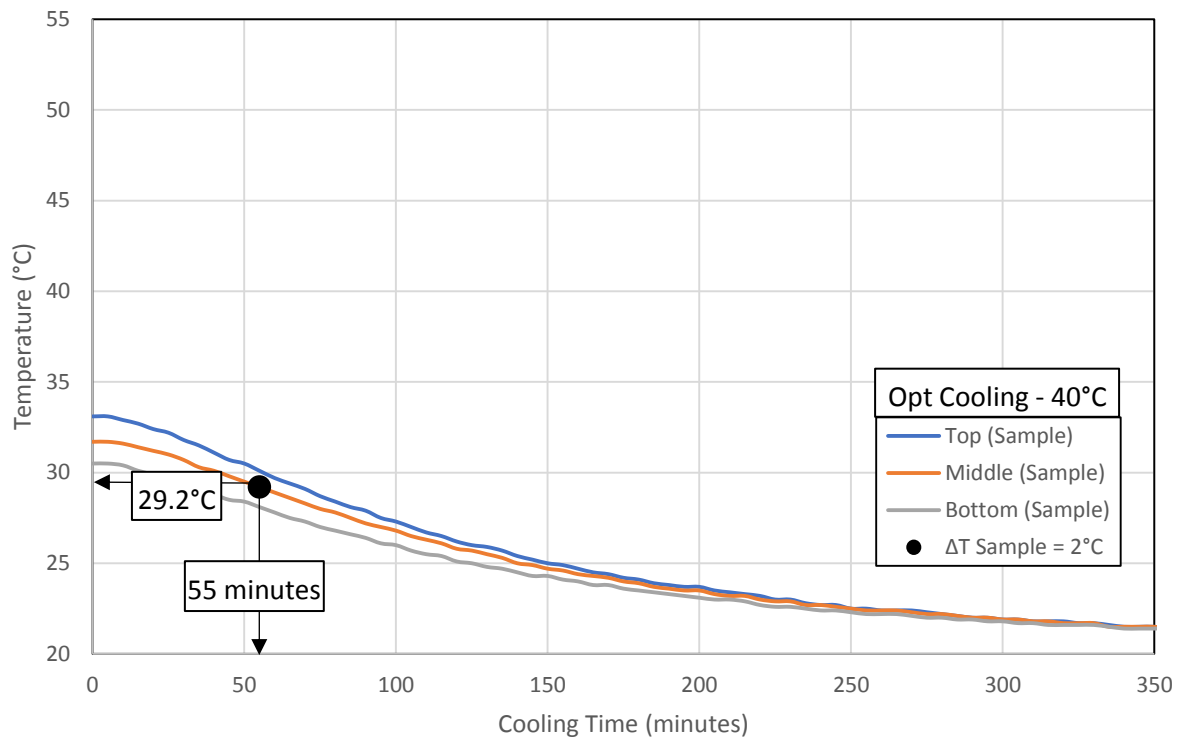

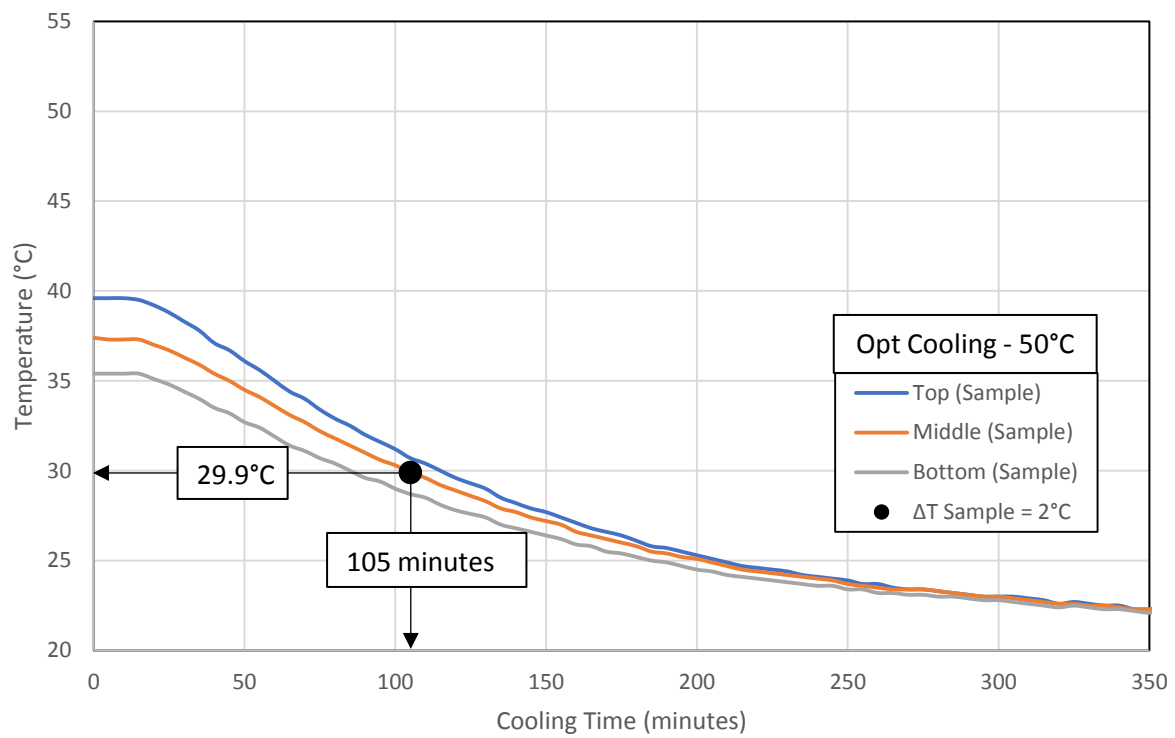Figure 4-24: Sample cooling for 40°C at 13.6% (optimum) moisture content

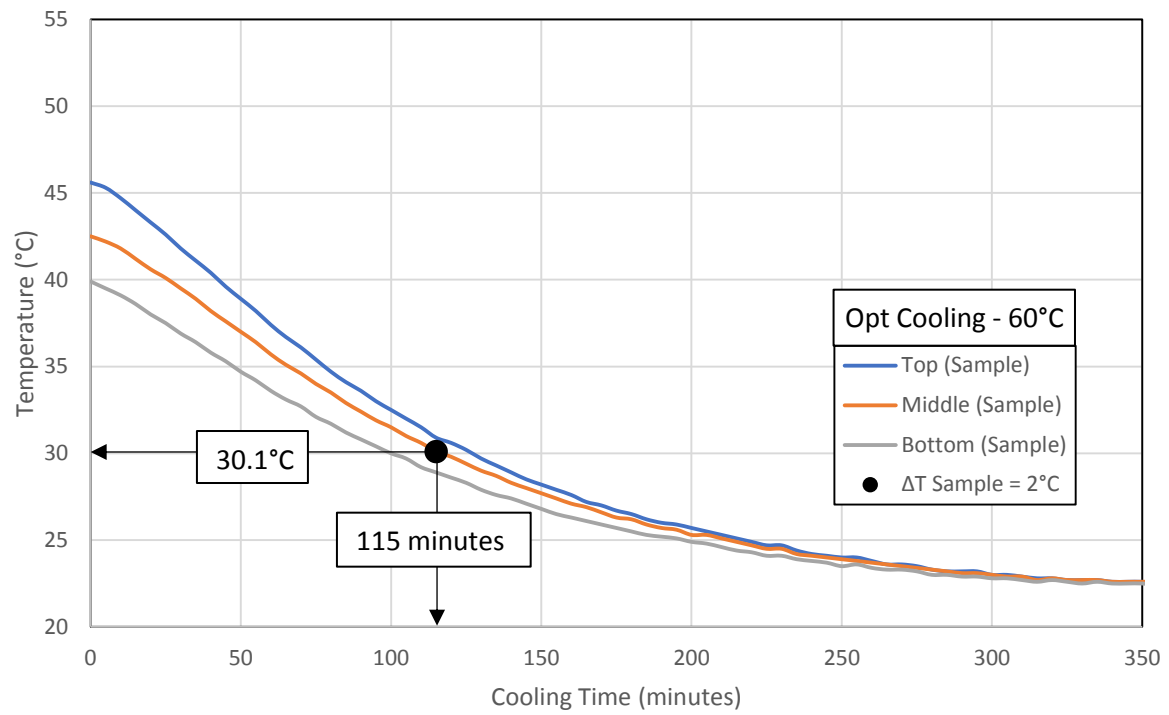Figure 4-25: Sample cooling for 50°C at 13.6% (optimum) moisture content

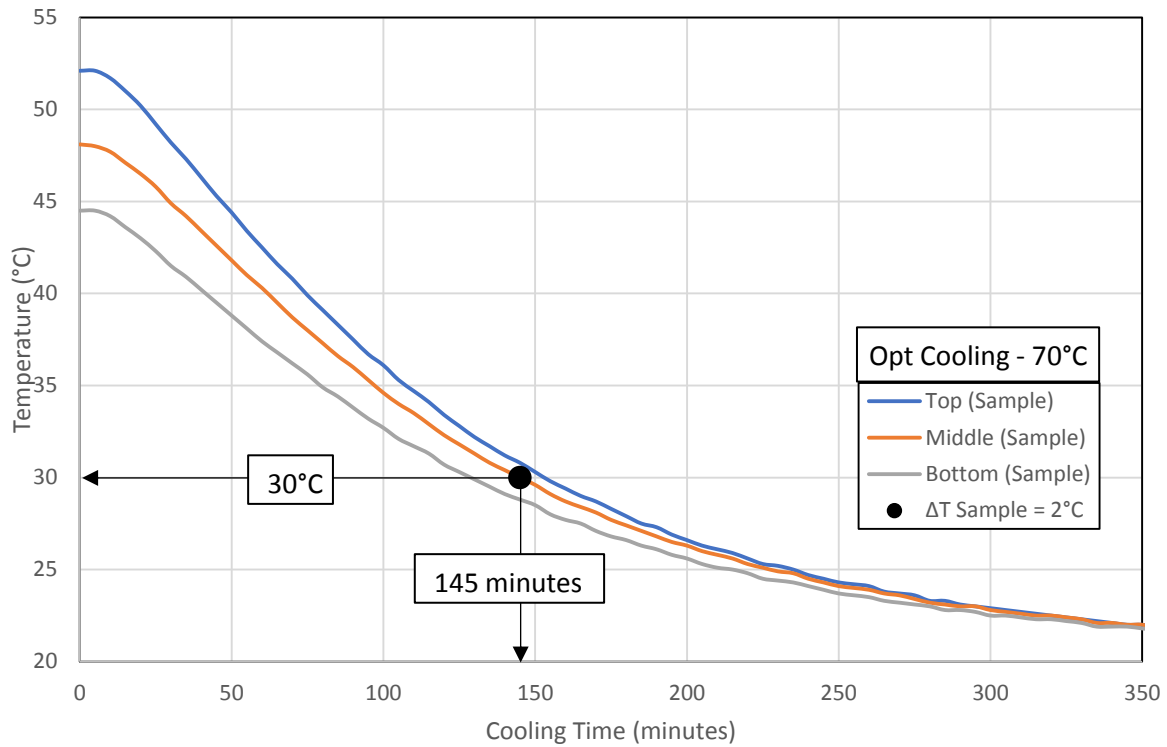Figure 4-26: Sample cooling for 60°C at 13.6% (optimum) moisture content

Figure 4-27: Sample cooling for 70°C at 13.6% (optimum) moisture content

Figure 4-28 shows change in temperature during cooling for 40, 50, 60, and 70°C for optimum moisture content. The graph shows that the same trend seen at a temperature variation of 2°C can also be seen at temperature variations of 3, 4, and 5°C. Despite initial temperatures, the samples reached a temperature variation of 2°C at an average soil temperature of 30°C, 3°C at an average soil temperature of 33°C, 4°C at an average soil temperature of 36.5°C, and 5°C at an average soil temperature of 39.5°C. This data suggests that while temperatures within the soil sample converge during cooling, the rate of convergence is dependent on the temperature difference between the hot air inside the chamber and the cooler air in the room. Initially the samples cool at a rapid rate immediately after the heating element inside the chamber is deactivated, however, as the temperature within the chamber cools to 22°C (room temperature)

the rate of cooling slows. Thus, performing resonant column tests when the temperature variation within the sample is 2°C would result in only performing tests at soil temperatures of 30°C.
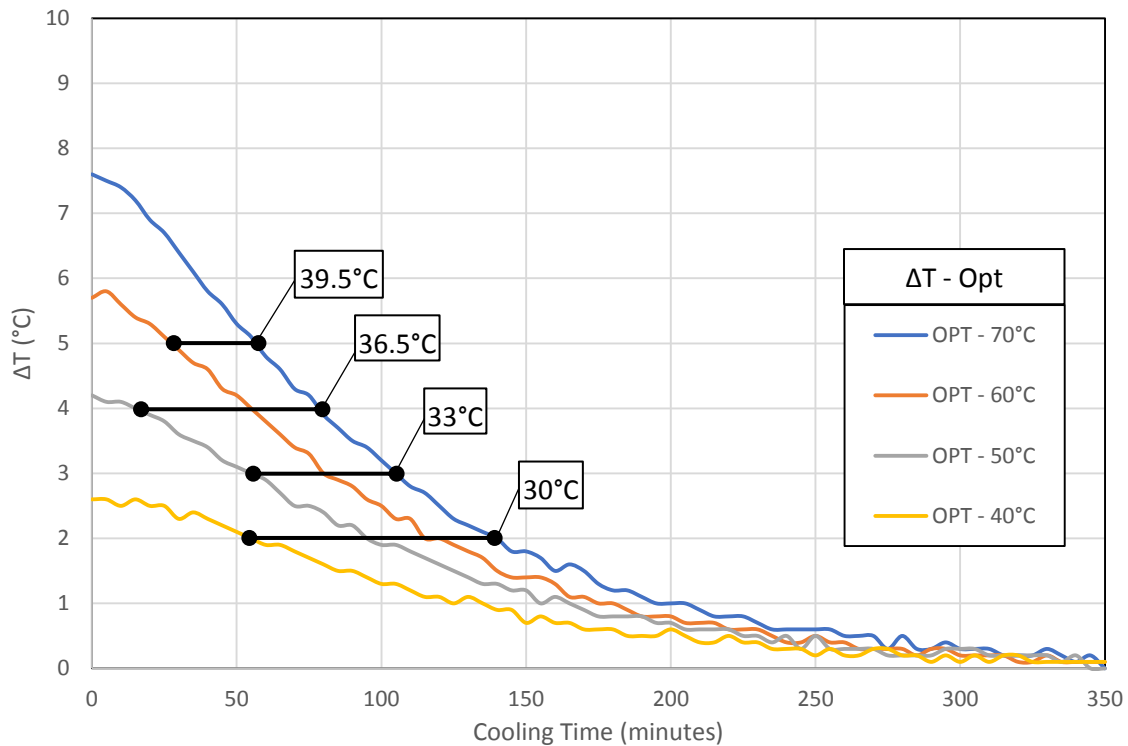

Figure 4-28: Change in temperature during cooling for 13.6% (optimum) moisture content

To visually depict the heating and cooling cycles shown in the graphs the Ti50 Fluke Thermal Imager previously described in chapter 3 was used to take infrared pictures of the heating chamber during heating and cooling, as well as a picture of the soil sample after heating. The figures show the progression of hot air in the chamber during heating and the convergence trend during cooling. The infrared picture of the soil sample is used to visually show the temperature variation during heating. In the infrared pictures, higher temperature areas show up as red and lower room temperature areas show up as blue. Figures 4-29 through 4-35 show images taken during the 70°C heating and cooling cycle of the wet sample.
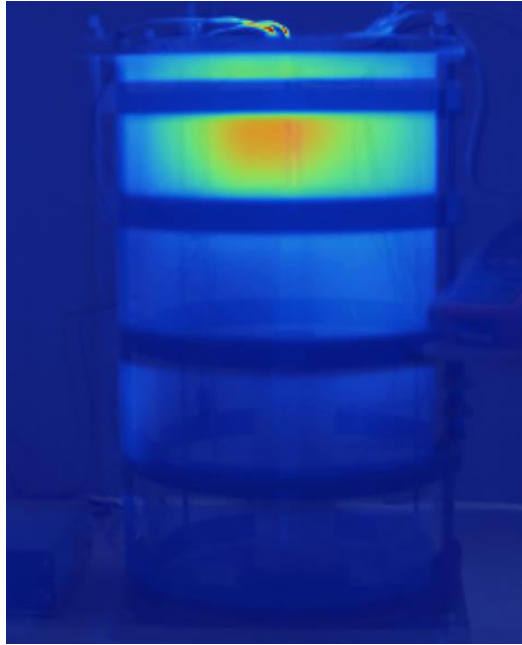
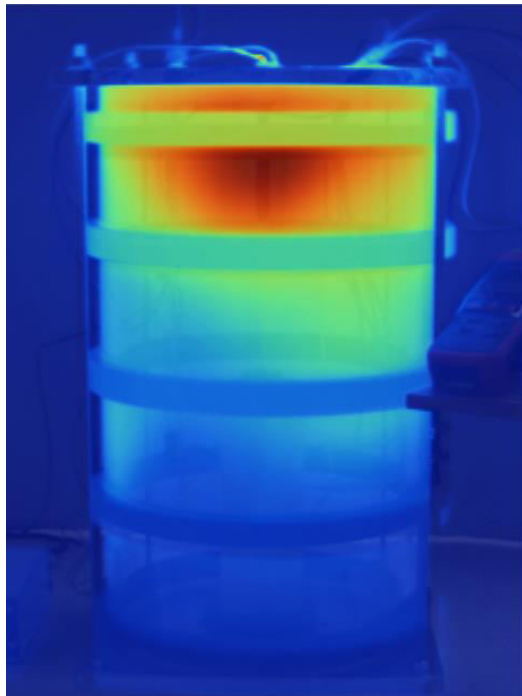Figure 4-29: Heating chamber immediately after being turned on (70°C)

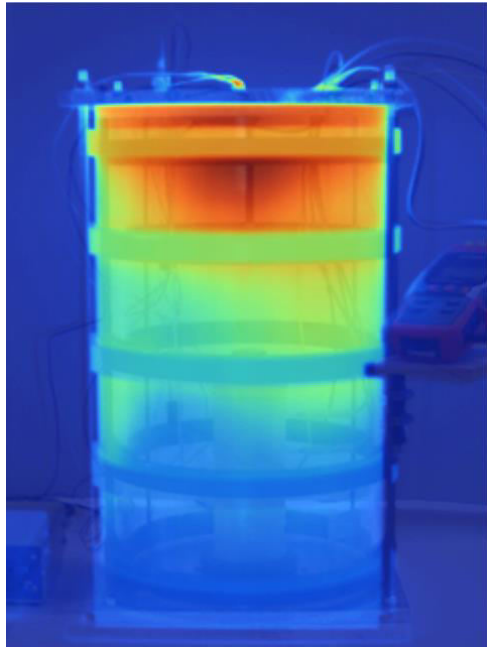Figure 4-30: Heating chamber 1 hour after being turned on (70°C)

Figure 4-31: Heating chamber 2 hours after being turned on (70°C)
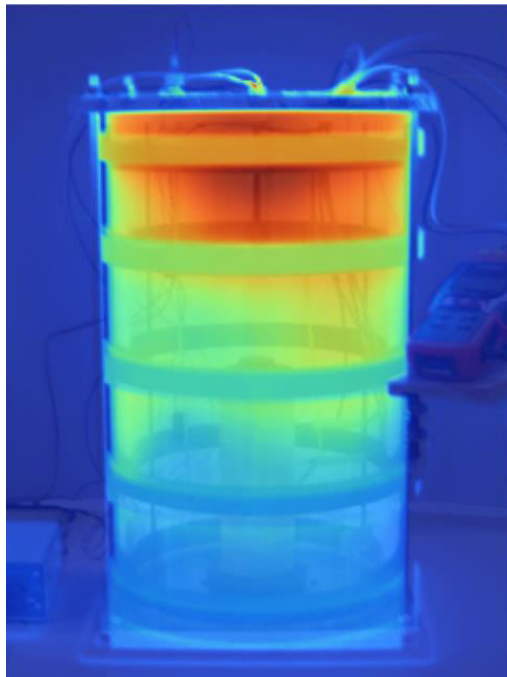

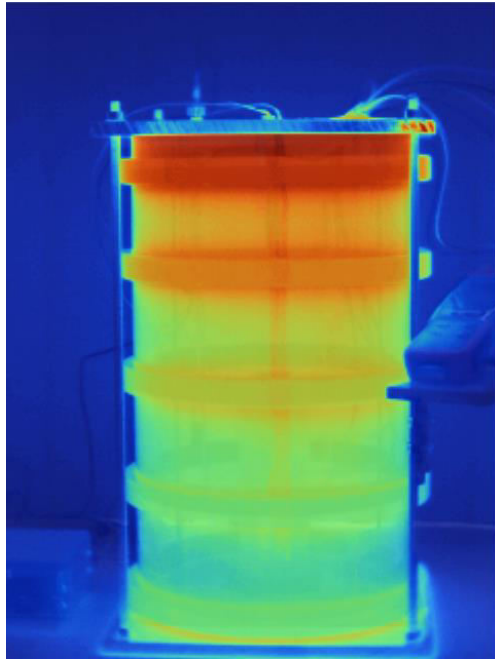Figure 4-32: Heating chamber 24 hours after being turned on (70°C)

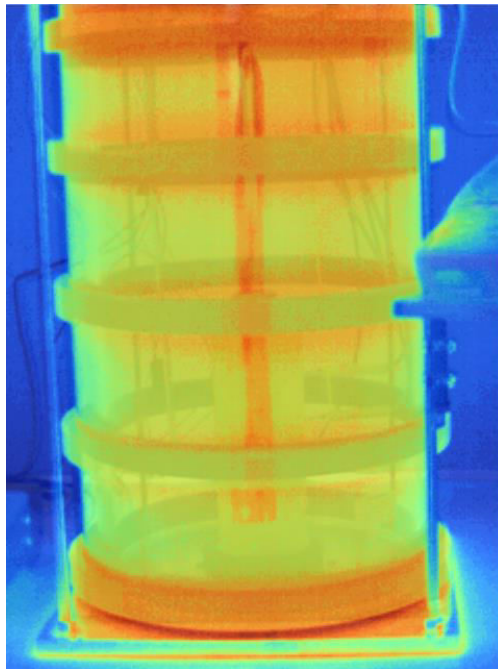Figure 4-33: Heating chamber 1 hour after shutting off

Figure 4-34: Heating chamber 2 hours after shutting off
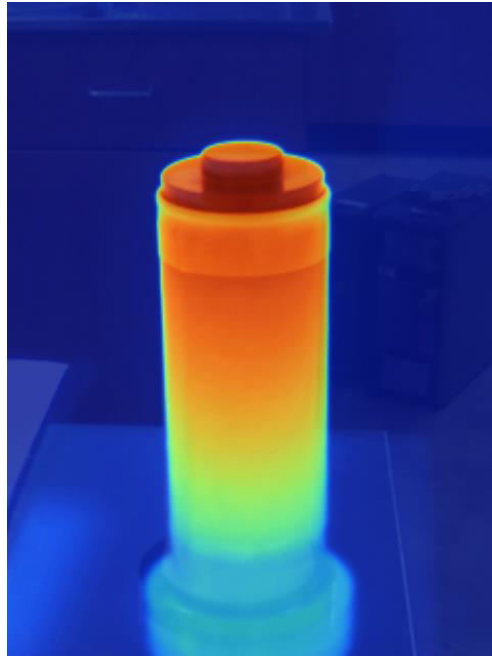
Figure 4-35: Soil sample compacted wet of optimum (17.6% moisture content) after 24 hours of heating (70°C)

Figure 4-36: Ti50 Fluke Thermal Imager

Comparing figures 4-29 through 4-32 shows that air temperature inside the chamber quickly peaks, however, increased heating time does not correlate to increased uniformity in heat distribution inside the chamber. Figures 4-33 and 4-34 show that air temperature becomes more uniform inside the chamber after the heat source has been shut off and the air temperature begins to equalize with the room temperature. Figure 4-35 visually depicts the temperature variation in the soil sample during heating.

Chapter 5

Preliminary Thermo-controlled Resonant Column Testing

5.1 - Introduction

Two preliminary resonant column tests were performed on a soil sample compacted at optimum water content (13.6% water content, 110.9 lb/ft^3 dry density). The sample was consolidated for 24 hours at 68 kPa (~10 psi) air pressure and 21.4°C (room temperature) before the first test. After testing, the sample continued to consolidate at 68 kPa for an additional 19 hours at 21.4°C before temperature of the heating element was set to 50°C. The sample was heated for five hours, allowing the soil to reach its peak temperature before a second resonant column test was performed. This chapter shows the thermo-controlled resonant column apparatus in figures 5-1 through 5-3 and results obtained from two preliminary tests in figures 5-9 through 5-13.

5.2 - Thermo-controlled resonant column device

Figure 5-1 shows the major components of the thermo-controlled resonant column system. The system consists of the GCTS TSH-100 resonant column chamber, GCTS SCON-1500 digital system controller, GCTS SR-DF-FO-250 signal controller, GCTS TSH-AMP2 motor controller, GCTS Fredlund SWCC Device (air pressure controller), and GCTS HTC-250 heat controller. Figure 5-1 depicts the entire thermo-controlled resonant column system. Figure 5-2 shows the internal components of the resonant column chamber. The resonant column chamber uses the same thermo controlling mechanisms shown in the calibration chamber. The Omega Type E thermocouple, 2 Orion 12V DC fans, and 2 120V heating elements are labeled in Figure 5-2. Figure 5-3 provides a closer look at the thermo-controlled resonant column chamber with the plexiglass cylinder in place.
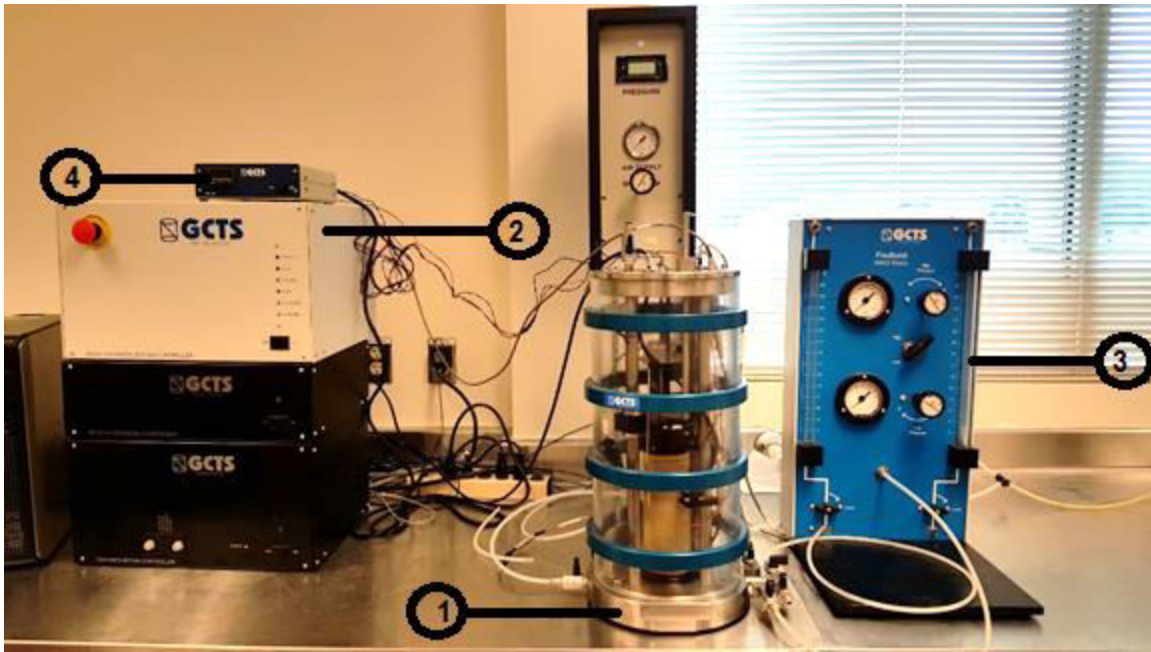
Figure 5-1: Thermo-controlled resonant column setup. 1) thermo-controlled RC chamber, 2) digital system, signal, and motor controllers, 3) confinement air pressure controller, 4) GCTS HTC-250 heat controller
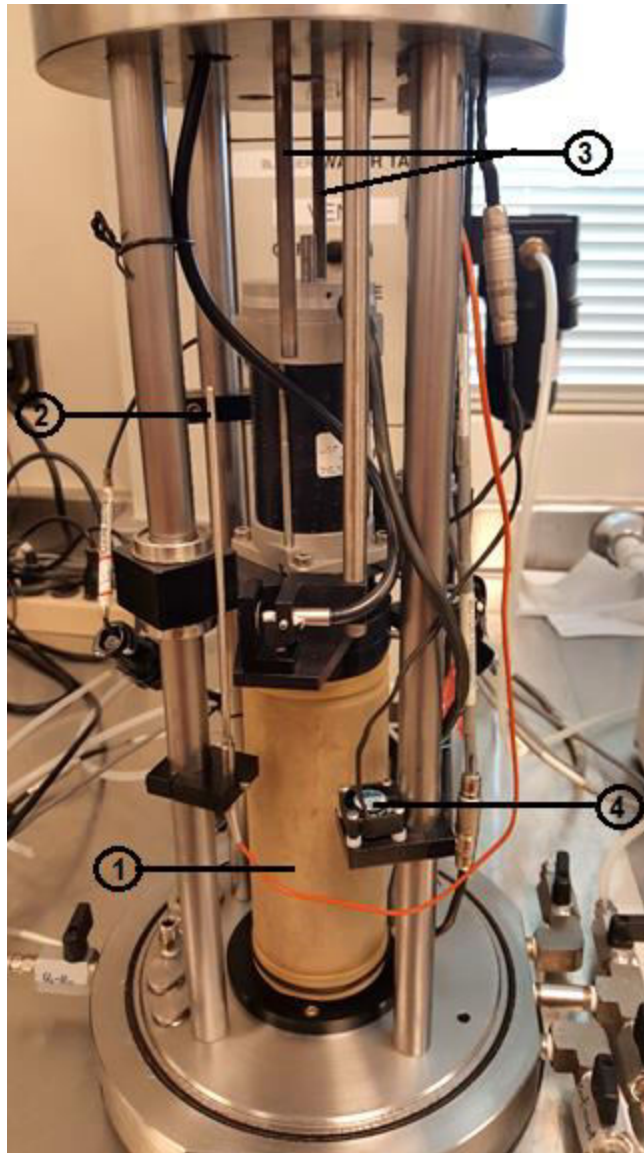
Figure 5-2: Internal components of thermo-controlled resonant column chamber. 1) soil sample, 2) Omega Type E thermocouple, 3) 2 120V heating elements, 4) 2 Orion 12V DC fans
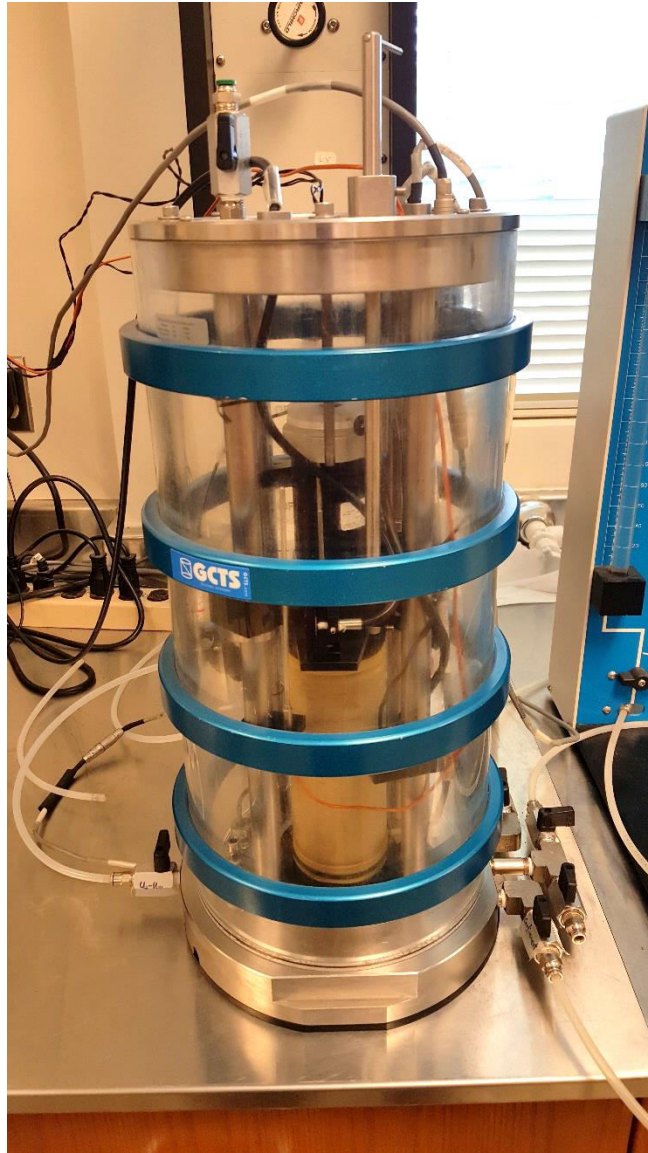
Figure 5-3: Thermo-controlled resonant column chamber during testing.

5.3 - Test Inputs and Variables

Both resonant column tests were performed on the same soil sample compacted at a target water content of 13.6% to a maximum dry density of 110.9 lb/ft^3. The sample was consolidated for 24 hours at a confinement pressure of 68 kPa and a temperature of 21.4°C as shown in Figure 5-4 prior to testing. After testing, the sample was consolidated for 19 additional hours at the same confinement pressure before a 5-hour period of heat application of 50°C under constant confinement. After heating, the second resonant column test was performed. As previously shown in Figure 4-6 and Figure 4-21 from chapter 4, the soil sample will have reached its peak temperature after four to five hours of heat application. For a source temperature of 50°C and a water content of 13.6% the middle of the soil sample is expected to have a temperature of 37°C with a variation of 4.2°C between the top and bottom of the sample. Input values for both tests are shown in Figure 5-5. A frequency increase from 10 to 280 Hz at a torque output amplitude of 10 pfs (percent of full scale) was used for both tests.

Figure 5-4: Resonant column confinement pressure gauge set to 68 kPa.
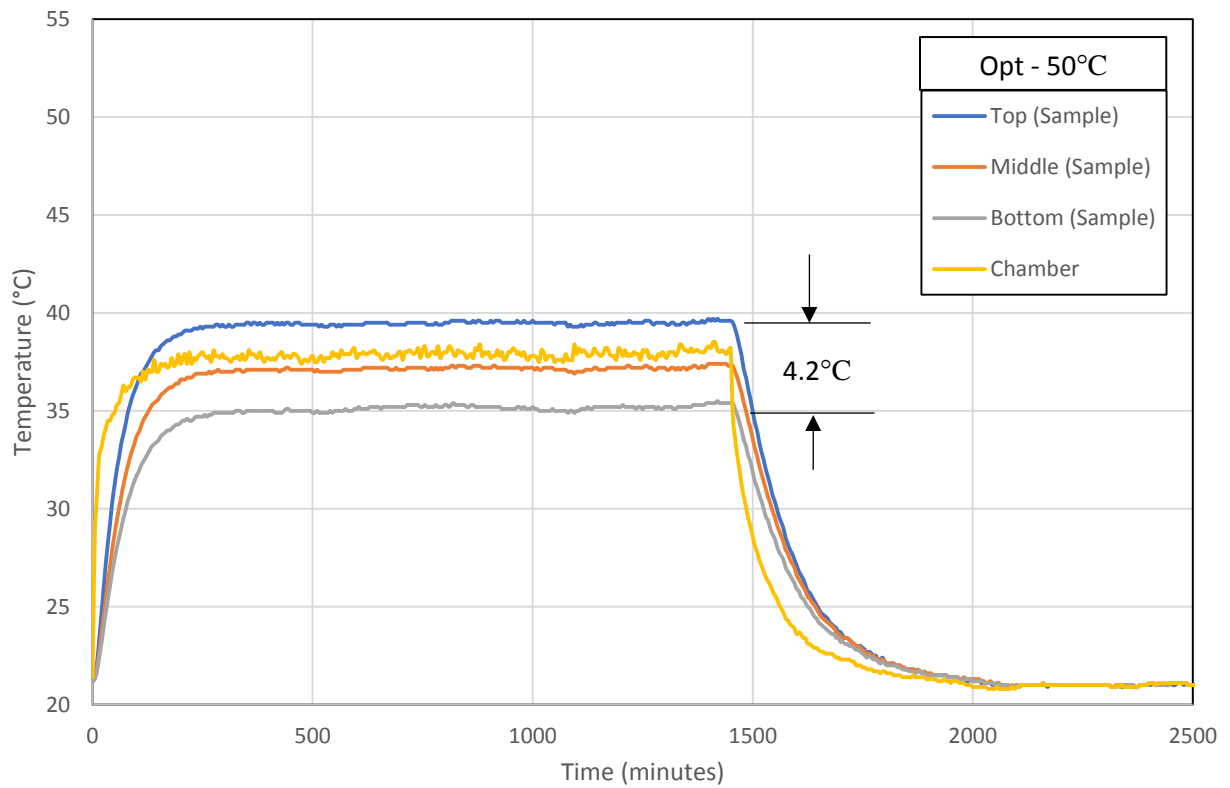
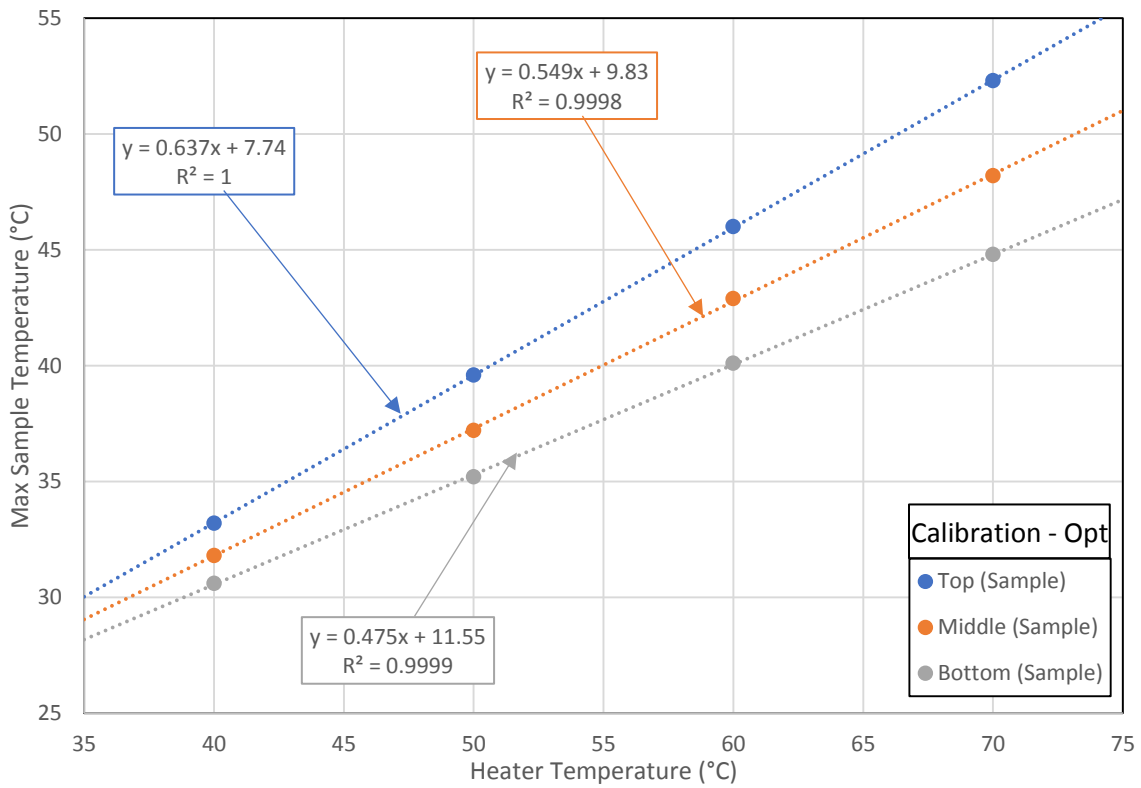Figure 4-6: Soil heating and cooling cycle for 50°C at 13.6% (optimum) water content

Figure 4-21: Heating chamber calibration for 13.6% (optimum) moisture content

Figure 5-5: Input values for resonant column tests

Figures 5-6 through 5-8 show proximitor and gauge deformation values obtained during consolidation. Figure 5-6 shows initial values prior to application of confinement pressure. Figure 5-7 shows a change of 0.43 mm in gauge deformation after 24 hours of 68 kPa confinement pressure prior to the first test at 21.4°C. Figure 5-8 shows a change of 0.02 mm in gauge deformation after an additional 24 hours of 68 kPa confinement pressure and temperature application prior to the second test at 37°C soil temperature (50°C source temperature).
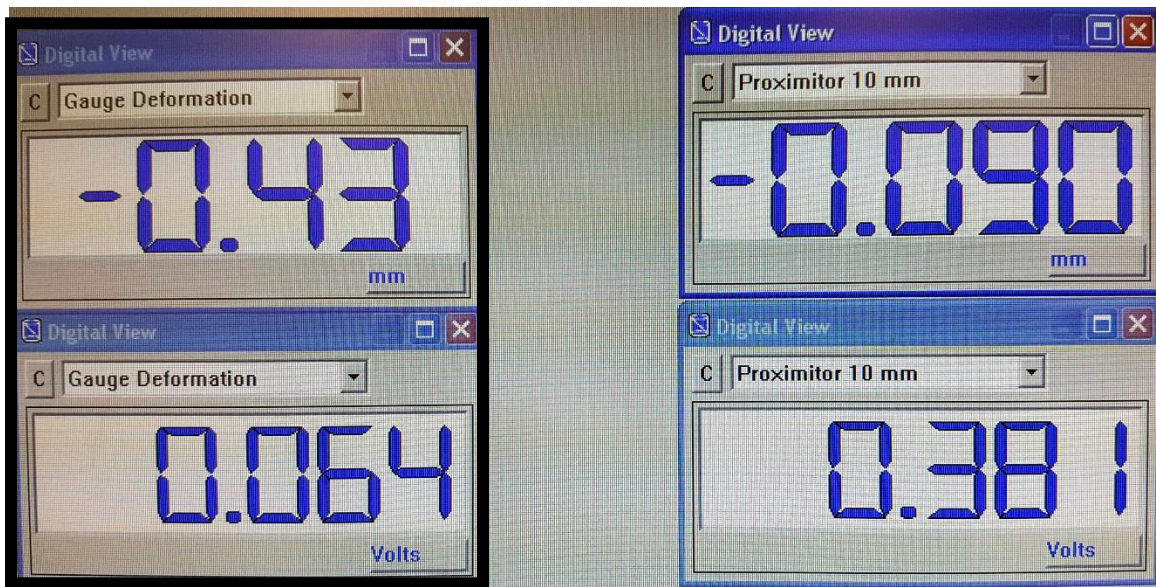

Figure 5-6: Initial proximitor and gauge deformation prior to consolidation
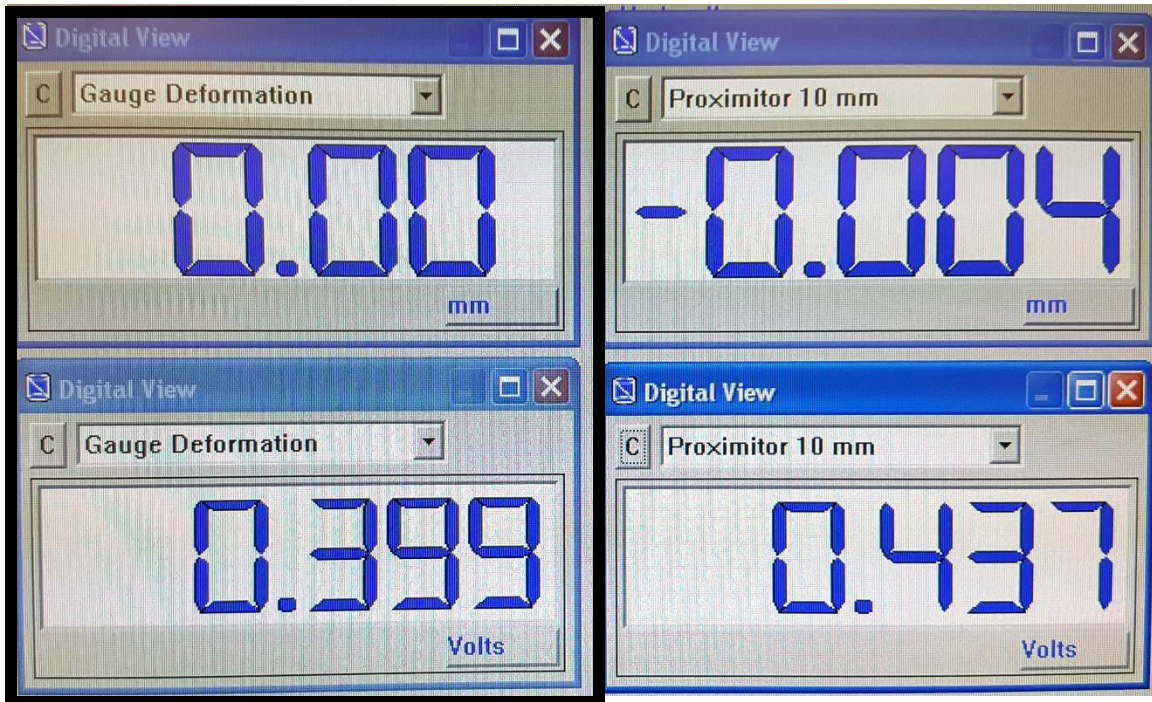
Figure 5-7: Proximitor and gauge deformation after 24-hour consolidation prior to first test
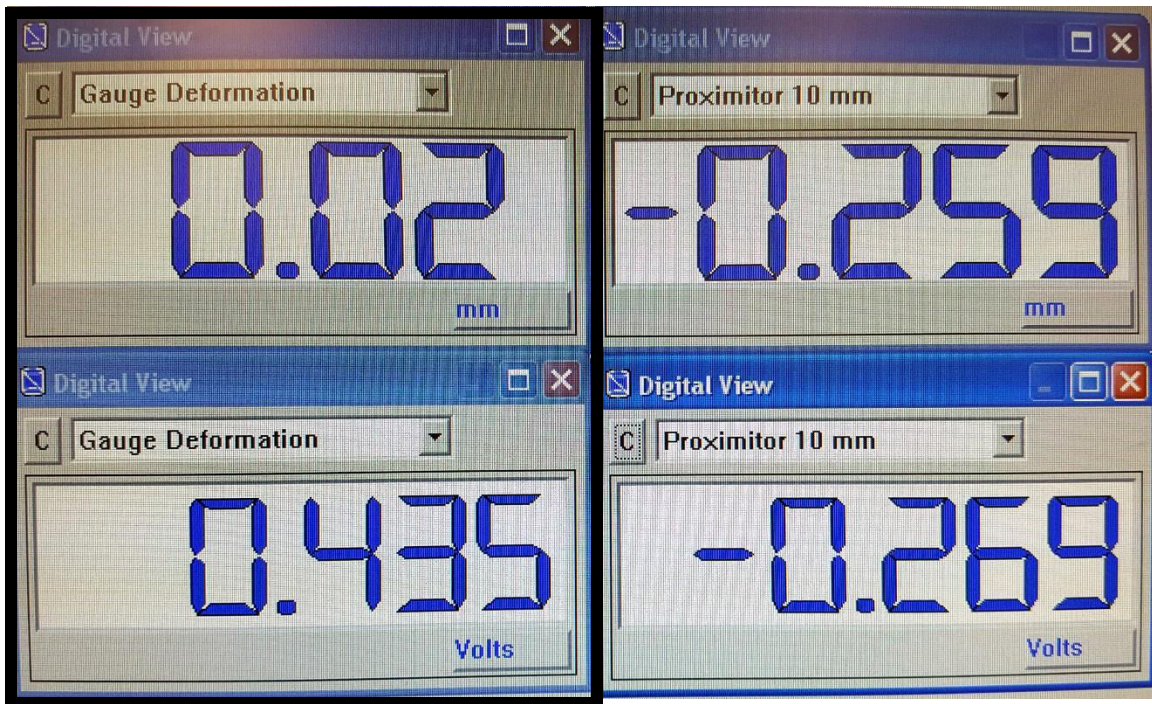
Figure 5-8: Proximitor and gauge deformation after 48-hour consolidation and 5-hour heat application prior to second test

5.4 - Preliminary Resonant Column Testing Results

Figures 5-9 through 5-11 show the results of the resonant column test at 68 kPa confinement and 21.4°C (room temperature). The damping ratio, D, was determined to be 11.5% from Figure 5-9 using the half power bandwidth method. Shear modulus, G, was output as 86.86 MPa. Figures 5-12 through 5-14 show the results of the resonant column test at 68 kPa confinement and 37°C (50°C source temperature). The damping ratio, D, was determined to be 9.25% from Figure 5-12 using the half power bandwidth method. Shear modulus, G, was output as 96.24 MPa. Heat application appeared to cause a decrease in damping ratio, D, and an increase in shear modulus, G.

Figure 5-9: Frequency sweep and damping ratio determination for 21.4°C
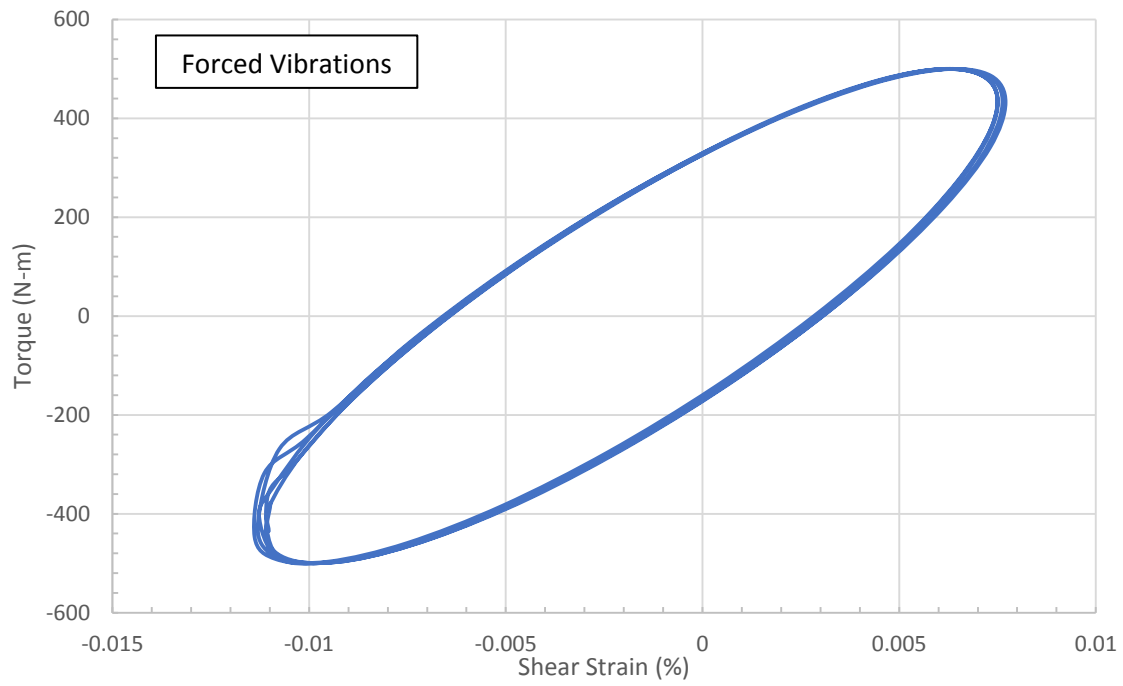
Figure 5-10: Shear Strain vs Torque (Forced vibrations) for 21.4°C

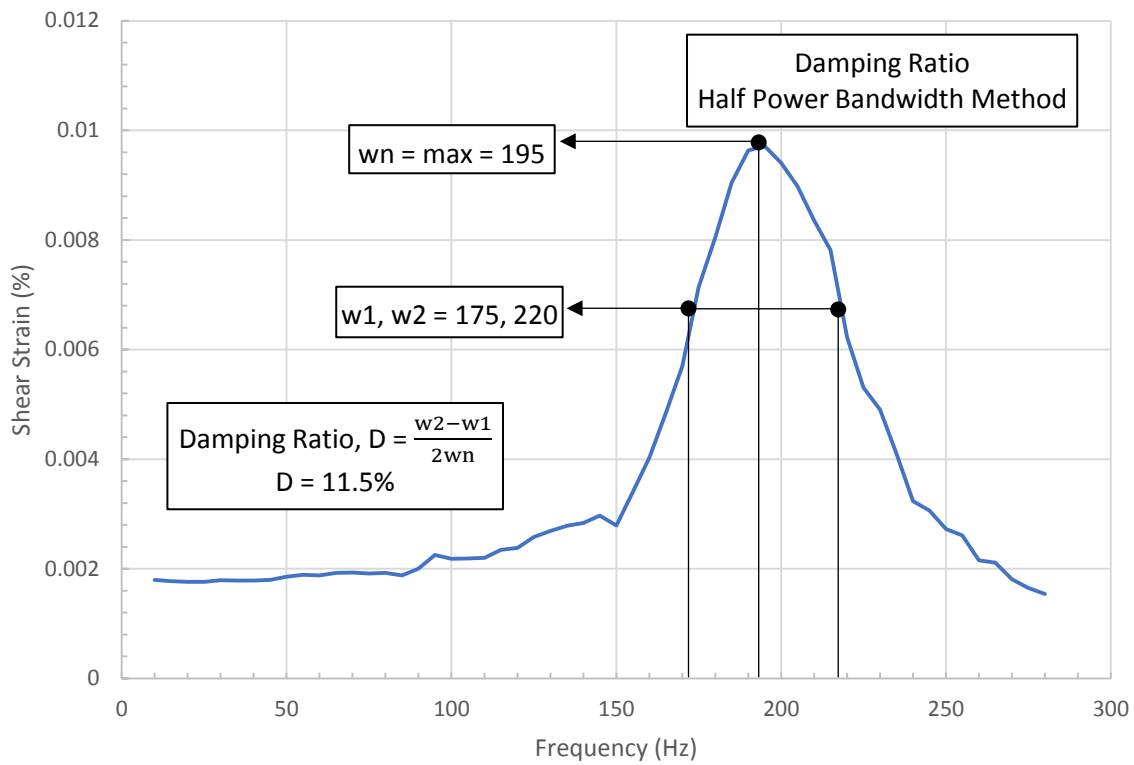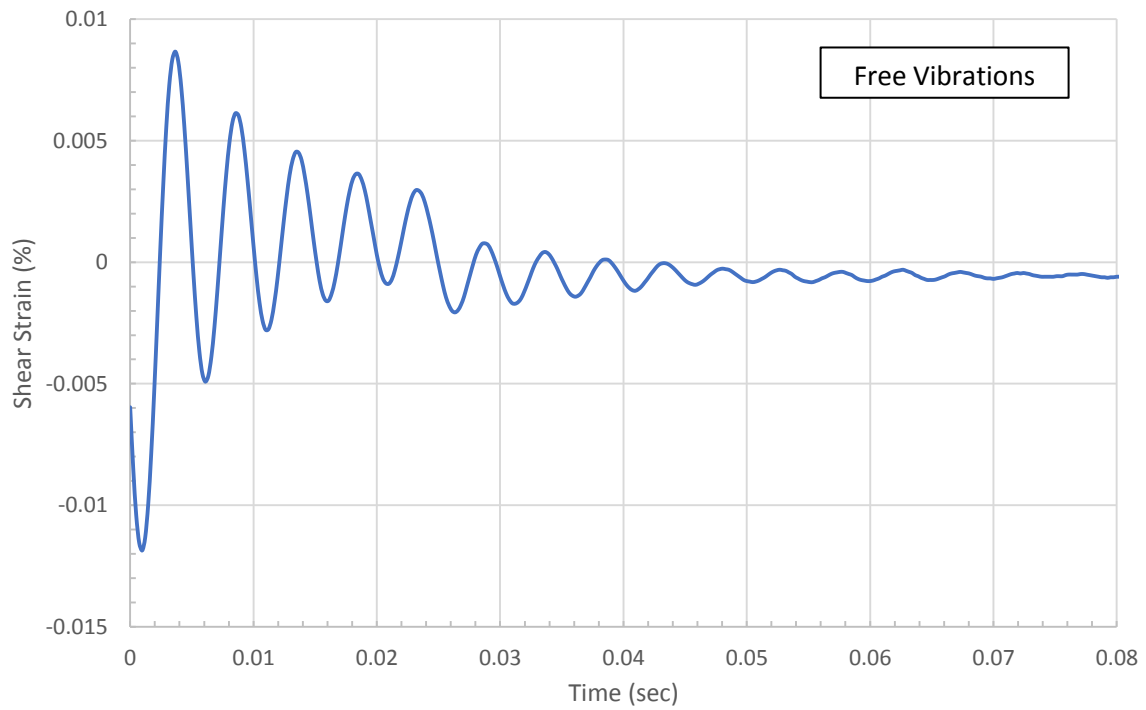Figure 5-11: Time vs Shear Strain (Free vibrations) for 21.4°C

97
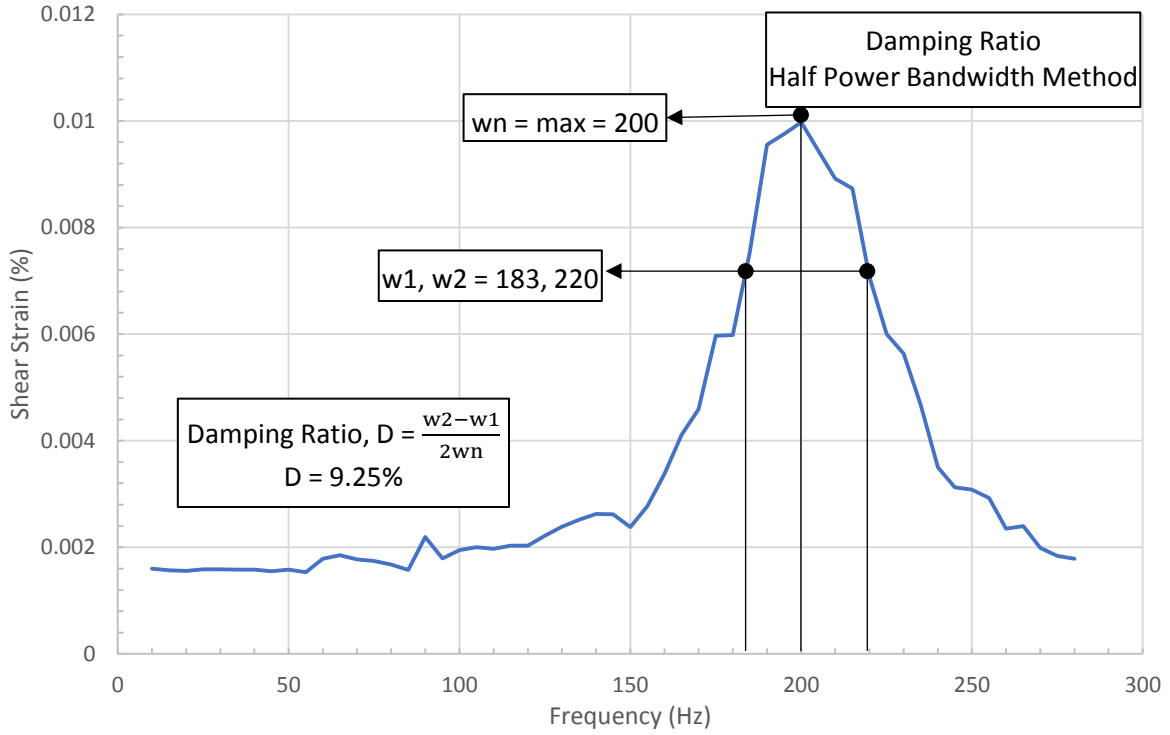
Figure 5-12: Frequency sweep and damping ratio determination for 37°C
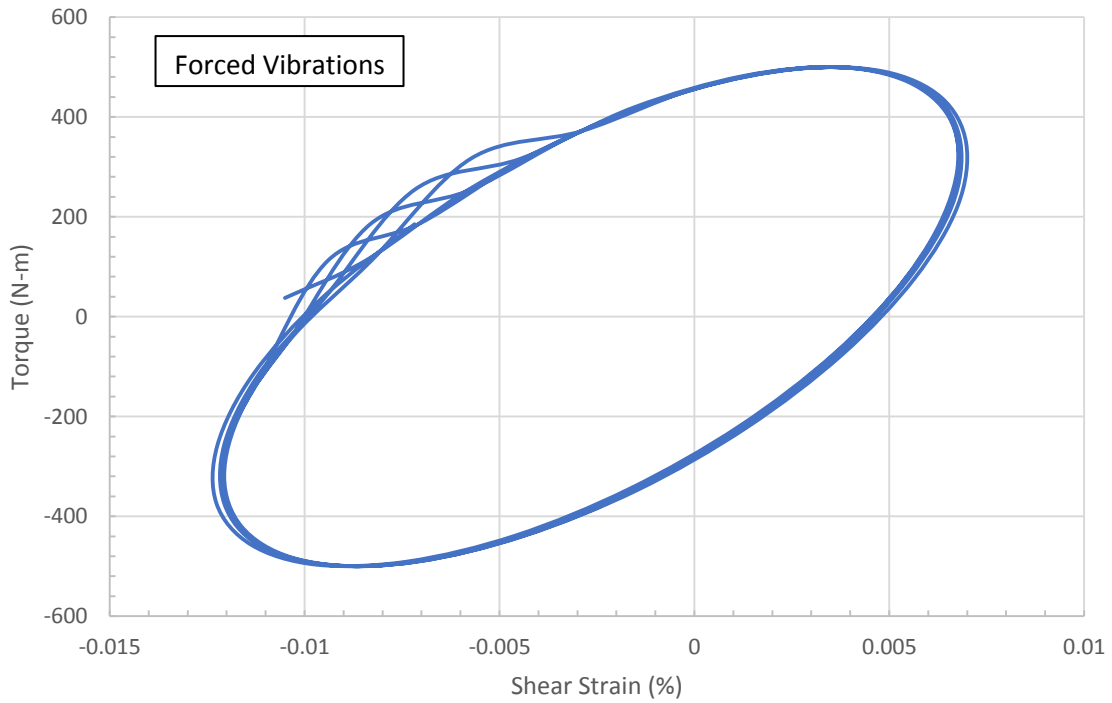
Figure 5-13: Shear Strain vs Torque (Forced vibrations) for 37°C
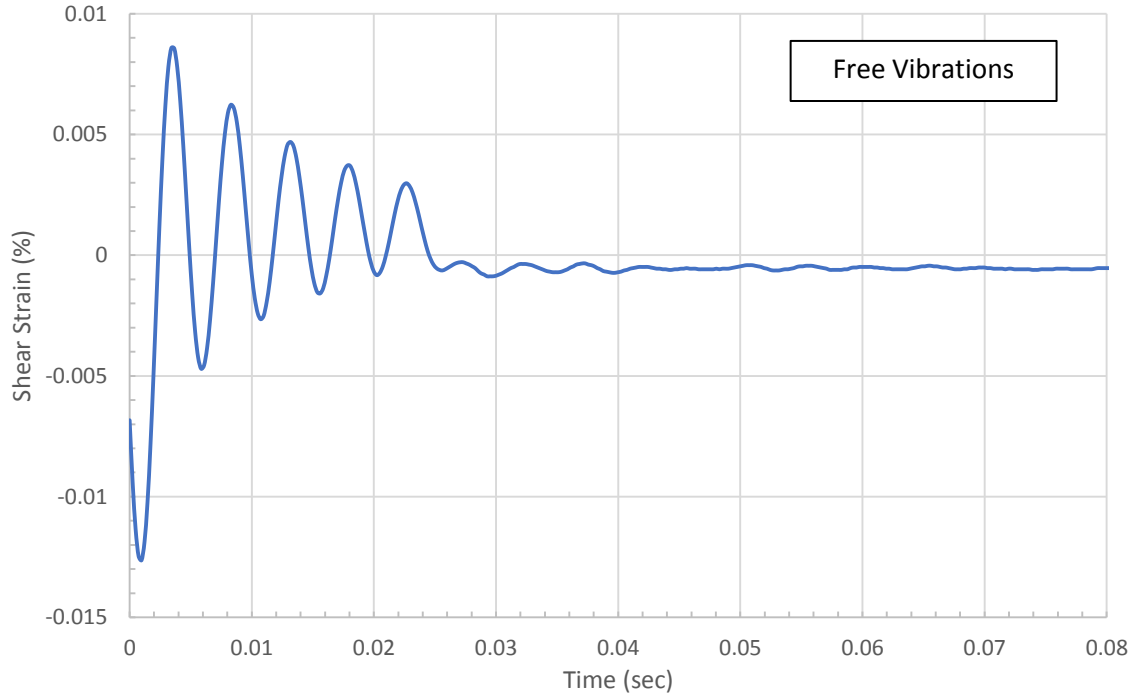
Figure 5-14: Time vs Shear Strain (Free vibrations) for 37°C

Tables 5-1 and 5-2 show moisture content calculations before compaction and after testing. As shown in Table 5-1, the target moisture content was 13.6%, however, the actual moisture content was slightly higher at 14.2%. Table 5-2 shows a moisture content of the sample after testing of 13.7%. A decrease in moisture content was observed. This decrease is more pronounced than decreases observed during calibration testing, possibly due to a thinner latex membrane used during resonant column testing. Table 5-3 summarizes the resonant column test results.

Table 5-1: Moisture content before compaction

Moisture Content Before Compaction			
Optimum, target = 13.6%			
Sample	1	2	3
Tare (g)	21.3	21.1	21.8
T+S (g)	43.2	40.9	49
T+S dry (g)	40.4	38.4	45.7
w%	14.6	14.4	13.8
avg	14.2		

Table 5-2: Moisture content after testing

Moisture Content After Testing			
Optimum, target = 13.6%			
Sample	Top	Middle	Bottom
Tare (g)	21.8	21	21.3
T+S (g)	44.8	38.6	52.8
T+S dry (g)	42	36.5	49
w%	13.9	13.5	13.7
avg	13.7		

Table 5-3: Resonant column test comparisons

Resonant Column Test Comparison		
	Test 1: 21.4°C	Test 2: 50°C
Mass (g)	1223.1	1223.1
Height (mm)	150	150
Diameter (mm)	72	72
Confinement (kPa)	68	68
Confinement Time (hr)	24	48
wn (Hz)	195	200
w1 (Hz)	175	183
w2 (Hz)	220	220
Damping Ratio (%)	11.5	9.25
Shear Modulus (MPa)	86.86	96.24

Chapter 6

Conclusions and Recommendations

6.1 – Summary

Geothermal power is a growing trend in green energy with steady annual increases both in the United States and internationally. However, efficient geothermal energy generation requires high underground temperatures, usually facilitated by hot steam and water reservoirs. The areas of the highest underground temperatures are located primarily in the western United States where thin layers in the earth's crust and tectonic plate boundaries let heat through. California and Nevada are two of the three most earthquake prone states and therefore are highly desirable candidates for geothermal energy. Earthquakes cause movement in the layers of the earth's crust, allowing heated water to circulate more freely, making the energy generation process easier.

On a smaller scale, geothermal pile use in foundation design is also increasing. LEED or leadership in energy and environment design is a rating system established by the United States Green Building Council, which rewards credits based on sustainable design practices. Geothermal piles meet the criteria for a credit and provide an efficient method for incorporating sustainable practices into foundations. Geothermal piles function as part of a ground source heat pump system, using the constant temperature zone below the surface for more efficient heating and cooling.

Despite the benefits of geothermal energy, the increase in soil temperature especially in earthquake prone areas creates new design challenges. Effects of temperature on strength properties of soil are well documented. Most studies report thermal softening trends with increasing temperatures causing a decrease in preconsolidation pressure and shear strength. However, the same comprehensive research has not been conducted on the stiffness properties of soil, such as, damping ratio, D, and shear modulus, G, under elevated temperatures.

To evaluate the stiffness properties of soil under elevated temperatures a GCTS TSH-100 resonant column device was outfitted with a GCTS HTC-250 heat controller to allow thermo-

controlled testing. However, prior to testing, thermo calibration of the resonant column chamber is required. Because the resonant column chamber is designed to hold air pressure, there are no openings for thermocouple probes to monitor air and soil temperature. Therefore, a similar chamber was designed for the sole purpose of thermo calibration. The new chamber was outfitted with the same heating mechanism and allowed for constant monitoring of soil and air temperature inside the device.

Prior to thermo calibration, soil classification and standard proctor tests were performed to obtain soil properties and compaction curve. After classification, heating and cooling cycles of 40, 50, 60, and 70°C were performed on samples of varying water contents and dry densities. Thermo calibration data was used to perform preliminary thermo-controlled resonant column tests.

6.2 - Conclusions

Based on the experimental data and analyses presented, the following conclusions can be made:

1. Heat distribution inside the thermo-controlled chamber is not uniform. The heating system is located at the top of the chamber and the fans are not powerful enough to circulate the heated air evenly throughout the chamber. Therefore, the air temperature is higher near the top and lower near the bottom. This same trend is evident in the soil samples. The top of the soil sample experiences a higher temperature than the bottom.

2. The temperature variation inside the soil sample increases as the temperature of the heating elements increases, from 2.5°C at 40°C to 7.5°C at 70°C. This trend can be seen in figures 4-5 through 4-8.

3. Samples compacted at optimum moisture content (13.6%) and maximum dry density (110.9 lb/ft^3) reached higher peak temperatures and experienced less temperature

variation than samples compacted at moisture contents lower (9.9%) or higher

(17.6%) than optimum. These trends can be seen in figures 4-9 through 4-20.

4. Heat transfers well between the heated air inside the chamber and the soil. At similar

    elevations inside the chamber, the temperature of the air is within 1-2°C of the

    temperature of the soil.

5. Soil temperatures peak and become steady near the 5-hour mark during heating.

6. The relationship between peak soil temperature and heating element temperature

    appears to be linear, allowing for accurate soil temperature prediction despite the

    chamber temperature not being uniform. Figures 4-21 through 4-23 show

    temperature calibration curves and linear heating trends.

7. Soil temperatures converge, and temperature variation decreases during cooling.

    Cooling trends and decrease in temperature variation is shown in Figures 4-24

    through 4-28. Despite temperature variation decreasing during cooling, the

    temperature variation does not equalize at a high enough temperature for cooling to

    be considered a viable method for obtaining a uniform temperature in the soil sample

    prior to testing.

8. Preliminary resonant column testing showed a decrease in damping ratio, D, from

    11.5% to 9.25% during heating and an increase in shear modulus, G, from 86.86

    MPa to 96.24 MPa. These results indicate an increase in soil stiffness during heating.

    More thorough thermo-controlled resonant column testing is required to fully

    understand the effect elevated temperatures has on the stiffness properties of soil.

6.3 – Recommendations

The following recommendations are made to improve the thermo calibration chamber and

resonant column chamber to provide more uniform heat distribution and better test results:

1. A more uniform heat distribution inside the calibration chamber and inside the

    resonant column chamber is achievable. The location of the heating elements inside

the chambers is suboptimal. The heating elements would be more effective if they were located near the bottom of the chamber, closer to the soil sample. If moving the heating elements is problematic, more powerful fans could be used to provide greater air circulation.

2. Only two resonant column tests were performed during preliminary testing. More thorough testing at different temperatures and varying moisture contents is necessary to fully understand the effects of temperature on stiffness properties of soil.

3. A testing schedule should be outlined prior to resonant column testing to ensure similar consolidation and heating time of each sample to eliminate as many variables as possible.

References

[1]   Alsherif, N. A., & Mccartney, J. S. (2015). Yielding of Silt at High Temperature and Suction Magnitudes. *Geotechnical and Geological Engineering,34*(2), 501-514. doi:10.1007/s10706-015-9961-x

[2]   Ashmawy, A. K.; Salgado, R.; Guha, S.; and Drnevich, V. P. (1995). Soil Damping and Its Use in Dynamic Analyses. *International Conferences on Recent Advances in Geotechnical Earthquake Engineering and Soil Dynamics. 9*. http://scholarsmine.mst.edu/icrageesd/03icrageesd/session01/9

[3]   Cekerevac, C., & Laloui, L. (2004). Experimental study of thermal effects on the mechanical behaviour of a clay. *International Journal for Numerical and Analytical Methods in Geomechanics,28*(3), 209-228. doi:10.1002/nag.332

[4]   Cekerevac, C., Laloui, L., & Vulliet, L. (2005). A Novel Triaxial Apparatus for Thermo-Mechanical Testing of Soils. *Geotechnical Testing Journal,28*(2), 161-170. doi:10.1520/gtj12311

[5]   Ghasemi-Fare, O., & Basu, P. (2016). Predictive assessment of heat exchange performance of geothermal piles. *Renewable Energy,86*, 1178-1196. doi:10.1016/j.renene.2015.08.078

[6]   Lanzo, G., & Vucetic, M. (1999). Effect of Soil Plasticity on Damping Ratio at Small Cyclic Strains. *Soils And Foundations,39*(4), 131-141. doi:10.3208/sandf.39.4_131

[7]   Matek, Benjamin. (2013). 2013 Annual US Geothermal Power Production and Development Report. Geothermal Energy Association. http://geo-energy.org/reports.aspx

[8]   Matek, Benjamin. (2013). 2013 Geothermal Power: International Market Overview. Geothermal Energy Association. http://geo-energy.org/reports.aspx

[9]   Matek, Benjamin. (2016). 2016 Annual US & Global Geothermal Power Production Report. Geothermal Energy Association. http://geo-energy.org/reports.aspx

[10]   Olgun, Guney & Ozudogru, Tolga & Abdelaziz, Sherif & Senol, Aykut. (2015). Long-term performance of heat exchanger piles. *Acta Geotechnica*. 10. 553-569. doi:10.1007/s11440-014-0334-z.

[11]   Perpetual Industries Inc. Everything that rotates needs to be balanced. (2011, November 21). Retrieved June, 2018, from http://www.xyobalancer.com/xyo-balancer-blog/material_damping_ratio_measurement

[12]   Rubio, Carles & Josa, Ramon & Ferrer, F. (2008). Thermal properties as a function of water content in a silt porous media under laboratory conditions. *15th International Congress of ISCO*. ResearchGate.

[13]   Stewart, Jonathan & Afshari, Kioumars & Hashash, Y.M.A.. (2014). Guidelines for performing hazard-consistent one-dimensional ground response analysis for ground motion prediction. ResearchGate

[14]   Tang, A., Cui, Y., & Barnel, N. (2007). A New Isotropic Cell for Studying the Thermo-Mechanical Behavior of Unsaturated Expansive Clays. *Geotechnical Testing Journal,30*(5), 341-348. doi:10.1520/gtj100623

[15]   Uchaipichat, A., & Khalili, N. (2009). Experimental investigation of thermo-hydro-mechanical behaviour of an unsaturated silt. *Géotechnique,59*(4), 339-353. doi:10.1680/geot.2009.59.4.339

[16]   Vassallo, R., Mancuso, C., & Vinale, F. (2007). Effects of net stress and suction history on the small strain stiffness of a compacted clayey silt. *Canadian Geotechnical Journal,44*(4), 447-462. doi:10.1139/t06-129

[17]   Vucetic, M., & Dobry, R. (1991). Effect of Soil Plasticity on Cyclic Response. *Journal of Geotechnical Engineering,117*(1), 89-107. doi:10.1061/(asce)0733-9410(1991)117:1(89)

Appendix

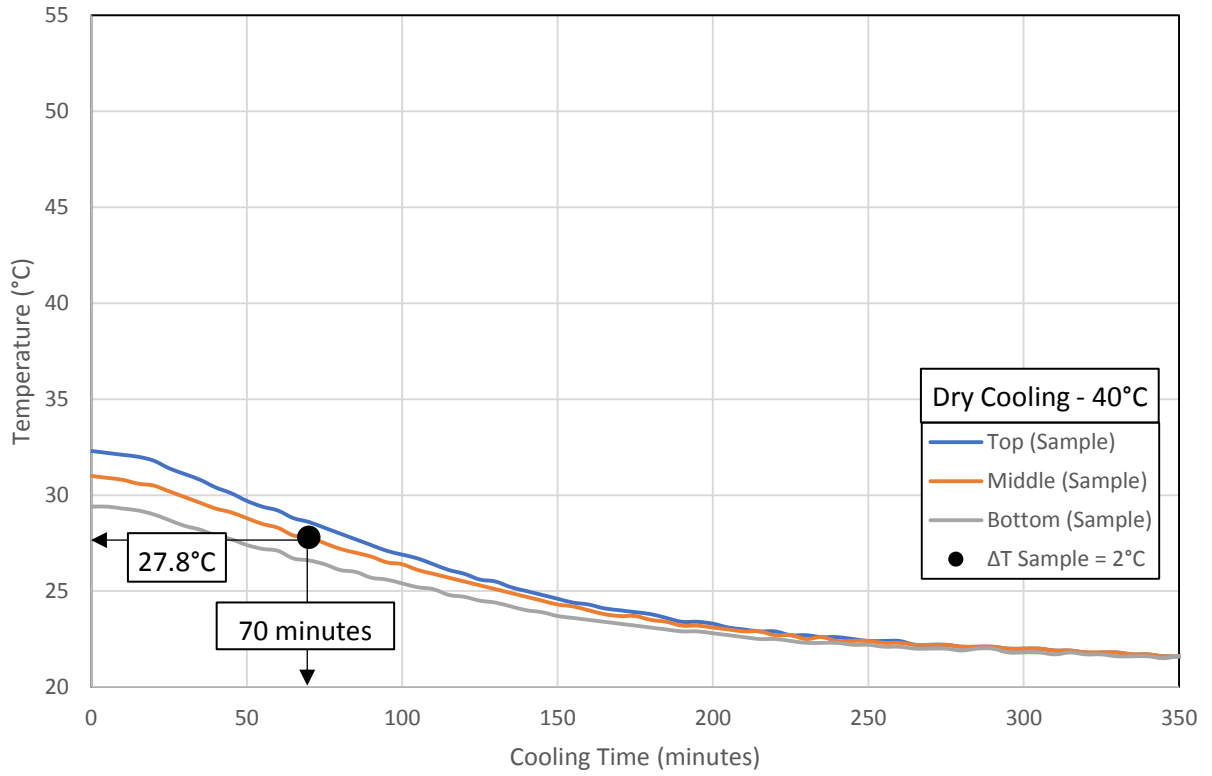Cooling trends for 9.9% (dry) and 17.6% (wet) moisture content

Figure A-1: Sample cooling for 40°C at 9.9% (dry) moisture content
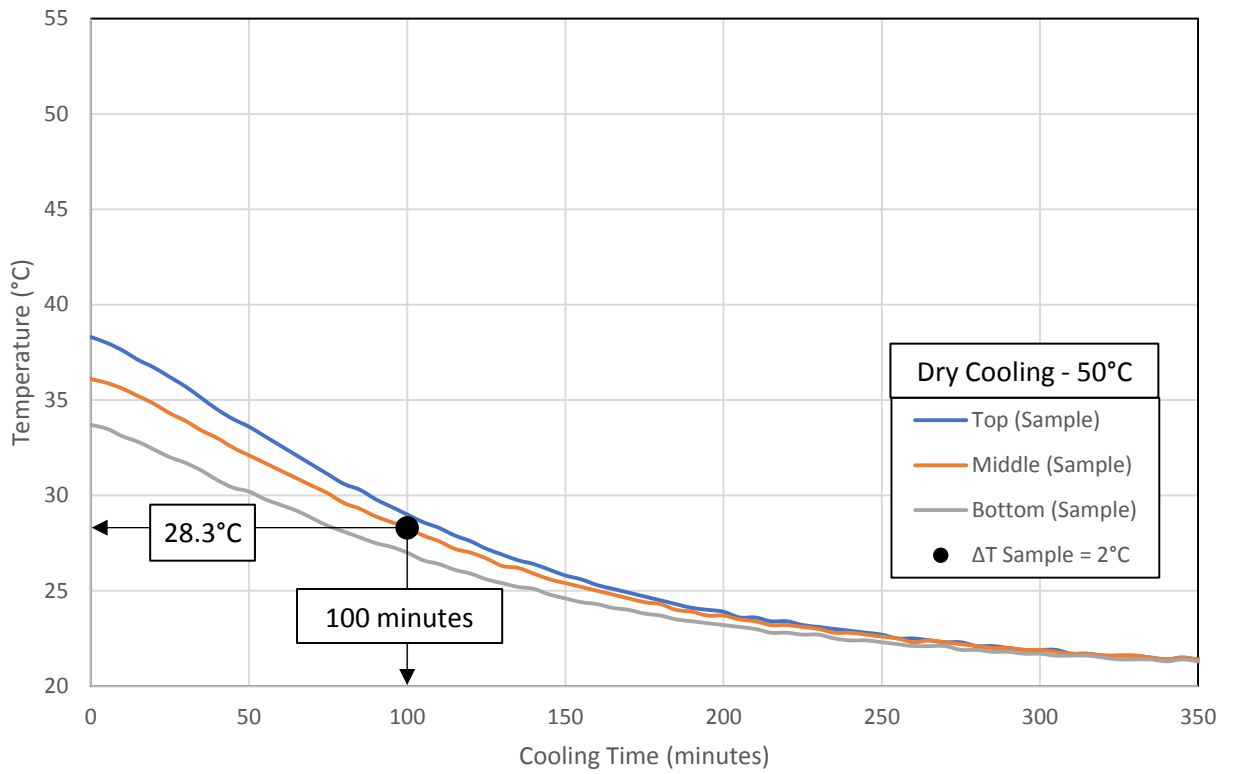
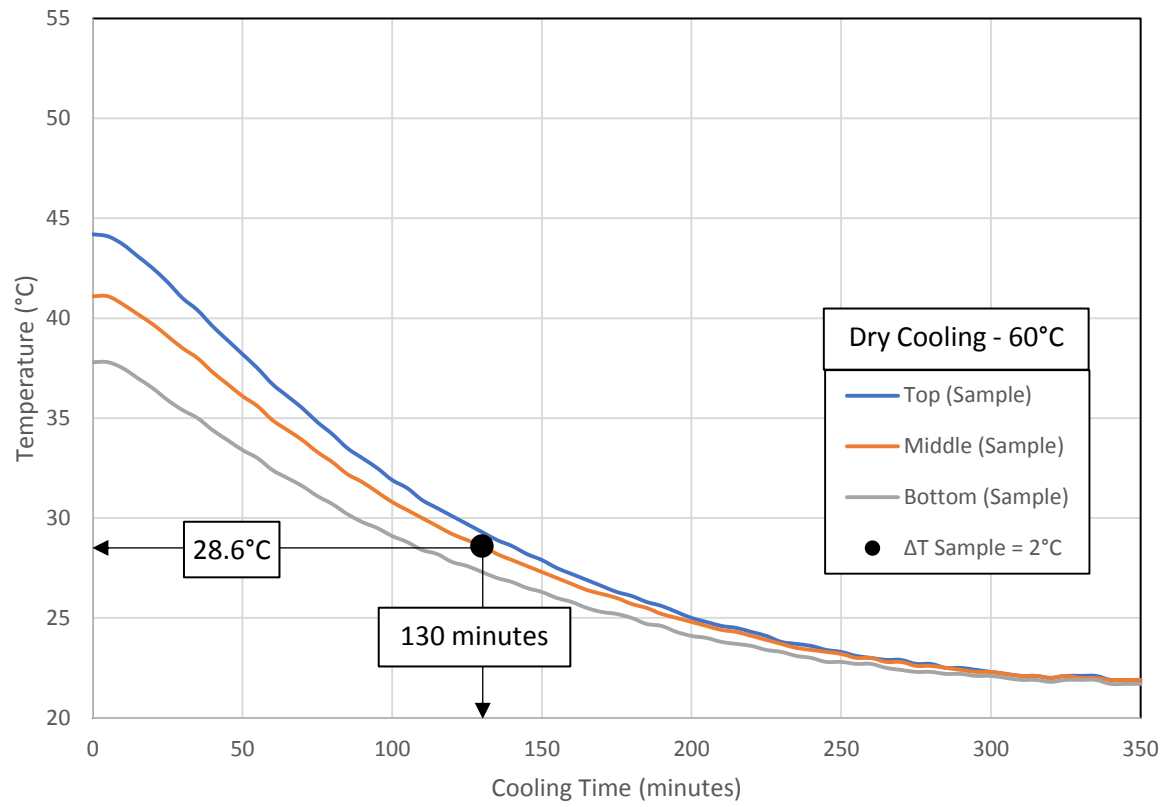Figure A-2: Sample cooling for 50°C at 9.9% (dry) moisture content

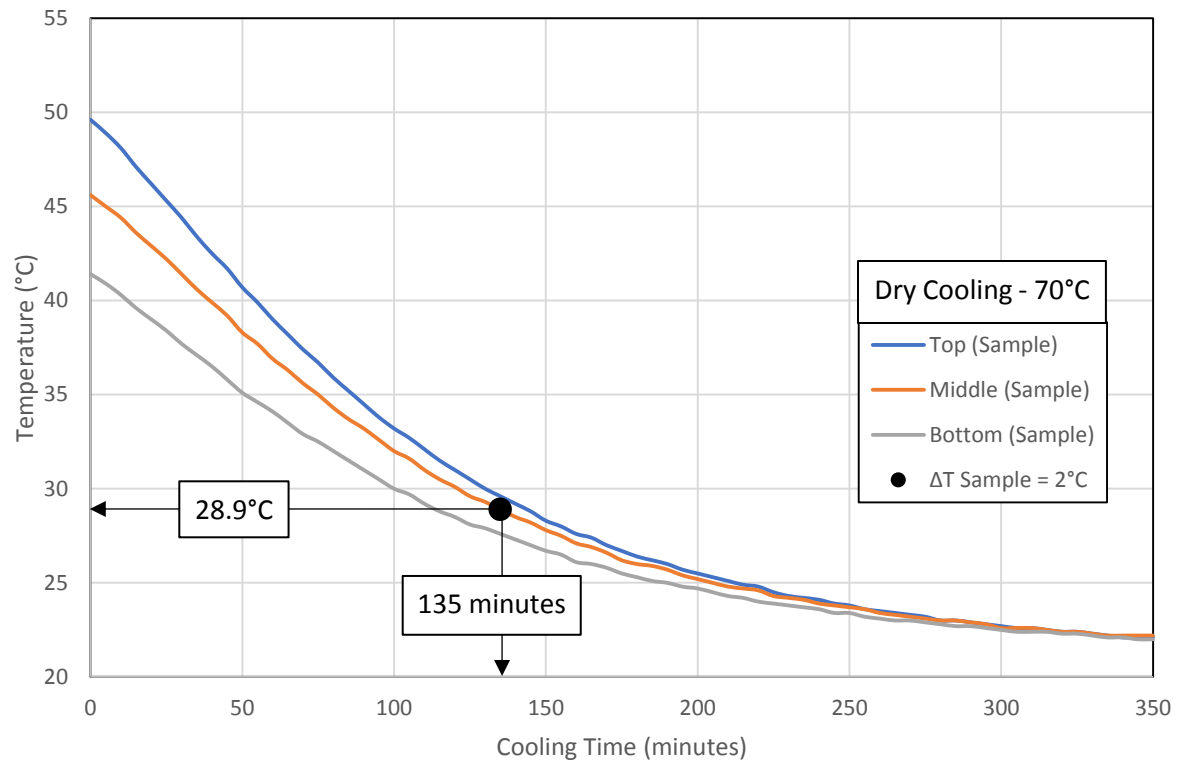Figure A-3: Sample cooling for 60°C at 9.9% (dry) moisture content

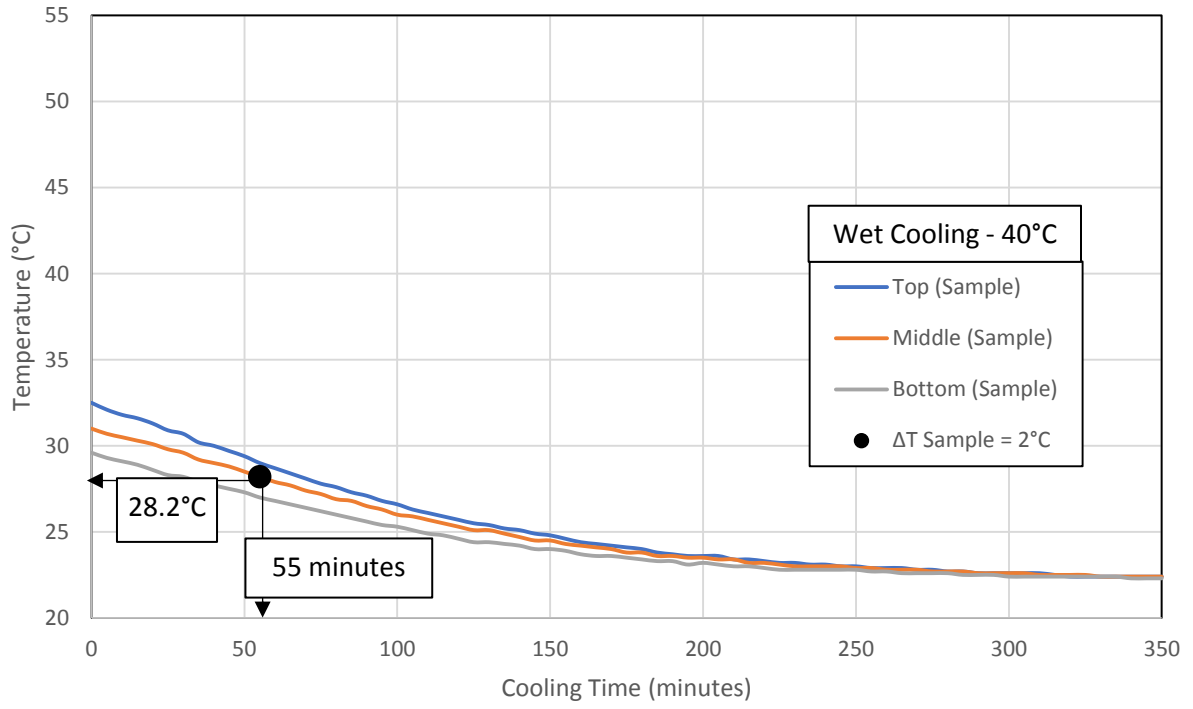Figure A-4: Sample cooling for 70°C at 9.9% (dry) moisture content

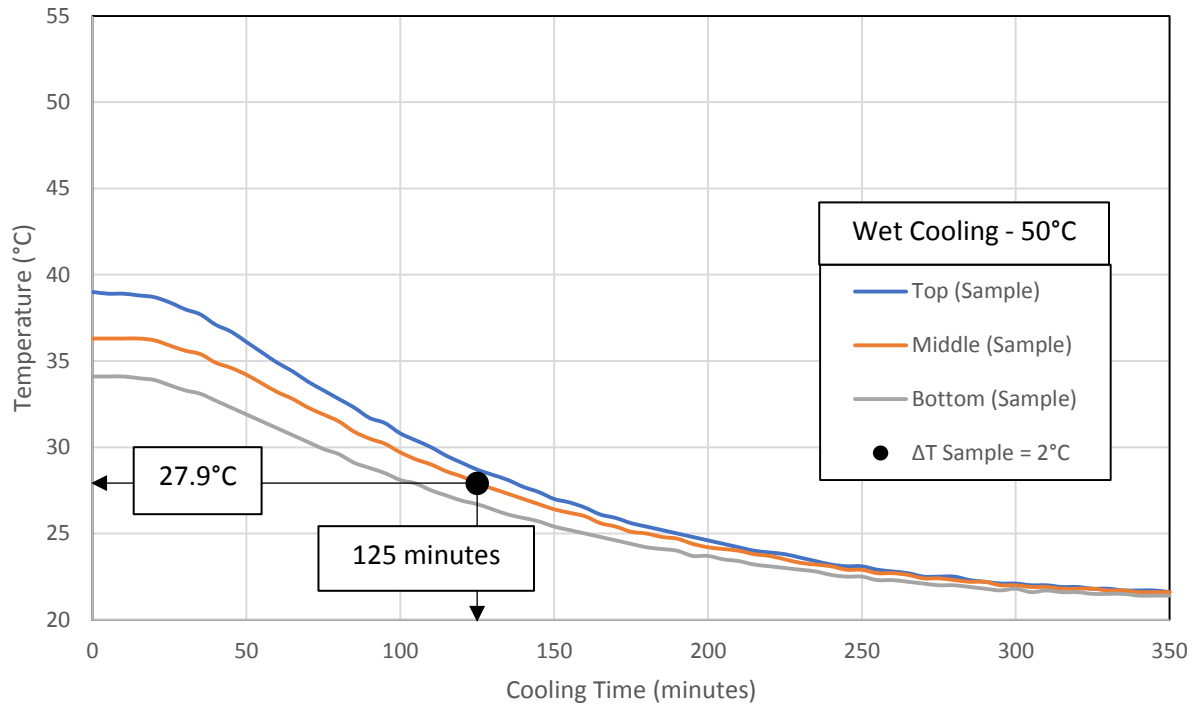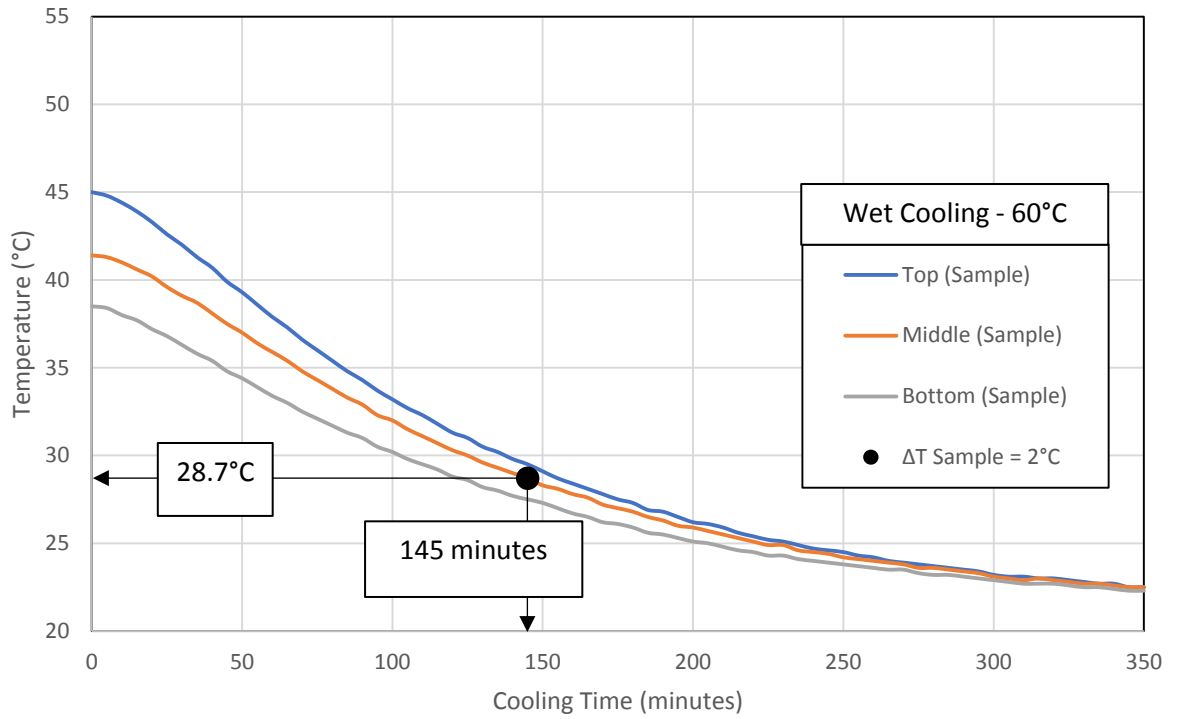Figure A-5: Sample cooling for 40°C at 17.6% (wet) moisture content

Figure A-6: Sample cooling for 50°C at 17.6% (wet) moisture content

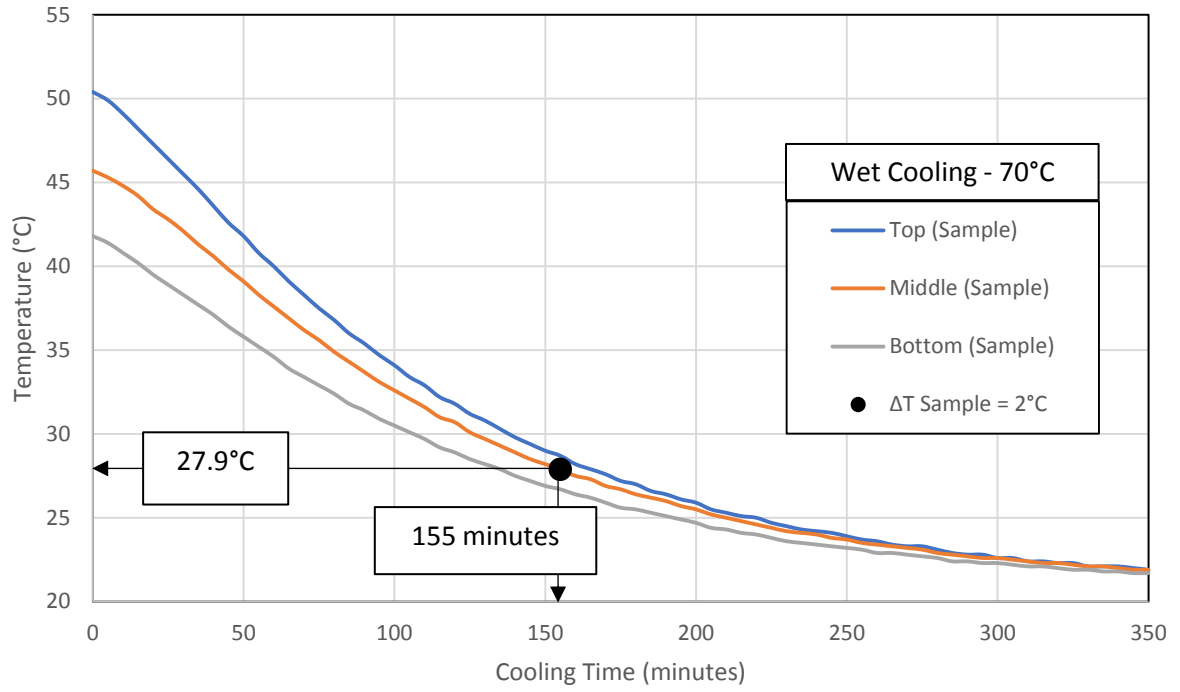Figure A-7: Sample cooling for 60°C at 17.6% (wet) moisture content

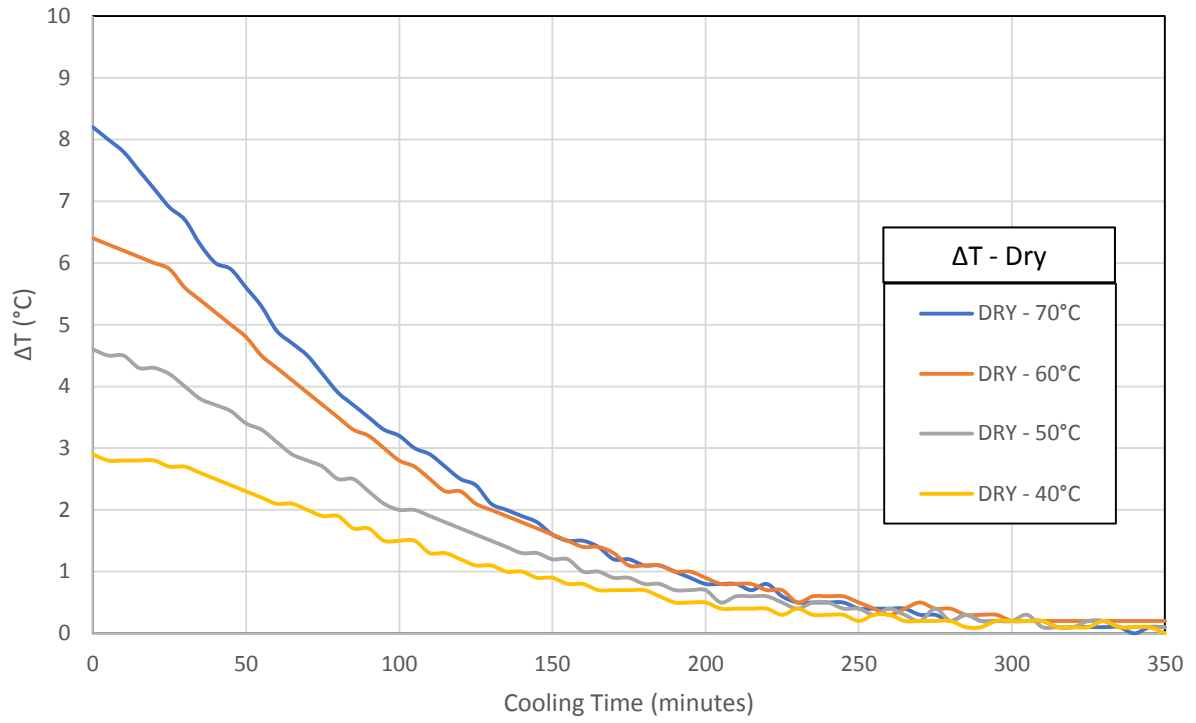Figure A-8: Sample cooling for 70°C at 17.6% (wet) moisture content

Figure A-9: Change in temperature during cooling for 9.9% (dry) moisture content
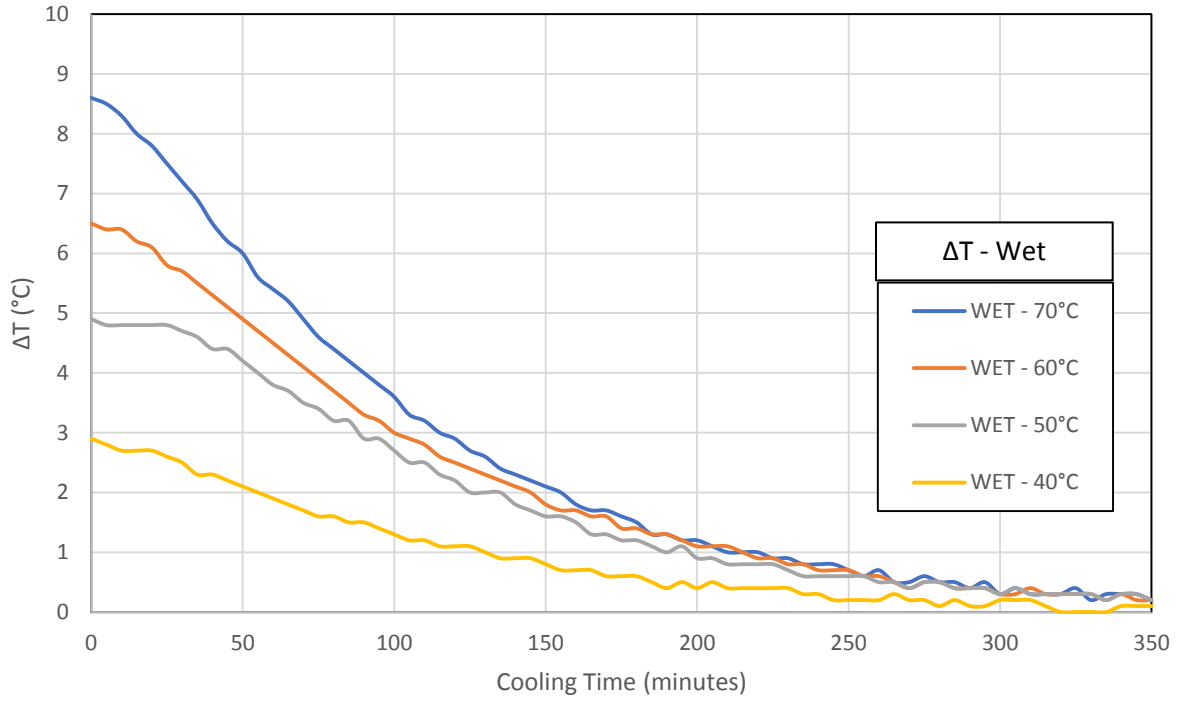
Figure A-10: Change in temperature during cooling for 17.6% (wet) moisture content